INTERACTION NOTES

Note 180

1968

# A GENERALIZED EXPANSION FOR RADIATED AND SCATTERED FIELDS

by

Robert John Garbacz

Ohio State University

It is shown that a denumerably infinite set of functions is associated with any loss-free obstacle and that these can be used to expand the fields radiated or scattered by that obstacle under a variety of excitation conditions. In the special case of a perfectly conducting obstacle, each such "characteristic" function is associated with a real "characteristic" current on its surface which gives rise to equiphase fields throughout the volume occupied by the obstacle. Several examples are treated briefly: the infinite circular cylinder, the sphere, the array of infinite, parallel wires, coaxial circular loops, and short, thin filaments of wire. The treatise ends with a discussion of topics for future investigation.

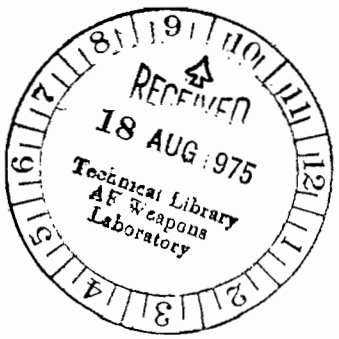

ACKNOWLEDGEMENT

The author is pleased to acknowledge the help of all his associates at the ElectroScience Laboratory, but especially of two individuals whose influence is reflected throughout this work: Dr. David Moffatt, friend and colleague, without whose patient encouragement this treatise might never have been completed; and Professor Edward Kennaugh, advisor and mentor without peer, a singular researcher whose maturing influence will always be appreciated.

CONTENTS

LIST OF TABLES

LIST OF TABLES (Continued)

LIST OF FIGURES

LIST OF FIGURES (Continued)

LIST OF FIGURES (Continued)

# CHAPTER I
# INTRODUCTION

Problems in the theory of electromagnetic and acoustic fields may be divided into two parts: (1) The mathematical representation of fields as functions of space, frequency, polarization, etc., and (2) The application of these representations for the solution of radiated or scattered fields associated with particular boundaries and excitations. Although these two aspects of field theory may be considered independently of each other, they in fact rarely are because, very often, the proper choice of field representation greatly simplifies the solution of a given problem. For example, when scattering objects are very large in terms of wavelength, a ray optic representation of the field is often postulated which involves reflection and attenuation factors. The evaluation of these factors for a given object leads to a solution which often is quite accurate and which can be arrived at only with great difficulty (if at all) if other field representations are assumed. Another example, closer to the subject of this study, is the solution for the scattering or radiation from a spherically symmetric object. We know that in the spherical coordinate system the vector (and scalar) time independent wave equation is separable and has for solutions the spherical vector (or scalar) wave functions, sometimes called spherical multipoles or spherical modes. Any radiated or scattered field can be represented

as an infinite (in general) weighted sum, i.e., modal expansion, of these functions. The presence of an object constrains the field to satisfy boundary conditions on its surface, and it is the satisfaction of these conditions that determines whether or not the field expansion is a useful representation for the solution of the fields radiated or scattered by the object. In the present instance, the spherical wave functions are "proper" to the solution of scattering or radiation from a spherically symmetric object because they possess orthogonality properties over the surface of such an object and, in the case of vector functions, they have components which are tangential to spherical surfaces.

For any other object shape, the spherical wave functions do not form a field representation directly suited to solution of the associated radiation or scattering problem. The question arises, therefore, whether or not a field representation of the modal expansion type exists which can be associated with a scatterer or radiator of any given arbitrary shape. In this treatise, we show that, given a loss-free obstacle, a set of characteristic functions exists which possesses properties similar to the set of spherical functions, and can be used to form a modal representation of a field scattered or radiated by that obstacle.

To aid the development, Chapter II presents a brief introduction to Hilbert space and the concept of an operator which transforms elements of one such space into elements of another. This mathematical background is used in Chapter III, where the scattering process

is interpreted in terms of operator language. This interpretation, together with physical reasoning, lead to the conclusion that for each perfectly conducting obstacle a particular set of surface currents and corresponding radiated fields exists which characterizes the obstacle shape independently of any specific excitation. These so-called "characteristic modes" form a useful basis set in which to expand fields radiated or scattered at a far distance from the obstacle. Certain properties of characteristic modes are inferred and these lead to methods for determining them in particular cases.

In Chapter IV several examples of characteristic modes associated with certain simple geometries are presented. First, the infinitely long circular cylinder and the sphere are elaborated from the characteristic mode viewpoint, and, although they are time-worn classical obstacles, the development is instructive. A less trivial obstacle composed of N infinitely long, thin, parallel wires arrayed arbitrarily in space is examined next. Two cases, where N = 3 and 8, are worked out in detail to illustrate the resulting modal currents and field patterns. Another example of characteristic modes is given for two coaxial circular loops of thin wire. The rotational symmetry of this obstacle gives some *a priori* knowledge of its modal currents which simplifies their determination. The representation in terms of characteristic modes is shown to be consistent with published results for the single circular loop scatterer. Finally, the thin finite wire of arbitrary shape is treated. Contrary to the infinite wire array, the modal currents for this obstacle have no neat expression in terms of

well known functions. Therefore, computer techniques are outlined for determining these currents which utilize certain properties of characteristic modes.

Chapter V presents a summary of the defining properties of characteristic modes. Some of the difficulties encountered in their determination are discussed as are their potential use in the solution of scattering and radiation problems.

One appendix is included in which the concept of modal impedances are discussed, specifically for the case of two coaxial circular loops.

An $e^{+i\omega t}$ time convention is assumed throughout this work and is suppressed for convenience.

# CHAPTER II
# LINEAR OPERATORS IN HILBERT SPACE- A BRIEF INTRODUCTION*

## A. Abstract Linear Spaces

In order to understand what is meant by the term "operator," it is necessary to introduce the notion of abstract linear spaces. The concept of a "space" is an abstraction and generalization of the familiar three-dimensional Euclidean space ("people" space) in which distance between any two "points" is measured along the "straight-line" between them. The generalization of this space proceeds in two directions: (1) to spaces of dimension greater than three, even to infinite dimension and (2) the introduction of more general measures of distance between any two "points" (elements) in the space. The abstraction of three-dimensional Euclidean space induces us to think not of concrete objects like points or vectors in the space but abstract elements which must obey certain rules if they are to be considered members of the space. By defining different rules, one may define many different abstract linear spaces, some of which have found more interest than others. One of these is Hilbert space, named after the mathematician who first studied infinite dimensional spaces. Hilbert space has been of much use to science because its defining rules have an interpretation in terms of physically meaningful quantities.

---

*Many of the statements in this chapter are extracted from Reference 1.

B. Postulates Defining Hilbert Space, $H$

A Hilbert space $H$ is a system of elements, f,g,h,$\cdots$ satisfying the following rules (postulates):

1. $H$ is a linear space

This means that two operations are defined; addition between elements of $H$ and multiplication of elements in $H$ by complex numbers (scalars) $\lambda, \mu, \rho$, such that

$$f + g = g + f$$

$$f + (g + h) = (f + g) + h$$

$$\lambda(f + g) = \lambda f + \lambda g$$

$$(\lambda + \mu)f = \lambda f + \mu f$$

$$(\lambda\mu)f = \lambda(\mu f)$$

$$1 \cdot f = f$$

$$0 \cdot f = 0 \cdot g \text{ for all } f, g \text{ in } H$$

2. A distance function is defined by means of a scalar (or inner) product

The scalar product of two elements f and g is a complex number denoted by $\langle f,g \rangle$ and possesses the following properties:

$$\langle \lambda f,g \rangle = \lambda \langle f,g \rangle$$

$$\langle g,f \rangle = \langle f,g \rangle^c$$

where superscript c means complex conjugate

$$\langle f_1 + f_2,g \rangle = \langle f_1,g \rangle + \langle f_2,g \rangle$$

$$\langle f,f \rangle > 0 \text{ if } f \neq 0$$

$$\langle f,g \rangle = 0 \text{ for all } g \text{ is } f = 0.$$

The quantity $\sqrt{\langle f,f\rangle} \equiv ||f||$ is called the norm of f. If $||f|| = 1$ it is called a normalized element. The distance function between two elements f and g is defined by $||f-g||$.

3. *H* is complete, that is, every Cauchy sequence in *H* must converge to a limit which also is in *H*

If $f_1, f_2, f_3, \cdots$, is a sequence of elements in *H*, then it is a Cauchy sequence if $||f_n - f_m|| \to 0$ as $n \to \infty$, $m \to \infty$. We require that every Cauchy sequence must converge to a limit f in *H* if the space is to be a Hilbert space, where convergence is defined in the strong sense,

$$\lim_{n\to\infty} ||f_n - f|| \to 0, \text{ or } f_n \to f.$$

A sequence $f_1, f_2, f_3 \cdots$ of elements in *H* is weakly convergent to f in *H* if

$$\lim_{n\to\infty} \langle f_n, g\rangle \rightharpoonup \langle f, g\rangle \text{ for every element g in } H,$$

$$\text{or } f_n \rightharpoonup f.$$

Every strongly convergent sequence is also weakly convergent; the converse is false.

4. The dimension of *H* is denumerably infinite

Let $\tau$ be a subset of *H*. If every neighborhood of any element in *H* always contains at least one element of $\tau$, then we say that $\tau$ is dense in *H*. If $g_\alpha$ are the elements of $\tau$ and we form all possible linear combinations

$$\sum_{\alpha=1}^{\infty} c_\alpha g_\alpha,$$

and if the totality of these linear combinations comprises a dense set in $H$, then we say that $\tau$ is a fundamental set in $H$. By definition, the smallest possible cardinality of a fundamental set in $H$ is called the dimension of $H$. By the present postulate, therefore, a Hilbert space must contain an infinite but denumerable fundamental set.

C. Two Realizations of Hilbert Space, $H_0$ and $L_2(a,b)$

There are two realizations of $H$ which are important to our later development. One is the Hilbert space of sequences (or infinite dimensional Euclidean space) and is denoted by $H_0$; the other is the Hilbert space of all complex-valued square integrable (in the sense of Lebesque) functions f(t) defined in the real interval $a \leq t \leq b$ with a suitable definition of scalar product, and is denoted by $L_2(a,b)$.

The space $H_0$ has as its elements all infinite sequences of complex numbers with finite norm. If two typical elements (sometimes called vectors) are denoted by $x = (x_1,x_2,x_3,\cdots)$ and $y = (y_1,y_2,y_3,\cdots)$, then

$$\langle x,y\rangle = \langle y,x\rangle^c = \sum_{\alpha=1}^{\infty} x_\alpha\, y_\alpha^c ,$$

is defined to be the inner product and

$$||x|| = \sqrt{\langle x,x\rangle} = \left[\sum_{\alpha=1}^{\infty} |x_\alpha|^2\right]^{\frac{1}{2}} ,$$

and

$$||y|| = \sqrt{\langle y,y \rangle} = \left[ \sum_{\alpha=1}^{\infty} |y_\alpha|^2 \right]^{\frac{1}{2}}$$

are finite. If $\langle x,y \rangle = 0$, the two elements (vectors) are said to be orthogonal.

The space $L_2(a,b)$ has as its elements all functions $f(t)$ such that

$$\int_a^b |f(t)|^2 \, dt \quad \text{and} \quad \int_\alpha^\beta f(t) \, dt,$$

where $a \leq \alpha \leq \beta \leq b$, exist. The interval $a \leq t \leq b$ can be infinite, but the sub-interval $\alpha \leq t \leq \beta$ must be finite. A suitable scalar product is defined by

$$\langle f,g \rangle = \int_a^b f(t) \, g^c(t) dt.$$

If $\langle f,g \rangle = 0$, the two elements $f(t)$ and $g(t)$ are said to be orthogonal.

D. Orthonormal Systems of Elements in $H$

A set $\{\phi\}$ of elements in $H$ such that each element $\phi$ is normalized, i.e., $||\phi|| = 1$, and any two different elements, say $\phi_m$ and $\phi_n$, are orthogonal, i e., $\langle \phi_m, \phi_n \rangle = 0$, is said to form an orthonormal system in $H$. Such an orthonormal system contains at most a countable infinity of elements. If $\{\phi\}$ also is a fundamental set, then any element $f$ in $H$ can be expanded in terms of $\phi_\alpha$ as

$$f = \sum_{\alpha=1}^{\infty} \langle f, \phi_\alpha \rangle \, \phi_\alpha \, ,$$

where the weighting coefficients are the scalar products $\langle f,\phi_\alpha \rangle$, called the Fourier coefficients of f. The set $\{\phi\}$ is then said to be a complete orthonormal system in $H$. As an example, in the Hilbert space $L_2(-\pi,\pi)$, the set of trigonometric functions

$$\{\phi\} = \begin{cases} 1/\sqrt{2\pi} \\ 1/\sqrt{\pi}\ \sin nt \\ 1/\sqrt{\pi}\ \cos nt \end{cases} \quad n = 1,2, \cdots \text{forms a complete orthonormal}$$

system in which any element f(t) in $L_2(-\pi,\pi)$ may be expanded. The resulting expansion,

$$f(t) = a_0 + \sum_{n=1}^{\infty} [a_n \cos nt + b_n \sin nt],$$

is the familiar Fourier series for f(t) and the coefficients

$$a_0 = \langle f,\ 1/\sqrt{2\pi} \rangle = \frac{1}{\sqrt{2\pi}} \int_{-\pi}^{\pi} f(t)dt,$$

$$a_n = \langle f, \frac{1}{\sqrt{\pi}} \cos nt \rangle = \frac{1}{\sqrt{\pi}} \int_{-\pi}^{\pi} f(t) \cos nt\, dt,$$

$$b_n = \langle f, \frac{1}{\sqrt{\pi}} \sin nt \rangle = \frac{1}{\sqrt{\pi}} \int_{-\pi}^{\pi} f(t) \sin nt\, dt,$$

are the Fourier coefficients of f(t).

E. Isomorphism Between $H$ and $H_0$

Having chosen an orthonormal system $\{\phi\}$ in $H$, one can form the infinite sequence of complex numbers (expansion coefficients) $x = (\langle f,\phi_1\rangle, \langle f,\phi_2\rangle, \langle f,\phi_3\rangle,\cdots)$ for any typical element f in $H$. But this sequence is one in the space $H_0$, and in fact it can be shown that there corresponds to any element f in $H$ a unique element x in $H_0$ and vice-versa, thereby defining a one-to-one correspondence between $H$ and $H_0$. If this one-to-one correspondence, denoted by T, satisfies the conditions

$$T(f + g) = Tf + Tg, \qquad \text{for all } f,g \text{ in } H$$

$$T(\lambda f) = \lambda Tf, \qquad \text{for all } f \text{ in } H \text{ and all scalars } \lambda$$

$$\langle Tf,Tg\rangle = \langle f,g\rangle, \qquad \text{for all } f,g \text{ in } H$$

then we say that the Hilbert space $H$ is isomorphic to the Hilbert space $H_0$. Thus, if a function f, which is an element of $H$, is expanded in a complete orthonormal set in $H$, the sequence formed by the corresponding expansion coefficients, which is an element of $H_0$, can be used to represent f in subsequent operations on f. Such images in $H_0$ of functions in $H$ will be useful in later developments.

F. Linear Operators in $H$

Having introduced the concept of abstract Hilbert space, we now are prepared to discuss operators in that space.

A map $M$ which associates with each element x belonging to a subset $\mathcal{D}$ of a Hilbert space $H$ with an element y belonging to a Hilbert space $H'$ is said to be an operator with domain of definition $\mathcal{D}$. The spaces $H$ and $H'$ need not be distinct. The operator $M$ is called linear if:

(1) $\mathcal{D}$ is a linear manifold, i.e., if $x_1$ and $x_2$ belong to $\mathcal{D}$, so does $(c_1x_1 + c_2x_2)$ for any complex numbers $c_1$ and $c_2$, and (2) $M(c_1x_1 + c_2x_2) = c_1Mx_1 + c_2Mx_2$. If the domain of definition of $M$ is all of $H$, and if there exists a constant $C \geq 0$ such that $||Mf|| \leq C||f||$ for all f in $H$, then the operator $M$ is a special one said to be bounded. The smallest such C always exists and is called the norm of $M$, denoted by $||M||$.

Suppose $M$ is a bounded linear operator relating an element x in $H$ to an element y in $H'$. Symbolically, this operation is written,

$$Mx = y.$$

If x is expanded in an orthonormal system $\{\phi\}$ with associated expansion coefficients $\langle x,\phi_\alpha\rangle = x_\alpha$ in $H_0$ and similarly, y is expanded in an orthonormal system $\{\psi\}$ with associated expansion coefficients $\langle y,\psi_\beta\rangle = y_\beta$ in $H_0'$, then $Mx = y$ implies that

$$y_\beta = \sum_{\alpha=1}^{\infty} \langle M\phi_\alpha,\psi_\beta\rangle x_\alpha.$$

In other words, the components of x and y are related by a matrix whose $\beta\alpha^{th}$ element is $\langle M\phi_\alpha,\psi_\beta\rangle$. This matrix, which can be denoted by $M = [M_{\alpha\beta}]$, is called the kernel matrix of the operator with respect to the $\{\phi\}$ and $\{\psi\}$ orthonormal systems. Thus, the symbolic equation $Mx = y$ for a bounded operator, $M$, can be transformed into an equivalent algebraic system of simultaneous equations of infinite number with infinitely many unknowns as a consequence of the isomorphism between $H$ and $H_0$ as well as between $H'$ and $H_0'$.

G. Completely Continuous Normal Operators in $H$

Bounded operators are a special case of the larger class of continuous operators; completely continuous operators are a special case of bounded operators. Whereas a bounded operator in $H$ implies only that if $x_n \to x$ (strong convergence) then $Mx_n \to Mx$, or if $x_n \rightharpoonup x_s$ (weak convergence) then $Mx_n \rightharpoonup Mx$ the completely continuous operator in $H$ implies that if $x_n \rightharpoonup x$ then $Mx_n \to Mx$. Thus, an operator $M$ which transforms any weakly convergent sequence in $H$ into a strongly convergent sequence in $H'$ and for which the domain of definition is all of $H$ is called completely continuous. There are alternative equivalent definitions and interpretations which will be pointed out later.

It may be shown[2] [3] that a sufficient condition for an operator to be completely continuous is that the elements, $M_{\alpha\beta} = \langle M\phi_\beta, \psi_\alpha \rangle$, of its kernel matrix $[M]$, with respect to complete orthonormal systems $\{\phi\}$ in $H$ and $\{\psi\}$ in $H'$, satisfy

$$\sum_{\alpha=1}^{\infty} \sum_{\beta=1}^{\infty} |M_{\alpha\beta}|^2 < \infty .$$

This property of the kernal matrix suggests that in performing the operation $M$ on an element $x$ in $H$, all but a finite number of terms in the expansion formula of the element $y = Mx$ in $H'$ may be neglected. More precisely, an operator $M$ is called completely continuous if it can be represented in the form[4]

$$y = Mx = M'x + M''x,$$

where $M'$ is a degenerate or finite dimensional operator and $||M''|| < \varepsilon$ for any $\varepsilon > 0$. This implies that the expansion formula for the element y can be truncated after a finite number of terms and the result will be within an $\varepsilon$ neighborhood of the correct y.

The kernel matrix which represents a completely continuous operator is "almost" finite dimensional, and its rows and columns can be ordered in such a manner that all entries, $M_{\alpha\beta}$, where $\alpha > N(\delta)$, $\beta > N(\delta)$, have absolute values less than any preassigned $\delta$. Thus, certain properties of completely continuous operators are analogous to those of finite-dimensional matrices. In particular, the adjoint, $M^*$ of a completely continuous operator, $M$, is the operator whose kernel matrix is the complex conjugate transpose of the kernel matrix of $M$.

A normal operator, $N$, is one whose kernel matrix commutes with that of its adjoint, $N^*$. For a bounded operator to be normal, it is necessary and sufficient that its self-adjoint or Hermitian components, defined by $R = \frac{1}{2}(N+N^*) = R^*$ and $J = \frac{1}{2i}(N-N^*) = J^*$, commute.

A symmetric operator is one whose kernel matrix is symmetric, that is, equal to its transpose. If an operator is both normal and symmetric, its self-adjoint components become its real and imaginary parts and therefore the real and imaginary parts of its kernel matrix commute.

If an operator $M$ is normal and completely continuous a special set of basis vectors, called the set of eigenvectors, exists, such that any element x in $H$ may be expressed in terms of the weighted sum,

$$x = A_1 x_1 + A_2 x_2 + \cdots + x_o,$$

where $x_o$ are a set of null vectors, i.e., those for which $Mx_o = 0$. Likewise, for any element y in $H'$,

$$y = Mx = \frac{A_1 x_1}{\gamma_1} + \frac{A_2 x_2}{\gamma_2} + \cdots ,$$

whence

$$\langle Mx, x \rangle = \frac{|A_1|^2}{\gamma_1} + \frac{|A_2|^2}{\gamma_2} + \cdots$$

The $\gamma_n$ are called eigenvalues and satisfy the equations

$$\gamma_n \, Mx_n = x_n \qquad |\gamma_1| \leq |\gamma_2| \leq \cdots ,$$

where $|\gamma_n| \to \infty$. The values $1/\gamma_n$ are the diagonal elements of the diagonalized kernel matrix [M].

The formula for $\langle Mx, x \rangle$ is called the fundamental formula and the formula for $y = Mx$ is called the expansion formula; if the sequence of eigenvectors is finite, then $M$ is called a degenerate or finite dimensional operator and [M] has only a finite number of

non-zero diagonal elements. A degenerate operator is always completely continuous. All the above statements lead to the following

spectral theorem for completely continuous normal operators:[5][6]

> Every completely continuous normal operator $M$ distinct from the null operator possesses either a finite number of eigenvalues (degenerate case) or else an infinity of eigenvalues, $1/(\mu_n + i\nu_n)$ (in general complex numbers) with no finite point of accumulation. Each eigenvalue has finite multiplicity. The union of the null vectors and eigenvectors of this operator contains a complete, orthonormal system. The expansion formula and the fundamental formula both hold. The self-adjoint components $R$ and $J$ of $M$ have the respective eigenvalues $1/\mu_n$ and $1/\nu_n$. If all the eigenvalues of $M$ are real, then $J = 0$ and $M$ is self-adjoint. In any case, $M$ and $M^*$ possess the same null vectors and eigenvectors. Conversely, if a completely continuous operator $M$ has the same null vectors and eigenvectors as $M^*$, and if the union of its null vectors and eigenvectors contains a complete orthonormal system, then $M$ must be normal.

Before stating additional mathematical concepts necessary to the development of characteristic modes, it may help to interpret those already presented in terms of the physics of scattering, for which we have some intuitive feeling.

# CHAPTER III
# THE CONCEPT OF CHARACTERISTIC MODES

## A. Scattering and Perturbation Operators

In the previous chapter we have introduced the notion of a linear space and an operator. In this chapter we shall relate these concepts to a physical problem, namely, the problem of electromagnetic scattering by a perfectly conducting object in space.

We choose an origin within the volume occupied by the scatterer and consider all the complex vector fields which satisfy the vector Helmholtz equation,

$$\nabla \times (\nabla \times \underline{E}^i) - k^2 \underline{E}^i = 0, \tag{1}$$

in a homogeneous region outside a sphere just enclosing the obstacle, and also satisfy the condition

$$\lim_{r\to\infty} \{r(r \times (\nabla \times \underline{E}^i) + ik \underline{E}^i)\} = 0, \tag{2}$$

on the sphere $\Sigma$ at $r\to\infty$. These will be called converging vector fields, i.e., fields which travel inward toward the chosen origin. Similarly, we consider all the complex vector fields which satisfy the vector Helmholtz equation in a homogeneous region outside a sphere just enclosing the obstacle and also satisfying the (radiation) condition

$$\lim_{r\to\infty} \{r(\hat{r} \times \nabla \times \underline{E}^0 - ik\underline{E}^0)\} = 0 \tag{3}$$

on the sphere $\Sigma$ at $\infty$. These will be called <u>diverging</u> vector fields, i.e., fields which travel outward from the chosen origin.

The scalar product of two fields $\underline{E}_1$ and $\underline{E}_2$, both of the same type (converging or diverging), is defined as

$$\langle \underline{E}_1, \underline{E}_2 \rangle = \lim_{r\to\infty} \frac{1}{Z_0} \iint_\Sigma \underline{E}_1 \cdot \underline{E}_2^c \, r^2 \sin\theta \, d\theta \, d\phi \tag{4}$$

where the surface integral is evaluated on the sphere of radius r. We limit our consideration to fields of finite norm.

The fields of either type form a linear space and, further, through their representation in terms of vector spherical wave functions (multipoles), may be made to correspond to elements in the Hilbert space, $H_0$. In order to create an isomorphism between the space of fields $\underline{E}^i(\underline{E}^0)$ and the space $H_0$ ($H_0'$), we shall adjoin to $\underline{E}^i$ ($\underline{E}^0$) fields which are discontinuous (and therefore do not satisfy the vector Helmholtz equation) but whose discontinuities do not affect the inner product integral. Then, for every element in $H_0(H_0')$, a unique element $\underline{E}^i$ ($\underline{E}^0$) in $H(H')$ exists, which by isomorphism, implies that $H(H')$ is a Hilbert space.

In particular, the isomorphism holds between $H_0$ ($H_0'$) and the tangential vector pattern functions $\{ r\, e^{ikr}\, \underline{E}^i \}$ ($\{ r\, e^{-ikr}\, \underline{E}^0 \}$) on $\Sigma$ at $\infty$ since these distributions completely define the associated multipole expansions. We shall refer to these sets of vector functions

(pattern functions) as $\{\underline{f}^i(\theta,\phi)\}$ in $H$ and $\{\underline{f}^o(\theta,\phi)\}$ in $H'$. We understand that they are functions of $\theta$ and $\phi$ on $\Sigma$ and, except where clarity is jeopardized, shall omit the explicit functional notation.

In the absence of an obstacle, any incoming function $\underline{f}^i$ in $H$ is transformed without disturbance into an outgoing function $\underline{f}^o$ in $H'$. That is,

$$\underline{f}^o = I\underline{f}^i, \tag{5}$$

where $I$ is the identity operator and may be viewed as the scattering operator associated with unbounded free space. By placing an obstacle at the origin, this unit operator is perturbed to form the scattering operator, $S$, indicating that the function $\underline{f}^i$ in $H$ is transformed into a function in $H'$ which is perturbed from $\underline{f}^o$. That is,

$$\underline{f}^o + \underline{\Delta f}^o = S\underline{f}^i \tag{6}$$

The perturbation is represented by the operator $(S-I)$, so that

$$\underline{\Delta f}^o = (S-I)\underline{f}^i \tag{7}$$

The operator $\frac{1}{2}(S-I)$ will be called the perturbation operator, denoted by $P$, and the perturbation $\underline{\Delta f}^o/2$ of the outgoing function from its value in the absence of the obstacle will be called the scattered function, $\underline{f}^s$. Thus

$$\underline{f}^s = P\underline{f}^i, \tag{8}$$

where $\underline{f}^i$ is an element of $H$ and $\underline{f}^s$ is an element of $H'$. The reason

for the factor $\frac{1}{2}$ in the definition $P = \frac{1}{2}(S-I)$ will become clear later.

Consider next, that a particular function exciting the obstacle as well as the resultant scattered function are expanded into a denumerably infinite, complete, orthonormal set of vector spherical waves or multipoles (a convenient basis system) with respect to the chosen origin within the scatterer surface. The resultant kernel matrix [S] associated with the scattering operator $S$ of the obstacle will be called the scattering matrix.[7] [8] [9] [10] It represents the transformation of all spherical multipoles converging upon the origin into all spherical multipoles diverging to the spherical surface at infinity. The scattering matrix generally is infinite dimensional but can be arranged so that only a finite number of off-diagonal elements are non-infinitesimal and only a finite number of diagonal elements differ significantly from unity. Since the unit matrix [I] is the kernel matrix of the identify operator $I$, and the matrix $\frac{1}{2}$ [S-I] = [P] is the kernel matrix of the perturbation operator $P$, then [P] may be decomposed into a sum of an infinite dimensional matrix all of whose non-zero elements lay in an $N \times N$ finite submatrix and an infinite dimensional matrix which has an infinitude of small elements. If the contribution of this latter matrix to the scattered field can be made arbitrarily small, then the perturbation operator $P$ and its kernel matrix [P] may be considered to be "almost finite dimensional".[11]

In the following section, some important mathematical properties of the operators $S$ and $P$ are inferred from the physics of the scattering phenomenon.

## B. Some Properties of Scattering and Perturbation Operators

In the previous section we have suggested that the operator concept provides a convenient mathematical description of how an obstacle scatters. By choosing a basis system, this operator concept is articulated in the form of an infinite dimensional kernel matrix which relates one vector whose components are the expansion coefficients of the incoming part of the exciting function to another vector whose components are the expansion coefficients of the outgoing scattered functions. We now are prepared to apply knowledge of the physics of scattering problems to infer certain interesting mathematical properties of the operators and their kernel matrices.

For isotropic media, the reciprocity condition on the fields and a proper choice of phase conventions for the wave functions ensure that the scattering operator $S$ and the scattering matrix $[S]$ are complex symmetric, i.e., $S^{c*} = S$ and $[S]^t = [S]$, where $S^{c*}$ is the complex conjugate of the adjoint of $S$ and $[S]^t$ is the transpose of $[S]$. Furthermore, since the obstacles under study are lossless, an energy balance must be maintained between incoming and outgoing waves.

This energy conservation condition together with the properties of the fields under time reversal implies that the scattering operator and the scattering matrix are unitary,[12] i.e., $S^*S = SS^* = I$ and $[S]^{ct}[S] = [S][S]^{ct} = [I]$, where $[S]^{ct}$ is the complex conjugate transpose of $[S]$. Since $S$ and $[S]$ are unitary they are also bounded[13] and normal,[14] [15] $S^*S = SS^*$ and $[S]^{ct}[S] = [S][S]^{ct}$. Since $S$ and $[S]$ are normal, so are $(S-I)$ and $[S-I]$, or in other words, the perturbation operator $P$ and perturbation matrix $[P]$ are normal. Clearly, $P$ and $[P]$ are also complex symmetric.

In the previous section we suggested that $P$ and $[P]$ are "almost finite dimensional," that is, that they can be expressed as a sum of a degenerate or finite-dimensional operator and an operator whose influence on the scattered field is very small (whose norm may be made less than any preassigned number). To say that this is indeed the case, we must prove that $P$ is a completely continuous operator.

To do this, it is sufficient to show that the elements, $p_{mn}$, of the kernel matrix of $P$ satisfy the relation

$$(9) \qquad \sum_{m=1}^{\infty} \sum_{n=1}^{\infty} |p_{mn}|^2 < \infty \quad .$$

To show that $[P]$ does satisfy this condition, consider the case of a plane wave illuminating a perfectly conducting finite obstacle from a direction, $(\theta^i,\phi^i)$. If this plane wave is expanded in terms of standing spherical multipoles, we find that the associated expansion coefficients have functional variations with $(\theta^i,\phi^i)$ equal to

the spherical multipoles, $\underset{o}{\underline{m}}^{(2)}_{emn}$ and $\underset{o}{\underline{n}}^{(2)}_{emn}$, given by Stratton. If these coefficients form a vector $(u^i(\theta^i,\phi^i))$, it is transformed by the kernel matrix, $[P]$, into a vector $(u^o(\theta^i,\phi^i))$, i.e.,

$$(10) \qquad (u^o) = [P]\ (u^i).$$

Note that, in a strict sense, the incoming part of the plane wave function does not belong to the Hilbert space, $H$, since its represenation in $H_o$ would be a vector of unbounded norm. However, we can approach the plane wave excitation by a sequence of excitations, $\{u^i_n\}$, which are weakly convergent, and for each of which the representation in $H_o$ consists of a vector with a finite number, N, of non-zero components. As N increases, this sequence converges weakly to a vector $(u^i)$ representing the plane wave excitation. The resultant outgoing function belongs to the Hilbert space, $H'$, since its representation $(u^o)$ in $H_o'$, must be of bounded norm as a consequence of the finiteness of the total scattered energy. That is,

$$(11) \qquad ||u^o||^2 = (u^o)^{ct}\ (u^o) = (u^i)^{ct}\ [P]^{ct}\ [P]\ (u^i) < \infty \quad .$$

In fact, if we consider all possible angles of incidence, $(\theta^i,\phi^i)$, of the illuminating plane wave with all possible polarization states, $\alpha$, we can state from the physics of scattering that the total power averaged over every such excitation is finite. That is,

$$(12) \qquad \int_\alpha \iint \ ||u^o(\theta^i,\phi^i)||^2 \sin\theta^i\, d\theta^i\, d\phi^i\, d\alpha < \infty,$$

which, together with the orthogonality of the spherical multipoles, implies that

$$(13) \qquad \sum_{m=1}^{\infty} \sum_{n=1}^{\infty} |p_{mn}|^2 < \infty ,$$

which is the desired conclusion.

With the assurance that $P$ is a normal completely continuous operator in $H$, we may apply the spectral theorem which states that $P$ possesses either a finite number of eigenvalues (degenerate case) or else an infinity of eigenvalues of the form $(a_{rn} + i\, a_{in})^{-1}$ (complex numbers in general) with no finite point of accumulation and of finite multiplicity. The union of the null vectors and the vectors of $P$ contains a complete orthonormal set in which to expand an arbitrary element in the vector space. More specifically, since the kernel matrix $[P] = \frac{1}{2}[S-I]$ is complex symmetric, its self-adjoint components are its real and imaginary components, $[P] = \frac{1}{2}[S-I] = \frac{1}{2}[S_r-I] + i\,\frac{1}{2}[S_i]$. Hence, by the spectral theorem

$$(14) \qquad a_{rn}(U_n) = \tfrac{1}{2}[S_r-I]\ (U_n) = [P_r]\ (U_n),$$

and

$$(15) \qquad a_{in}(U_n) = \tfrac{1}{2}[S_i]\ (U_n) = [P_i]\ (U_n),$$

where $1/a_{rn}$ and $1/a_{in}$ are eigenvalues* or else zeros and $(U_n)$ are the associated orthonormal eigenvectors. Since $[S_r-I]$ and $[S_i]$ are real, $a_{rn}$ and $a_{in}$ as well as all the components of $(U_n)$ are real numbers. Hence, we imply that the perturbation matrix $[P] = \frac{1}{2}[S-I]$ possesses a set of complex eigenvalues $1/a_n = 1/(a_{rn} + ia_{in})$ and an associated set of eigenvectors in $H_o$ which are real and orthonormal. That is,

$$(16) \qquad a_n(U_n) = \frac{1}{2}[S-I]\ (U_n) = [P]\ (U_n).$$

The diagonalized perturbation matrix has entries on its diagonal equal to its characteristic values $a_n$, or zero. The diagonalized scattering matrix has entries on its diagonal equal to its characteristic values $s_n = 2a_n + 1$ or unity[17] and the unitary property of $[S]$ assures that $s_n = e^{i2\sigma n}$, i.e., $|s_n| = 1$. Clearly, in the complex plane the $s_n$ lie on the unit circle centered at the origin and the $a_n$ lie on the circle of half-unit radius centered at $(-\frac{1}{2},io)$. In later work it will be convenient to relate $s_n$ and $a_n$ to a parameter, $\lambda_n$, by means of bilinear transforms,

$$(17) \qquad s_n = \frac{1 - \left(\frac{1}{i\lambda_n}\right)}{1 + \left(\frac{1}{i\lambda_n}\right)} \quad ,$$

---

*In the literature $a_n$ are called characteristic values and $1/a_n$ are called eigenvalues. See Reference 16. In this work, we shall refer to $(U_n)$ as eigenvectors or characteristic vectors, interchangably.

and

$$a_n = -\frac{1}{1 + i\lambda_n} \quad . \tag{18}$$

The Smith impedance chart, which graphically represents these transforms, may be superimposed on the unit circle as shown in Figs. 1 and 2.

C. Discussion

As a consequence of the complete continuity of the symmetric normal operator, $P$, we have implied certain mathematical results. It is important to the later development that the physical implications be understood at this point.

Once the oscillation frequency is fixed, a loss-free object of given composition and surface shape has associated with it a denumerable set of special electromagnetic fields, each unique to within a multiplicative constant. Each such field may be produced by primary sources located outside some sphere enclosing the obstacle and is characterized by a cavity-mode total field behavior between the scatterer and the enclosing sphere. If the scatterer is removed and replaced by the ambient medium, the primary sources also produce a cavity-mode field in the region formerly occupied by the scatterer. A harmonic field is said to be a cavity-mode field in a three dimensional region if $\underline{E}$ (and $\underline{H}$) vanishes instantaneously throughout the region twice per period. Equivalently, the vector distribution of $\underline{E}$ or $\underline{H}$ throughout the region is independent of time, but varies sinusoidally in amplitude with time.

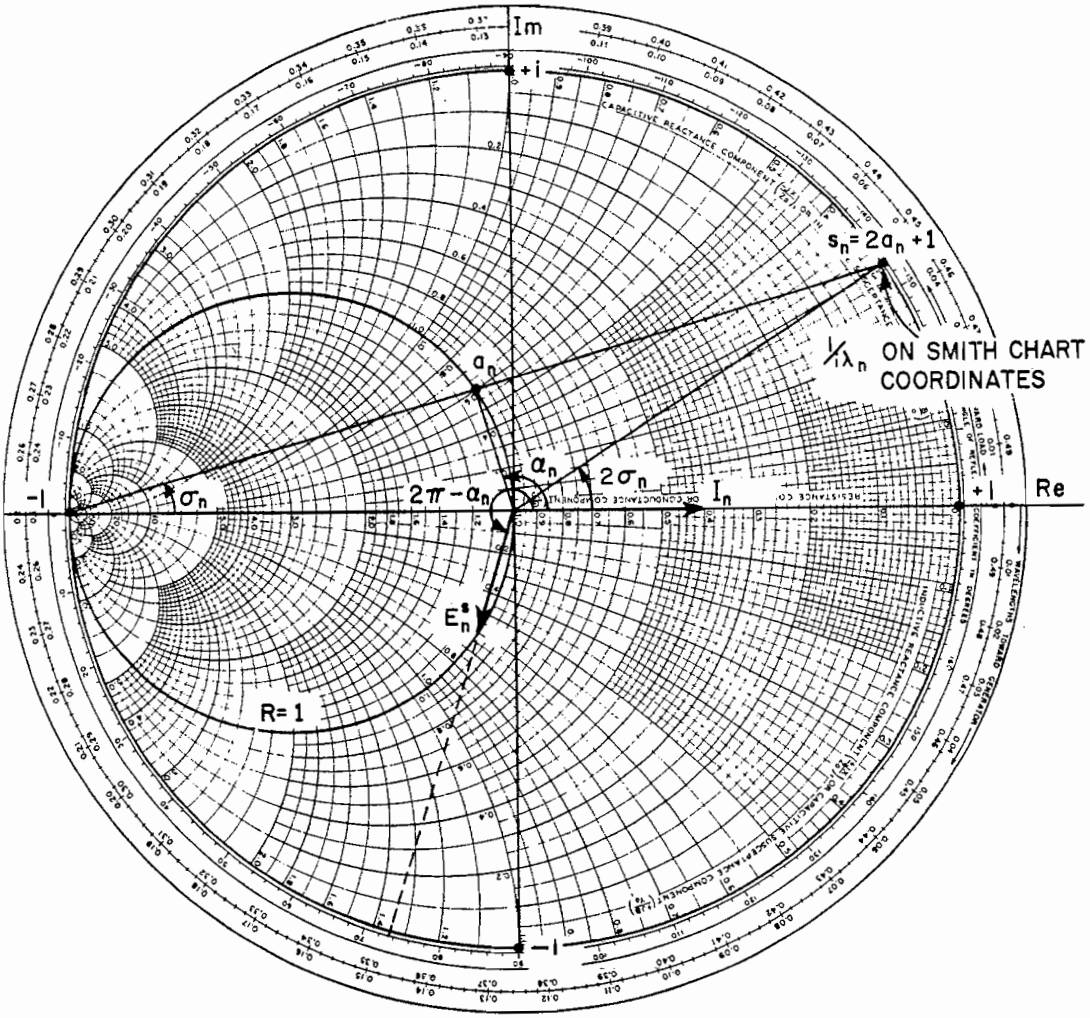


Fig. 1--Geometrical relationships between the characteristic values of [S] and $[P] = \frac{1}{2}[S-I]$.

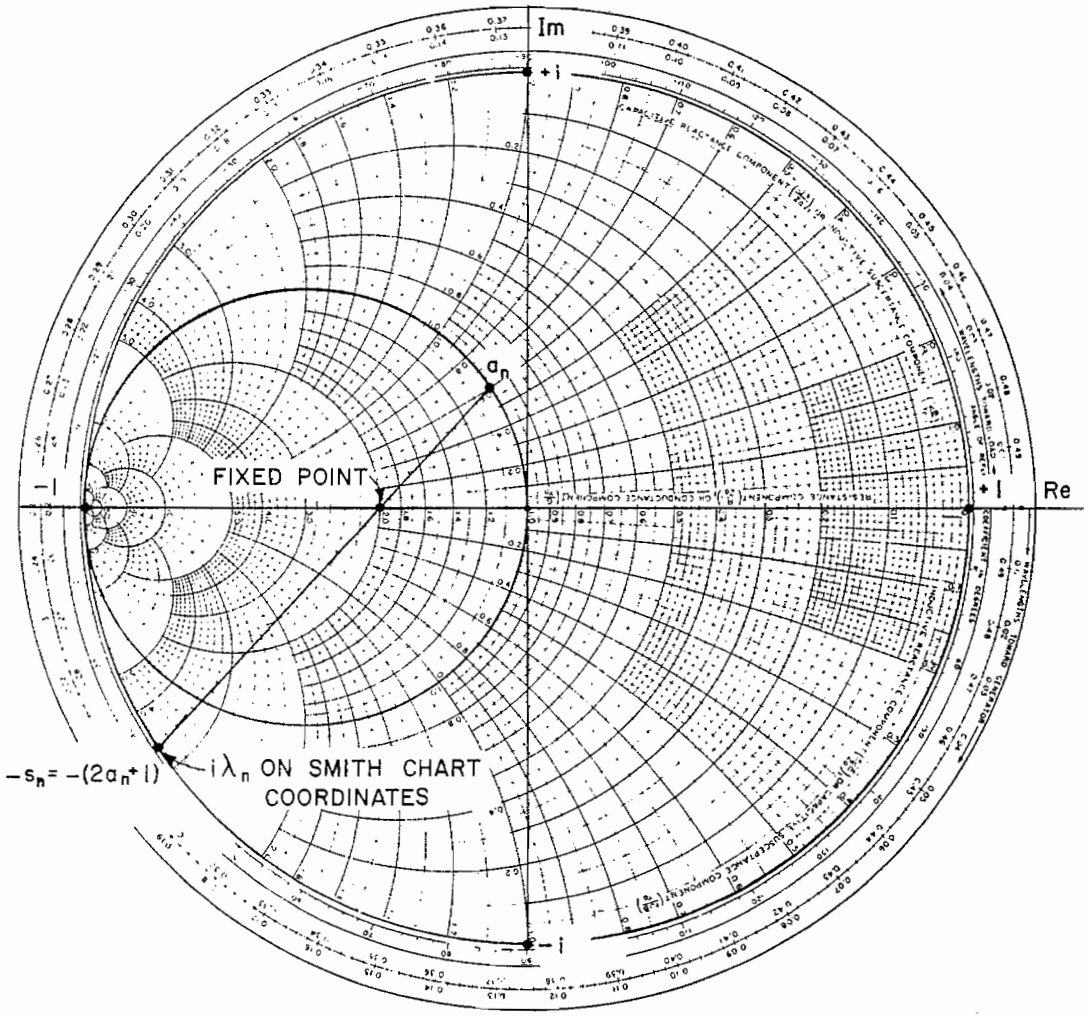


Fig. 2--An alternative construction.

These physical properties possessed by the special set of fields are a consequence of two facts: (1) in the absence of the scatterer, the incoming and outgoing vector spherical wave expansions of each such field have identical real coefficients, and (2) in the presence of the scatterer, the coefficients in the expansion for each outgoing field undergo a uniform phase shift. These fields may be ordered naturally according to the magnitude of their phase shifts, only a finite number having phase shifts greater than $\varepsilon > 0$ in magnitude, where $\varepsilon$ is an arbitrarily small quantity.

In the case where the obstacle is a perfect electric conductor, which henceforth shall be assumed in this work, a further interpretation of the special fields and associated surface current distributions may be made. Since the total fields exterior to the scatterer surface are cavity-mode, the associated surface current distribution (electric type) will have a standing-wave character, i.e., its strength varies sinusoidally with time, but its spacial distribution over the surface does not. Furthermore, in the absence of the scatterer, this current distribution generates a cavity mode field throughout the region formerly occupied by the scatterer (since the sum of the fields produced by the induced surface current and the primary sources present in the absence of the scatterer must be zero within the volume occupied by the scatterer).

Thus, for a perfectly conducting scatterer with a surface S, at a specified angular frequency $\omega$, we may define a set of characteristic

mode current distributions $\underline{J}_n$ on S which radiate a set of characteristic mode electric fields $\underline{E}_n^{ext}(r,\theta,\phi)$ outside S, such that

(1) $\underline{J}_n$ is a standing wave current distribution of the form $\underline{J}_n(u,v)\cos\omega t$, where u and v are surface coordinates on S.

(2) $\underline{J}_n$ generates a cavity mode field everywhere inside S and this interior field can be expressed as $\underline{E}_n^{int}(r,\theta,\phi)\cos(\omega t-\alpha_n)$, where $\frac{\pi}{2} \leq \alpha_n \leq \frac{3\pi}{2}$. The indices n are chosen so that the magnitudes $|\cos\alpha_n|$ form a decreasing sequence with increasing n and only a finite number of the $|\cos\alpha_n|$ are greater than $\varepsilon > 0$, where $\varepsilon$ is an arbitrarily small number.

(3) The electric field $\underline{E}_n^{ext}(r,\theta,\phi)$ is that radiated by the surface current distribution $\underline{J}_n$, and $\underline{J}_n$ is normalized so that it radiates unit power for each mode of finite order n. On the sphere $\Sigma$ at $r\to\infty$, $\underline{E}_n^{ext}(r,\theta,\phi) = \frac{-i\omega\mu}{4\pi}\frac{e^{-ikr}}{r}\underline{F}_n(\theta,\phi)$, where $\underline{F}_n(\theta,\phi)$ is the $n^{th}$ characteristic mode pattern function on $\Sigma$. The normalization to unit radiated power implies that

$$\langle \underline{F}_n, \underline{F}_n \rangle = \frac{1}{Z_o}\iint_\Sigma |\underline{F}_n|^2 \sin\theta\, d\theta\, d\phi = \frac{(4\pi)^2}{(kZ_o)^2} .$$

Furthermore, since $\underline{E}_n^{ext}(r,\theta,\phi)$ is the $n^{th}$ characteristic function of the perturbation operator P, and these

are orthonormal to all others according to the spectral theorem,

$$\langle \underline{F}_n, \underline{F}_m \rangle = \frac{1}{Z_o} \iint_{\Sigma} \underline{F}_n \cdot \underline{F}_m^c \sin\theta \, d\theta \, d\phi = 0, \quad m \neq n.$$

The characteristic mode current distributions as defined are an extension of the set of resonant current distributions, if any exist, for the cavity enclosed by S at angular frequency $\omega$. These familiar cavity modes, if they exist, are included as a degenerate subset of the set of characteristic modes; they correspond to values of $\alpha_n = \frac{\pi}{2}$ or $\frac{3\pi}{2}$, i.e., $|\cos \alpha_n| \equiv 0$, for which the radiated field is identically zero.* Such modes are not encountered for finite n because of the mode ordering chosen on $|\cos \alpha_n|$.

Having defined characteristic mode currents and characteristic mode radiated fields of a perfectly conducting scatterer with surface S and at angular frequency $\omega$, it seems natural to investigate methods for expanding an illuminating field (such as a plane wave arriving from an arbitrary direction) in terms of a linear combination of characteristic mode interior fields $\underline{E}_n^{int}(r,\theta,\phi)$ and then deriving an expression for the scattered field as a linear combination of the $\underline{E}_n^{ext}(r,\theta,\phi)$. In the following section we shall see that such an expansion is possible and in the process, reduces the expression

---

*For these resonant cavity modes, the tangential component of the electric field on S is identically zero.

for the far-zone scattered field due to plane wave illumination to a particularly simple bilinear form in terms of the characteristic pattern functions, $\underline{F}_n(\theta,\phi)$.

## D. The Bilinear or Characteristic Mode Expansion

Having defined a complete, orthonormal (in the sense of radiated power) set of modal fields, $\underline{E}_n^{int}(r,\theta,\phi)$ and $\underline{E}_n^{ext}(r,\theta,\phi)$, interior and exterior, respectively, to S, we wish to use them to expand the field due to a current source $\underline{J}$ arbitrarily located at $(r^i,\theta^i,\phi^i)$. In the absence of the obstacle, this field in the vicinity of the origin must be of standing wave type and can therefore be expanded as a weighted sum of the fields, $\underline{E}_n^{int}(r,\theta,\phi)$. The weight, $A_n$, of the $n^{th}$ term in this expansion is given by the reaction[18] [19] [20] of the $n^{th}$ radiated field, $\underline{E}_n^{ext}(r,\theta,\phi)$, with the source current. That is,

$$A_n = \iiint_V \underline{E}_n^{ext}(r,\theta,\phi) \cdot \underline{J}(r,\theta,\phi)\, dv, \tag{19}$$

where the integration is over the volume of the source. If the source is an electric dipole located at $(r^i,\theta^i,\phi^i)$, this simplifies to

$$A_n = i\omega \underline{E}_n^{ext}(r^i,\theta^i,\phi^i) \cdot \underline{p}\ , \tag{20}$$

where $\underline{p}$ is the electric dipole moment of the source. But it is precisely this incoming wave, with pattern function $F_n(\theta,\phi)$ on $\Sigma$, which is transformed by the obstacle into an outgoing wave with the same far field pattern, i.e., $2a_n \underline{F}_n(\theta^s,\phi^s) = 2P \underline{F}_n(\theta^i,\phi^i)$. Hence,

the $n^{th}$ characteristic mode field at an observer point, $(r^s,\theta^s,\phi^s)$, due to a dipole source at $(r^i,\theta^i,\phi^i)$ is

$$(21)\quad \underline{E}_n(r^s,\theta^s,\phi^s;r^i,\theta^i,\phi^i) = -i\omega a_n \underline{E}_n^{ext}(r^s,\theta^s,\phi^s)\underline{E}_n^{ext}(r^i,\theta^i,\phi^i) \cdot \underline{p},$$

and if the first N such modes are important,

$$(22)\quad \underline{E}(r^s,\theta^s,\phi^s;r^i,\theta^i,\phi^i) = -i\omega \sum_{n=1}^{N} a_n \underline{E}_n^{ext}(r^s,\theta^s,\phi^s)\underline{E}_n^{ext}(r^i,\theta^i,\phi^i) \cdot \underline{p} \ .$$

Clearly this is a bilinear expansion in the characteristic fields, $\underline{E}_n^{ext}(r,\theta,\phi)$.

If both the source and observer are at extreme distances from the scatterer,

$$(23)\quad \underline{E}(r^s,\theta^s,\phi^s;\ r^i,\theta^i,\phi^i) = -i\omega \frac{\omega^2\mu^2}{(4\pi)^2} \frac{e^{-ikr^i}}{r^i} \frac{e^{-ikr^s}}{r^s} \sum_{n=1}^{N} a_n \underline{F}_n(\theta^s,\phi^s)\ \underline{F}_n(\theta^s,\phi^s) \cdot \underline{p} \ .$$

If the source dipole is considered to cause an essentially plane wave in the vicinity of the obstacle, with unit electric field intensity of zero phase at the origin,

$$(24)\quad \frac{\omega^2\mu}{4\pi} \frac{e^{-ikr^i}}{r^i} \underline{p} = \hat{\xi}^i,$$

where $\hat{\xi}^i$ is polarization state vector of the plane wave. Hence,

$$(25)\quad \underline{E}(r^s,\theta^s,\phi^s;\theta^i,\phi^i) = + \frac{i\omega\mu}{4\pi} \frac{e^{-ikr^s}}{r^s} \sum_{n=1}^{N} a_n \underline{F}_n(\theta^s,\phi^s)\underline{F}_n(\theta^i,\phi^i) \cdot \hat{\xi}^i$$

$$= -\frac{i\omega\mu}{4\pi} \frac{e^{-ikr^s}}{r^s} \underline{F}(\theta^s,\phi^s;\theta^i,\phi^i) \cdot \hat{\xi}^i \ ,$$

where

$$(26) \qquad \underline{\underline{F}}(\theta^s,\phi^s;\theta^i,\phi^i) = -\sum_{n=1}^{N} a_n \underline{F}_n(\theta^s,\phi^s)\,\underline{F}_n(\theta^i,\phi^i),$$

is the dyadic pattern function represented as a bilinear expansion in the characteristic pattern functions, $\underline{F}_n(\theta,\phi)$.

Thus, in the bilinear or characteristic mode expansion we have a particularly compact formulation for bistatic-scattering from any loss-free obstacle (metallic, dielectric, or magnetic). With knowledge of the characteristic fields $\underline{E}_n^{ext}(r,\theta,\phi)$, or pattern functions $\underline{F}_n(\theta,\phi)$ on $\Sigma$, together with the characteristic values $a_n$ associated with the obstacle, it permits the evaluation of the scattered field in any direction due to a source near or far from the obstacle. In the next chapter we shall apply the bilinear expansion to express the scattered fields of several perfectly conducting obstacles.

## E. Summary

Summarizing the results of the previous sections, we find that an appropriate representation of the electromagnetic fields associated with a loss-free scatterer utilizes a special set of characteristic vector fields, determined uniquely by the scatterer shape and composition, together with the frequency. When the forms of the outgoing parts of each of these vector fields are known as a set of vector surface distributions, $\underline{F}_n(\theta,\phi)$ on the infinite sphere, $\Sigma$, surrounding the scatterer, together with an associated set of characteristic values

$a_n = |\cos \alpha_n| e^{i\alpha_n}$, where $\frac{\pi}{2} \leq \alpha_n \leq \frac{3\pi}{2}$, the scattering of plane waves arriving from arbitrary directions into arbitrary receiver directions may be evaluated concisely.

The determination of these characteristic fields and their characteristic values, $a_n$, is not a simple task, however. In the special case of a perfectly conducting scatterer, it has been inferred that a set of characteristic surface currents can be defined, together with their characteristic values, by certain cavity-mode properties of the associated fields within and on the mathematical surface defined by the scatterer. We shall later discuss the use of these defining properties to determine the characteristic modes in special cases.

It is appropriate at this point to consider the forms of the characteristic mode currents and fields on $\Sigma$ for special conducting scatterers, and illustrate the general bilinear formulation for bistatic scattering in each case.

# CHAPTER IV
# EXAMPLES OF CHARACTERISTIC MODES FOR PERFECTLY CONDUCTING OBSTACLES

## A. The Infinite Circular Cylinder

The problem of plane wave scattering by a perfectly conducting circular cylinder of infinite length viewed normal to its axis has a well-known solution in terms of cylindrical wave functions. In this section, the same problem will be discussed in terms of characteristic modes.

For normal incidence, the set of characteristic mode current densities on the surface of the cylinder have no variation along the cylinder axis and may be separated into TM and TE types. For a cylinder whose circumference in wavelengths is $ka$ (see Fig. 3), the characteristic mode current densities on S are:

TM Type:

$$\underline{J}_{e_n}^{(TM)}(\phi) = \hat{z}\,\frac{\sqrt{\varepsilon_n}}{2\pi a\, J_n(ka)} \begin{Bmatrix} \cos n\phi \\ \sin n\phi \end{Bmatrix} \cos \omega t, \tag{27}$$

TE Type:

$$\underline{J}_{e_n}^{(TE)}(\phi) = \hat{\phi}\,\frac{\sqrt{\varepsilon_n}}{2\pi a\, J_n'(ka)} \begin{Bmatrix} \cos n\phi \\ \sin n\phi \end{Bmatrix} \cos \omega t, \tag{28}$$

where

$\varepsilon_n = \begin{cases} 1, & n = 0 \\ 2, & n \neq 0 \end{cases}$ and $J_n(ka)$ is the $n^{th}$ order Bessel function and $J_n'(ka)$ is its derivative with respect to $k\rho$ evaluated at $\rho = a$.

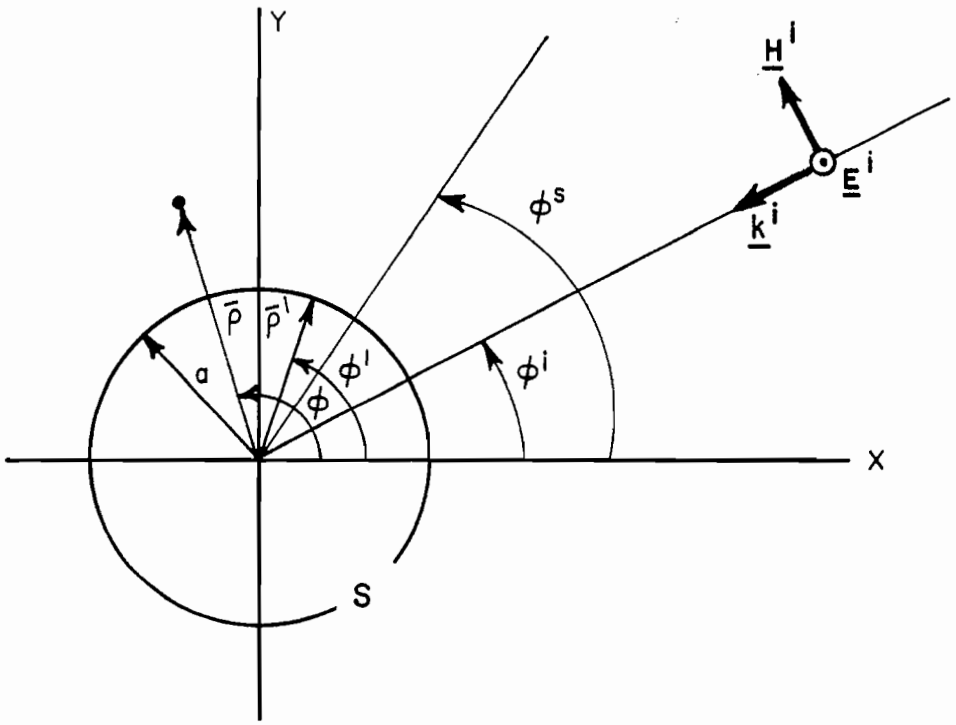


Fig. 3--Coordinate system for an infinite circular cylinder.

The characteristic fields radiated by these current densities at a large distance r are:

TM Type:

$$\underline{E}_{e_{o_n}}^{(TM)\ ext}(r,\phi) = -\sqrt{\frac{\omega\mu}{4}}\sqrt{\frac{2i}{\pi}}\ \frac{e^{-ik\rho}}{\sqrt{k\rho}}\ \underline{F}_{e_{o_n}}^{(TM)}(\phi)\ , \tag{29}$$

where

$$\underset{e}{F}_{o}^{(TM)}{}_{n}(\phi) = \hat{z}\sqrt{\varepsilon_n}\sqrt{\frac{\omega\mu}{4}}\,(i)^n \begin{matrix}\cos\\ \sin\end{matrix} n\phi \quad . \tag{30}$$

TE Type:

$$\underset{e}{E}_{o}^{(TM)ext}{}_{n}(r,\phi) = -\sqrt{\frac{\omega\mu}{4}}\sqrt{\frac{2i}{\pi}}\,\frac{e^{-ik\rho}}{\sqrt{k\rho}}\,\underset{e}{F}_{o}^{(TE)}{}_{n}(\phi), \tag{31}$$

where

$$\underset{e}{F}_{o}^{(TE)}{}_{n}(\phi) = \hat{\phi}\sqrt{\varepsilon_n}\sqrt{\frac{\omega\mu}{4}}\,i(i)^n \begin{matrix}\cos\\ \sin\end{matrix} n\phi \, . \tag{32}$$

The characteristic fields produced by these current densities interior to the cylinder of radius a are:

TM Type:

$$\underset{e}{E}_{o}^{(TM)int}{}_{n}(r,\phi) = \hat{z}\sqrt{\varepsilon_n}\,\frac{1}{a_n^{(TM)}}\,J_n(k\rho) \begin{matrix}\cos\\ \sin\end{matrix} n\phi \, . \tag{33}$$

TE Type:

$$\underset{e}{E}_{o}^{(TE)int}{}_{n}(r,\phi) = \hat{\phi}\sqrt{\varepsilon_n}\,\frac{1}{a_n^{(TE)}}\,J_n'(k\rho) \begin{matrix}\cos\\ \sin\end{matrix} n\phi \quad . \tag{34}$$

The symmetry of the circular cylinder causes a 2-fold degeneracy in the characteristic values, $a_n^{(TM)}$ and $a_n^{(TE)}$. These values are

$$a_n^{(TM)} = -\frac{J_n(ka)}{H_n^{(2)}(ka)} = |\cos\alpha_n^{(TM)}|\, e^{i\alpha_n^{(TM)}} \quad , \tag{35}$$

where

$$(36) \qquad \alpha_n^{(TM)} = \tan^{-1}\left\{-\frac{N_n(ka)}{J_n(ka)}\right\} \quad , \quad \frac{\pi}{2} \leq \alpha_n^{(TM)} \leq \frac{3\pi}{2} \quad ,$$

and

$$(37) \qquad a_n^{(TE)} = -\frac{[J_n(ka)]'}{[H_n^{(2)}(ka)]'} = |\cos \alpha_n^{(TE)}| \, e^{i\alpha_n^{(TE)}} \quad ,$$

where

$$(38) \qquad \alpha_n^{(TE)} = \tan^{-1}\left\{-\frac{[N_n(ka)]'}{[J_n(ka)]'}\right\} \quad , \quad \frac{\pi}{2} \leq \alpha_n^{(TE)} \leq \frac{3\pi}{2} \quad .$$

The bilinear expansion leads to the following expression for the $\hat{z}$ and $\hat{\phi}$ components of the far-zone scattered field observed in the direction, $\phi^s$, where a plane wave of polarization $\hat{\xi}^i = \cos \alpha \, \hat{z} + \sin \alpha \, \hat{\phi}$ is normally incident upon the cylinder from the direction $\phi^i$.

$$(39) \qquad \underline{E}(\rho, \phi^s; \phi^i) = -\sqrt{\frac{2i}{\pi}} \, \frac{e^{-ik\rho}}{\sqrt{k\rho}} \, \underline{\underline{F}}(\phi^s; \phi^i) \cdot \hat{\xi} \quad ,$$

where the dyadic pattern function is

$$(40) \qquad \underline{\underline{F}}(\phi^s; \phi^i) = -\sum_{n=0}^{N} a_n^{(TM)} \left[ \underline{F}_{en}^{(TM)}(\phi^s) \, \underline{F}_{en}^{(TM)}(\phi^i) + \underline{F}_{on}^{(TM)}(\phi^s) \, \underline{F}_{on}^{(TM)}(\phi^i) \right] - \sum_{n=0}^{N} a_n^{(TE)} \left[ \underline{F}_{en}^{(TE)}(\phi^s) \, \underline{F}_{en}^{(TE)}(\phi^i) + \underline{F}_{on}^{(TE)}(\phi^s) \, F_{on}^{(TE)}(\phi^i) \right] .$$

There are only a finite number of characteristic values, $a_n$, of magnitude significant enough to be included in the bilinear expansion for $\underline{E}$. The number that must be used, however, increases with the value of ka so that the characteristic mode expansion is most useful when ka does not exceed 10 or 20.

For cylinders of noncircular cross section, the trigonomentric functions no longer form characteristic modes. In these cases, the modes are unknown, except for the perfectly conducting elliptic cylinder where they take the form of Mathieu functions.[23]

B. The Sphere

As another illustration of characteristic modes, consider their application to the spherically symmetric scatterer. This classical obstacle has been investigated by many authors under a variety of exciting conditions. Of particular interest here is the illumination of a sphere by an arbitrarily located and oriented electric dipole,[24][25] or, more specially, such a dipole removed to an extreme distance from the sphere (plane wave excitation)[26][27][28] Conventional techniques fall into two categories: the use of vector and scalar potentials[29][30], and the use of a dyadic Green's function[31]. Results obtained by the latter formalism resemble in form those described here from the characteristic mode approach. A discussion of the spherical scatterer in terms of the scattering matrix appears in Newton[32].

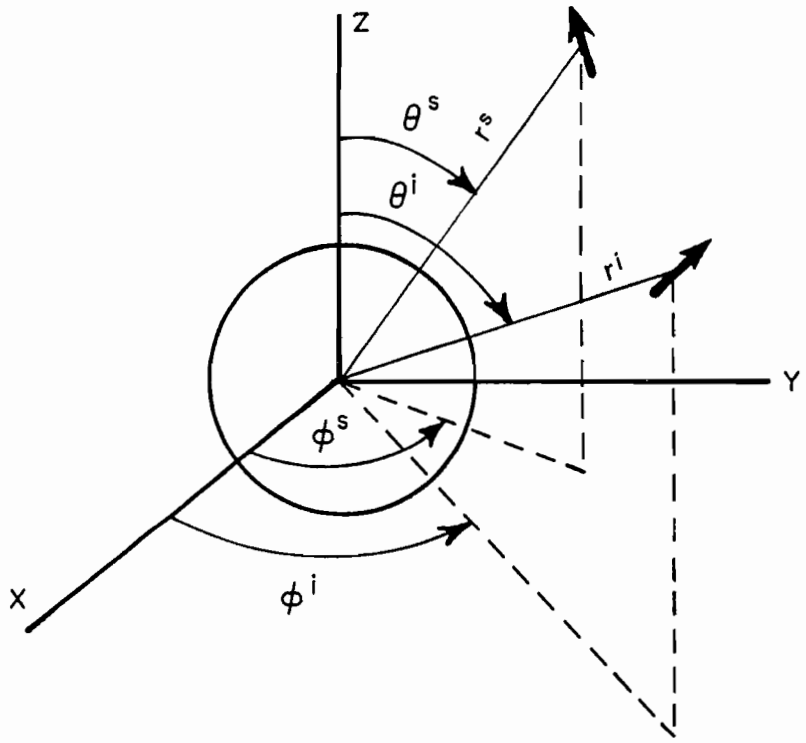


Fig. 4--Coordinate system for a sphere.

Referring to Fig. 4, the characteristic current densities and fields are described in a spherical coordinate system centered at the sphere. The sphere circumference in wavelengths is ka. The characteristic mode current densities and fields are separated into TM and TE types, with an "e" and "o" degeneracy similar to that encountered in the circular cylinder. The current densities, normalized to radiate unit power, are:

TM Type:

$$(41)\qquad \underset{e_{omn}}{J}^{(TM)}(a,\theta,\phi) = \frac{1}{k\sqrt{Z_o}}\ \frac{1}{a^2[kaj_n(ka)]'}\sqrt{\frac{\varepsilon_m}{4\pi}\ \frac{2n+1}{n(n+1)}\ \frac{(n-m)!}{(n+m)!}}\ \times$$

$$\left\{\frac{\partial P_n^m(\cos\theta)}{\partial\theta}\ \begin{matrix}\cos\\ \sin\end{matrix}\ m\phi\ \hat{\theta} \mp m\ \frac{P_n^m(\cos\theta)}{\sin\theta}\ \begin{matrix}\sin\\ \cos\end{matrix}\ m\phi\hat{\phi}\right\}.$$

TE Type:

$$(42)\qquad \underset{e_{omn}}{J}^{(TE)}(a,\theta,\phi) = \frac{1}{k\sqrt{Z_o}}\ \frac{1}{a^2 j_n(ka)}\sqrt{\frac{\varepsilon_m}{4\pi}\ \frac{2n+1}{n(n+1)}\ \frac{(n-m)!}{(n+m)!}}\ \times$$

$$\left\{\mp m\ \frac{P_n^m(\cos\theta)}{\sin\theta}\ \begin{matrix}\sin\\ \cos\end{matrix}\ m\phi\ \hat{\theta} - \frac{\partial P_n^m(\cos\theta)}{\partial\theta}\ \begin{matrix}\cos\\ \sin\end{matrix}\ m\phi\ \hat{\phi}\right\}.$$

The characteristic fields radiated by these current densities at large distance r are:

TM Type:

$$(43)\qquad \underset{e_{omn}}{E}^{(TM)ext}(r,\theta,\phi) = -\frac{i\omega\mu}{4\pi}\ \frac{e^{-ikr}}{r}\ \underset{e_{omn}}{F}^{(TM)}(\theta,\phi)\ ,$$

where

$$(44)\qquad \underset{e_{omn}}{F}^{(TM)}(\theta,\phi) = \frac{-4\pi}{k\sqrt{Z_o}}\ i(i)^n\sqrt{\frac{\varepsilon_m}{4\pi}\ \frac{2n+1}{n(n+1)}\ \frac{(n-m)!}{(n-m)!}}\ \times$$

$$\left\{\frac{\partial P_n^m(\cos\theta)}{\partial\theta}\ \begin{matrix}\cos\\ \sin\end{matrix}\ m\phi\ \hat{\theta}\ \mp m\ \frac{P_n^m(\cos\theta)}{\sin\theta}\ \begin{matrix}\sin\\ \cos\end{matrix}\ m\phi\ \hat{\phi}\right\}.$$

TE Type:

$$(45)\qquad \underline{E}_{\substack{e\\o}mn}^{(TE)ext}(r,\theta,\phi) = -\frac{i\omega\mu}{4\pi}\frac{e^{-ikr}}{r}\underline{F}_{\substack{e\\o}mn}^{(TE)}(\theta,\phi),$$

where

$$(46)\qquad \underline{F}_{\substack{e\\o}mn}^{(TE)}(\theta,\phi) = \frac{4\pi}{k\sqrt{Z_o}}(i)^n\sqrt{\frac{\varepsilon_m}{4\pi}\frac{2n+1}{n(n+1)}\frac{(n-m)!}{(n+m)!}}\times$$

$$\left\{\mp m\frac{P_n^m(\cos\theta)}{\sin\theta}\begin{matrix}\sin\\\cos\end{matrix} m\phi\,\hat{\theta} - \frac{\partial P_n^m(\cos\theta)}{\partial\theta}\begin{matrix}\cos\\\sin\end{matrix} m\phi\,\hat{\phi}\right\}.$$

The characteristic fields produced by these current densities interior to the sphere of radius a are:

$$(47)\qquad \underline{E}_{\substack{e\\o}mn}^{(TM)int}(r,\theta,\phi) = \frac{k\sqrt{Z_o}}{a_n^{(TM)}}\sqrt{\frac{\varepsilon_m}{4\pi}\frac{2n+1}{n(n+1)}\frac{(n-m)!}{(n+m)!}}\,[krj_n(kr)]'\times$$

$$\left\{\frac{\partial P_n^m(\cos\theta)}{\partial\theta}\begin{matrix}\cos\\\sin\end{matrix} m\phi\,\hat{\theta} \mp m\frac{P_n^m(\cos\theta)}{\sin\theta}\begin{matrix}\sin\\\cos\end{matrix} m\phi\,\hat{\phi}\right\}.$$

TE Type:

$$(48)\qquad \underline{E}_{\substack{e\\o}mn}^{(TE)int}(r,\theta,\phi) = \frac{k\sqrt{Z_o}}{a_n^{(TE)}}\sqrt{\frac{\varepsilon_m}{4\pi}\frac{2n+1}{n(n+1)}\frac{(n-m)!}{(n+m)!}}\,j_n(ka)\times$$

$$\left\{\mp m\frac{P_n^m(\cos\theta)}{\sin\theta}\begin{matrix}\sin\\\cos\end{matrix} m\phi\,\hat{\theta} - \frac{\partial P_n^m(\cos\theta)}{\partial\theta}\begin{matrix}\cos\\\sin\end{matrix} m\phi\,\hat{\phi}\right\}.$$

All the above currents and fields are defined for $m \leq n$, $n \geq 1$. The high order of symmetry present in the sphere produces a $(2n+1)$-fold degeneracy in the characteristic values, $a_n^{(TM)}$ and $a_n^{(TE)}$, which

depend only upon the index n and the TM or TE type. These values are

$$(49) \qquad a_n^{(TM)} = -\frac{[ka\, j_n(ka)]'}{[ka\, h_n^{(2)}(ka)]'} = |\cos \alpha_n^{(TM)}|\, e^{i\alpha_n^{(TM)}} ,$$

where

$$(50) \qquad \alpha_n^{(TM)} = \tan^{-1}\left\{ \frac{[ka\, n_n(ka)]'}{[ka\, j_n(ka)]'} \right\} , \quad \frac{\pi}{2} \leq \alpha_n^{(TM)} \leq \frac{3\pi}{2} ,$$

and

$$(51) \qquad a_n^{(TE)} = -\frac{j_n(ka)}{h_n^{(2)}(ka)} = |\cos \alpha_n^{(TE)}|\, e^{i\alpha_n^{(TE)}} ,$$

where

$$(52) \qquad \alpha_n^{(TE)} = \tan^{-1}\left\{ -\frac{n_n(ka)}{j_n(ka)} \right\} , \quad \frac{\pi}{2} \leq \alpha_n^{(TE)} \leq \frac{3\pi}{2} .$$

The bilinear expansion leads to the following expression for the $\hat{\theta}$ and $\hat{\phi}$ components of the scattered field observed at a large distance in the direction $(\theta^s,\phi^s)$ when a plane wave of polarization $\hat{\xi}^i = \cos\alpha\hat{\theta} + \sin\alpha\hat{\phi}$ is incident upon the sphere from the direction $(\theta^i,\phi^i)$:

$$(53) \qquad \underline{E}(r^s,\theta^s,\phi^s;\theta^i,\phi^i) = -\frac{i\omega\mu}{4\pi}\,\frac{e^{-ikr^s}}{r^s}\,\underline{\underline{F}}(\theta^s,\phi^s;\theta^i\phi^i)\cdot\hat{\xi}^i ,$$

where the dyadic pattern function is

$$(54)\qquad \underline{\underline{F}}(\theta^s,\phi^s;\theta^i,\phi^i) = -\sum_{n=1}^{N} a_n^{(TM)}\left[\sum_{m=0}^{N} \underline{\underline{F}}_{emn}^{(TM)}(\theta^s,\phi^s)\underline{\underline{F}}_{emn}^{(TM)}(\theta^i,\phi^i) + \sum_{m=0}^{n} \underline{\underline{F}}_{omn}^{(TM)}(\theta^s,\phi^s)\,\underline{\underline{F}}_{omn}^{(TM)}(\theta^i,\phi^i)\right] -$$

$$\sum_{n=1}^{N} a_n^{(TE)}\left[\sum_{m=0}^{n} \underline{\underline{F}}_{emn}^{(TE)}(\theta^s,\phi^s)\,\underline{\underline{F}}_{emn}^{(TE)}(\theta^i,\phi^i) + \sum_{m=0}^{n} \underline{\underline{F}}_{omn}^{(TE)}(\theta^s,\phi^s)\,\underline{\underline{F}}_{omn}^{(TE)}(\theta^i,\phi^i)\right] .$$

This is the most general form of the characteristic mode expansion for arbitrary directions and polarizations of source and receiver. It is simplified considerably without significant loss of generality by restricting the direction of incidence of the plane wave to the polar axis ($\theta^i = \pi$), in which case the finite sums on the index m reduce to a single term each, for m = 1. The number of terms needed in the characteristic mode expansion increases with ka so that it is of greatest utility when ka does not exceed 10 or 20.

## C. An Array of Infinitely Long, Thin Parallel Wires

Consider a scatterer whose perturbation operator $P$ is *a priori* known to be well approximated by a degenerate or finite dimensional operator. Such a scatterer might consist of an ensemble of N scatterers each of which supports a current distribution of fixed form but variable magnitude, under plane wave excitations. One example is an ensemble of short, thin conducting filaments arrayed in a

specified fashion throughout or on the surface of a given volume of space. If crossed filament pairs are arrayed to outline a closed surface, a quantized model of an arbitrary shape can be envisioned which may approximate the continuous closed surface in some sense. The far field patterns associated with such a scatterer ensemble are functions of $\theta$ and $\phi$ on $\Sigma$ and in general possess both $\theta$ and $\phi$ directed vector components. In order not to obscure the characteristic mode formulation with a vector formalism, we shall consider the simpler two dimensional analogue of the foregoing ensemble scatterer -- an array of N infinitely long, parallel wires, each of which is electrically thin under TM plane wave excitation. The far fields are functions only of $\phi$ and are longitudinally directed, implying an effectively scalar problem. Such wires arrayed around a closed contour have been used as an electrical model of a smooth conducting cylinder of the same contour.[33]

Consider the N-wire array sketched in Fig. 5, where the location of the $p^{th}$ wire is given in polar coordinates by $(\rho_p,\phi_p)$ and the radii of all the wires are assumed to be equal to b, where $b << \lambda$. (Wires of differing radii can be treated in the same manner so long as they are all small in terms of wavelength.) Because they are thin, the current density is assumed to be uniform around the surface of each wire such that the current flowing on the $p^{th}$ wire is given by $J_p$. With a specified ordering of the wires, a set of currents on the wires can be represented by an N component vector, (J) whose $p^{th}$ component is the current, $J_p$,

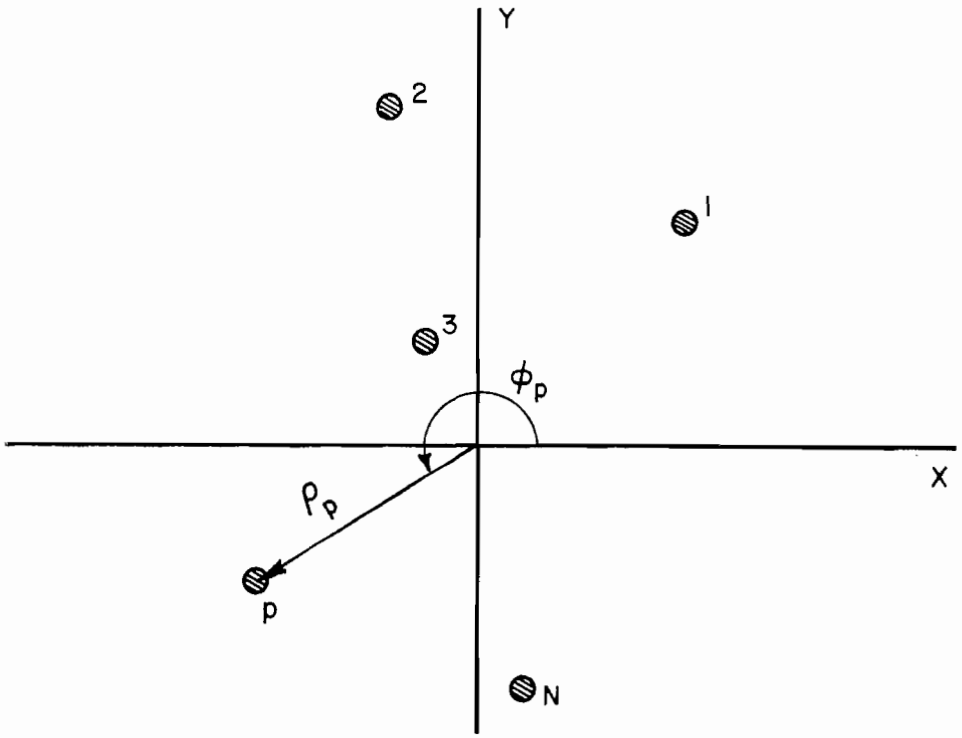


Fig. 5--Geometry associated with scattering by an array of infinitely long wires.

on wire "p". The field radiated by such an arbitrary set of currents (J), evaluated at position $\bar{\rho}$, is given by

$$\hat{z}E(\bar{\rho}) = -\hat{z}\frac{\omega\mu}{4}\sum_{n=1}^{N} H_o^{(2)}(k|\bar{\rho}_p - \bar{\rho}|)\, J_p. \tag{55}$$

If this field is evaluated at the center of the $q^{th}$ wire, Eq. (55) becomes

$$E(\bar{\rho}_q) = -\frac{\omega\mu}{4}\sum_{p=1}^{N} H_o^{(2)}(k|\bar{\rho}_p - \bar{\rho}_q|)\, J_p, \tag{56}$$

or, in matrix notation,

$$(57) \qquad (E) = -\frac{\omega\mu}{4}\left[ H_o^{(2)}(k|\bar{\rho}_p - \bar{\rho}_q|)\right] (J),$$

$$= [Z] (J).$$

The quantity $|\bar{\rho}_p - \bar{\rho}_q|$ is the distance between the $p^{th}$ and $q^{th}$ wire centers and $|\bar{\rho}_p - \bar{\rho}_p| \equiv b$ by definition.

Thus, an $N \times N$ matrix, $[Z]$, whose elements have been defined, relates the current vector (J) for N filamentary currents to the electric field intensity vector these produce at the centers of the N wires. From our previous observations regarding characteristic current distributions of a perfectly conducting object, we would expect in this case to define N real characteristic current vectors, $(J_n)$, by the requirement that the associated electric field intensity vector, $(E_n)$, must have equiphase components. That is, the characteristic current vectors would satisfy,

$$(58) \qquad \lambda_n [R] (J_n) = [X] \ (J_n),$$

where

$$(59) \qquad [R] = \text{Re } [Z] = \frac{1}{2} \{[Z] + [Z]^c\} ,$$

and

$$(60) \qquad [X] = \text{Im } [Z] = -\frac{i}{2} \{[Z] - [Z]^c\} .$$

There should exist N real values, $\lambda_n$, in general, related to the characteristic phases, $\alpha_n$, between the currents and the fields they produce, where

(61) $$\alpha_n = \tan^{-1}(-\lambda_n),\ \frac{\pi}{2} \leq \alpha_n \leq \frac{3\pi}{2}$$ .

We shall show that this can be done, and that corresponding to each characteristic current vector ($J_n$), there is a normalized far field radiation pattern, $F_n(\phi)$ which it produces. These characteristic mode patterns, in a manner completely analogous to that shown earlier for TM excitation of a circular cylinder, may be used to obtain the scattered field intensity. Thus, the field scattered in a direction $\phi^s$, produced by a plane wave incident from $\phi^i$, is given by

(62) $$\underline{E}(\phi^i,\phi^s) = +\hat{z}\sqrt{\frac{2i}{\pi}}\frac{e^{-ik\rho}}{\sqrt{k\rho}}\sum_{n=1}^{N}|\cos\alpha_n|e^{i\alpha_n}F_n(\phi^i)F_n(\phi^s).$$

To prove the foregoing statements, let us return to the [Z] matrix of the array. We see that the $\lambda_n$ are solutions of the determinantal equation,

(63) $$\det[X - \lambda R] = 0,$$

or

(64) $$\det[x_{ij} - \lambda r_{ij}] = 0,$$

where the elements of [X] are $x_{ij} = +\frac{\omega\mu}{4}N_o(k|\bar{\rho}_i-\bar{\rho}_j|) = x_{ji}$ and the elements of [R] are $r_{ij} = -\frac{\omega\mu}{4}J_o(k|\bar{\rho}_i-\bar{\rho}_j|) = r_{ji}$. Since [X] and [R] are symmetric matrices, the solutions, $\lambda_n$, of the determinantal equation must be real.[34] The associated characteristic current vectors ($J_n$) are then easily found from the defining Eq. (58).

At this point, let us digress for a brief observation. Given a set of N radiating current filaments (J) and along these filaments an impressed electric field intensity (E), the complex power input per unit length is

$$(65) \qquad P = -(J)^{ct}\,(E) = -\sum_{j=1}^{N} E_j\, J_j^c \,.$$

The real part of P measures the radiated power per unit length of the array and the imaginary part measures the $2\omega$ times the net average reactive power per unit length associated with near-field energy storage. Using the $[Z]$ matrix of the array and assuming that the currents are real, we can express P compactly as,

$$(66) \qquad P = -(J)^{t}\,[Z]\,(J),$$

and

$$(67) \qquad Re\{P\} = -(J)^{t}\,[R]\,(J),$$

$$(68) \qquad IM\{P\} = -(J)^{t}\,[X]\,(J).$$

The ratio of the reactive and radiated powers is

$$(69) \qquad \frac{Im\{P\}}{Re\{P\}} = \frac{(J)^{t}\,[X]\,(J)}{(J)^{t}\,[R]\,(J)} \,,$$

which is a ratio of real, symmetric quadratic forms. Since the quadratic form in the denominator represents power radiated it is negative semi-definite at least. Furthermore, since the set of N

wires does not form a closed interior region which can support resonant cavity fields, there is no non-zero current set of the assumed type which radiates zero power, implying that the denominator quadratic form is negative definite. With these facts established, theorems concerning the extremal properties of the ratio may be stated.[34]

(1) The extrema of the ratio

$$\frac{(J)^t[X](J)}{(J)^t[R](J)}$$

are associated with the roots of the determinantal equation $\det[X - \lambda R] = 0$. These roots are real and may be arranged in non-descending order according to their absolute values, $\lambda_1, \lambda_2, \cdots \lambda_N$, where $|\lambda_j| \leq |\lambda_{j+1}|$.

(2) The maximum ratio of radiated to net reactive power for real currents is equal to $1/|\lambda_1|$, and the current $(J_1)$ associated with this value satisfies $\lambda_1[R](J_1) = [X](J_1)$, i.e., it is a characteristic current vector of the array with a phase shift $\alpha_1 = \tan^{-1}(-\lambda_1)$.

(3) The minimum ratio of radiated to reactive power for real currents is equal to $1/|\lambda_N|$, and the current $(J_N)$ associated with this value satisfies $\lambda_N[R](J_N) = [X](J_N)$, i.e., it is a characteristic current vector of the array with a phase shift $\alpha_N = \tan^{-1}(-\lambda_N)$.

(4) The N real characteristic vectors $(J_n)$ associated with the $\lambda_n$ form the columns of a matrix $[J]$ such that $[J]^t\,[R][J]$ and $[J]^t\,[X][J]$ both are diagonal matrices. Further, when the vectors $(J_n)$ are normalized, each radiates unit power per unit length of the array,

$$[J]^t\,[R][J] = -\,[I]\ , \tag{70}$$

and

$$[J]^t\,[X][J] = -[\Lambda]\ , \tag{71}$$

where

$$[I] = \begin{bmatrix} 1 & & 0 \\ & 1 & \\ & \ddots & \\ 0 & & 1 \end{bmatrix}\ , \tag{72}$$

and

$$[\Lambda] = \begin{bmatrix} \lambda_1 & & 0 \\ & \lambda_2 & \\ & \ddots & \\ 0 & & \lambda_N \end{bmatrix}\ . \tag{73}$$

While the characteristic mode current vectors $(J_n)$ do not, in general, form an orthonormal set (nor do the associated field intensity vectors, $(E_n)$, where $(E_n) = [Z]\,(J_n)$ , they satisfy the orthogonality property,

(74) $$(J_k)^t (E_1) = 0, \; k \neq 1 \quad ,$$

and

(75) $$(J_k)^t (E_k) = - \{1 + i\lambda_k\} \quad .$$

This orthogonality property ensures that the complex power associated with an excitation of the array of filamentary sources is equal to the sum of the complex powers associated with each of the characteristic mode excitations, when these are known.

Another important use of this orthogonality property arises when decomposing a given excitation into its characteristic mode components. Thus, if an incident TM field produces an excitation (E) on the set of wires, we may wish to express this as a weighted sum of the characteristic field vectors, $(E_k)$; that is,

(76) $$(E) = \sum_{k=1}^{N} A_k (E_k).$$

Since the $(E_k)$ are not orthogonal, the usual technique for obtaining the $A_k$ does not apply. However, if both sides of the equations are multiplied by $(J_n)^t$ (inner product operation),

(77) $$(J_n)^t (E) = \sum_{n=1}^{N} A_k (J_n)^t (E_k) = - A_n(1 + i\lambda_n),$$

whence

(78) $$A_n = - \frac{1}{1 + i\lambda_n} (J_n)^t (E).$$

Returning to the development of the bilinear expansion formula for bistatic scattering by the wire array, we define the far field characteristic radiated fields, $\underline{E}_n(\rho,\phi)$, by

$$(79) \qquad \underline{E}_n(\rho,\phi) = \lim_{\rho\to\infty} \; -\hat{z}\,\frac{\omega\mu}{4} \sum_{p=1}^{N} H_o^{(2)}(k|\bar{\rho}_p-\bar{\rho}|)\, J_{pn},$$

$$= -\hat{z}\sqrt{\frac{\omega\mu}{4}}\,\sqrt{\frac{2i}{\pi}}\,\frac{e^{-ik\rho}}{\sqrt{k\rho}}\,F_n(\phi),$$

where the $n^{th}$ characteristic pattern function is

$$(80) \qquad F_n(\phi) = \sqrt{\frac{\omega\mu}{4}} \sum_{p=1}^{N} J_{pn}\, e^{ik\rho_p \cos(\phi-\phi_p)},$$

and $J_{pn}$ is the current on the $p^{th}$ wire in the $n^{th}$ characteristic mode $(J_n)$.

Next, assume that the exciting field is that of a plane wave incident upon the array from a direction $\phi^i$ and represented by the vector $(E^i(\phi^i))$. We assume that the strength of this incident plane wave is normalized to unit incident field intensity at each wire. As indicated previously, we can determine the strengths of the induced characteristic currents by expanding $(E^i(\phi^i))$ in terms of the $(E_n)$, utilizing the inner product operation. That is,

$$(81) \qquad (E^i(\phi^i)) = \sum_{n=1}^{N} A_n(\phi^i)(E_n),$$

where

$$(82) \qquad A_n(\phi^i) = - \frac{1}{1 + i\lambda_n} (J_n)^t \, (E_n^i(\phi^i)).$$

The field scattered into a direction $\phi^s$ at a great distance is

$$(83) \qquad \underline{E}(\phi^i,\phi^s) = -\hat{z}\sqrt{\frac{\omega\mu}{4}}\sqrt{\frac{2i}{\pi}} \, \frac{e^{-ik\rho}}{\sqrt{k\rho}} \sum_{n=1}^{N} A_n(\phi^i) \cdot F_n(\phi^s).$$

Furthermore, since $(J_n)^t(E^i(\phi^i))$ measures the reaction between the unit plane wave source and the $n^{th}$ characteristic mode current, we can say

$$(84) \qquad \sqrt{\frac{\omega\mu}{4}} \, (J_n)^t \, (E^i(\phi^i)) = - F_n(\phi^i),$$

whereupon

$$(85) \qquad A_n(\phi^i) = + \frac{1}{1 + i\lambda_n} \sqrt{\frac{4}{\omega\mu}} \, F_n(\phi^i)$$

$$= - \sqrt{\frac{4}{\omega\mu}} \, a_n \, F_n(\phi^i),$$

and the expression for the scattered field becomes

$$(86) \qquad \underline{E}(\phi^i,\phi^s) = \hat{z} \sqrt{\frac{2i}{\pi}} \, \frac{e^{-ik\rho}}{\sqrt{k\rho}} \sum_{n=1}^{N} a_n \, F_n(\phi^i) \, F_n \, (\phi^s),$$

$$= \hat{z}\sqrt{\frac{2i}{\pi}} \, \frac{e^{-ik\rho}}{\sqrt{k\rho}} \sum_{n=1}^{N} |\cos \alpha_n| e^{i\alpha_n} \, F_n(\phi^i) \, F_n(\phi^s).$$

In the examples to follow, the quantity,

$$F(\phi^i,\phi^s) = - \sum_{n=1}^{N} a_n \, F_n(\phi^i) \, F_n(\phi^s),$$

is called the scattering pattern, so that

$$E(\phi^i,\phi^s) = -\hat{z}\sqrt{\frac{2i}{\pi}}\frac{e^{-ik\rho}}{\sqrt{k\rho}}\,F(\phi^i,\phi^s). \tag{87}$$

As in the previous examples,

$$a_n = -\frac{1}{1+i\lambda_n}\ , \tag{88}$$

and

$$s_n = 2a_n + 1 = \frac{1-\left(\frac{1}{i\lambda_n}\right)}{1+\left(\frac{1}{i\lambda_n}\right)}\ , \tag{89}$$

which are interrelated by the Smith chart constructions of Figs. 1 and 2.

We might point out that, although Eqs. (86) or (87) have been specialized to the case where source and receiver are distant from the array, it is possible to obtain a bilinear form similar to Eq. (22) for z-independent line sources near the array by applying reaction between the source and the characteristic mode field intensities.

The total power scattered per unit length of array is

$$P_T(\phi^i) = \frac{1}{Z_o}\int_0^{2\pi} |E(\phi^i,\phi^s)|^2\,\rho\,d\phi^s, \tag{90}$$

$$= \frac{4}{kZ_o}\sum_{n=1}^{N} |a_n|^2\,|F_n(\phi^i)|^2\ .$$

The average total power scattered per unit length of array is

$$(91) \qquad \hat{P}_T = \frac{1}{2\pi} \int_0^{2\pi} P_T(\phi^i)\, d\phi^i = \frac{4}{kZ_o} \sum_{n=1}^{N} |a_n|^2 ,$$

assuming the incident plane wave is of unit electric field intensity. These results are consistent with the total scattering cross section theorem.[35][36]

Assuming an incident plane wave of unit electric field intensity, average backscattered power per unit length of array is

$$(92) \qquad \hat{P}_{B.S.} = \frac{1}{2\pi} \frac{1}{Z_o} \int_0^{2\pi} |E(\phi,\phi)|^2 \rho\, d\phi ,$$

$$= \frac{1}{\pi^2} \frac{1}{kZ_o} \sum_{n=1}^{N} \sum_{m=1}^{N} a_n a_m^c \int_0^{2\pi} [F_n(\phi)\, F_m^c(\phi)]^2\, d\phi .$$

If the integrals in the above equation form the elements $\hat{p}_{mn} = \hat{p}_{nm}^c$ of an Hermitian symmetric matrix $[\hat{P}]$, and the $a_n$ are the components of an N-dimensional column vector, (a), then in matrix notation

$$(93) \qquad P_{B.S.} = \frac{1}{\pi^2} \frac{1}{kZ_o} (a)^{ct} [\hat{P}] (a).$$

As an example, consider scattering by the array of three wires sketched in Fig. 6. The wire circumferences in wavelengths are kb = 0.3 and their locations are given in Table I.

TABLE I

Wire Locations - 3 Wire Array

| Wire No. | kx | ky |
|---|---|---|
| 1 | 3.0 | 0.0 |
| 2 | 0.0 | 3.0 |
| 3 | -3.0 | 0.0 |

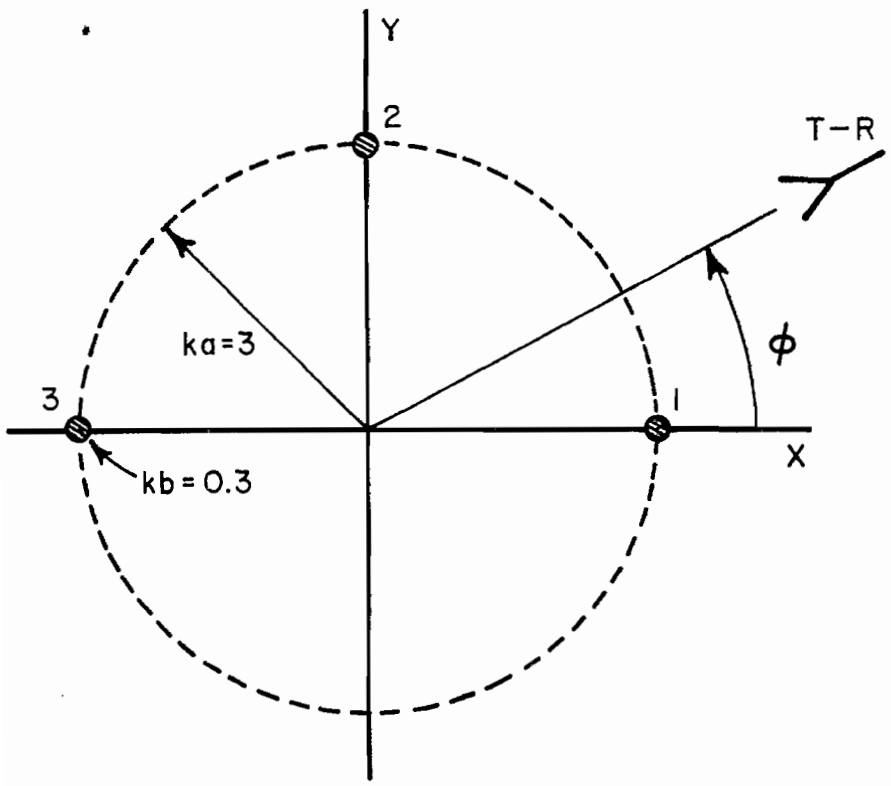


Fig. 6--An example of a 3-wire array.

The roots, $\lambda_n$, of the equation, $\det[X-\lambda R] = 0$ and the angles, $\alpha_n$, and coefficients, $a_n$, are given in Table II.

TABLE II

Values of $\lambda_n$, $\alpha_n$ and $|a_n|$ for 3 Wire Array

| Mode No. | $\lambda_n$ | $\alpha_n = \tan^{-1}(-\lambda_n)$ | $\lvert a_n\rvert = \lvert\cos \alpha_n\rvert$ |
|---|---|---|---|
| 1 | 0.4968 | $153.7^{o}$ | 0.896 |
| 2 | 0.6278 | $147.9^{o}$ | 0.846 |
| 3 | 2.090 | $115.6^{o}$ | 0.432 |

The coefficients $a_n$ have been plotted in the complex plane in Fig. 7.

The characteristic currents $(J_n)$, normalized such that $(J_m)^t\left[\frac{-4}{\omega\mu} R\right] (J_n) = \delta_{mn}$, are given in Table III.

TABLE III

Characteristic Currents for 3 Wire Array

| Mode No. | 1 | 2 | 3 |
|---|---|---|---|
| Wire No. | | | |
| 1 | 0.348981 | -0.777566 | 0.684139 |
| 2 | -0.636539 | 0.0 | 0.977887 |
| 3 | 0.348981 | 0.777566 | 0.684139 |

The characteristic fields $(E_n)$ produced on the axes of the respective wires by the $(J_n)$ of Table III are given in Table IV.

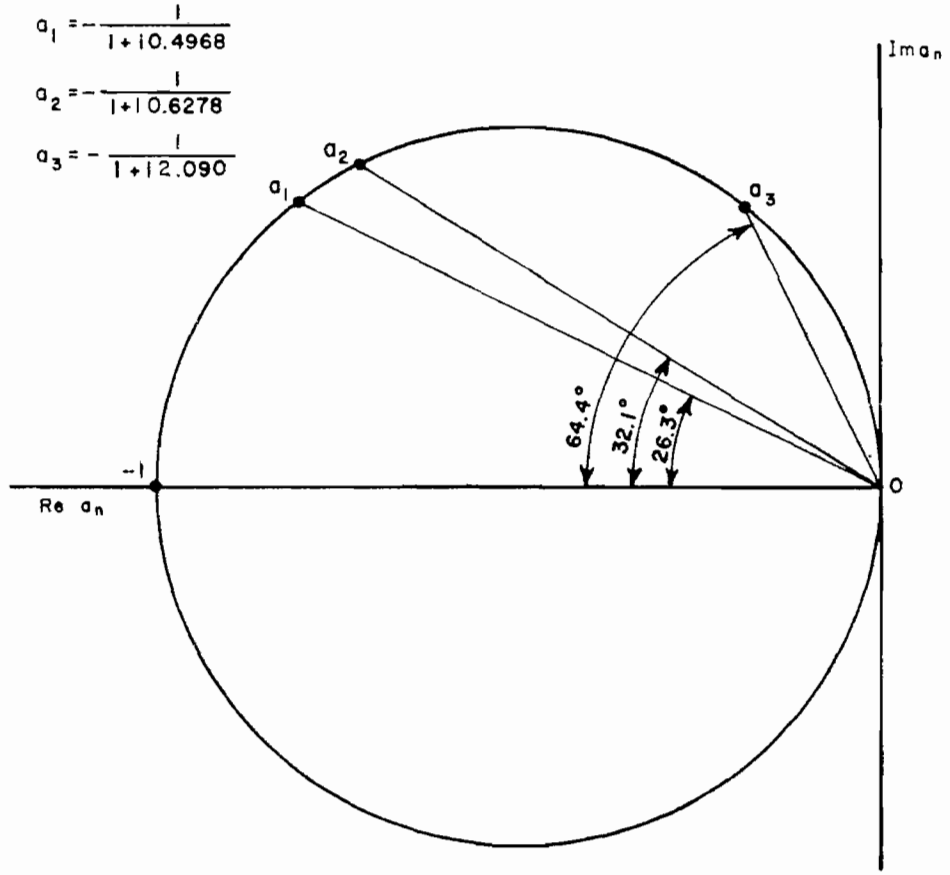


Fig. 7--The coefficients $a_n$ for the 3-wire array.

TABLE IV

Characteristic Fields for 3 Wire Array

| Mode No. | 1 | 2 | 3 |
|---|---|---|---|
| Wire No. | | | |
| 1 | -0.629478 -i0.312740 | 0.643032 +i0.403618 | -0.409748 -i0.856310 |
| 2 | 0.880777 +i0.437591 | 0 + i0 | -0.449287 -i0.938941 |
| 3 | -0.629478 -i0.312740 | -0.643032 -i0.403618 | -0.409748 -i0.856310 |

Note that the ratio of the imaginary to the real parts of each component of $(E_n)$ is equal to $\lambda_n$.

The far field modal patterns, $F_n(\phi)$, are plotted in Figs. 8, 9, and 10. The sum of their squares, weighted by the coefficients $a_n$ yields the far field backscattering pattern shown in Fig. 11. The pattern in Fig. 11 agrees with that arrived at by the method of Richmond. [33]

It is instructive to compare the 3 wire array described by the [Z] matrix to the hypothetical case of the same three wires without mutual coupling. In this latter case, the [Z] matrix is diagonal, its elements each equal to $-\frac{\omega\mu}{4} H_o^{(2)}(kb)$. Accordingly, for this example, kb = 0.3,

$$(94) \qquad a_1 = a_2 = a_3 = -\frac{1}{1 - i\frac{N_o(0.3)}{J_o(0.3)}} ,$$

$$= 0.77\, e^{i140.5^o}$$

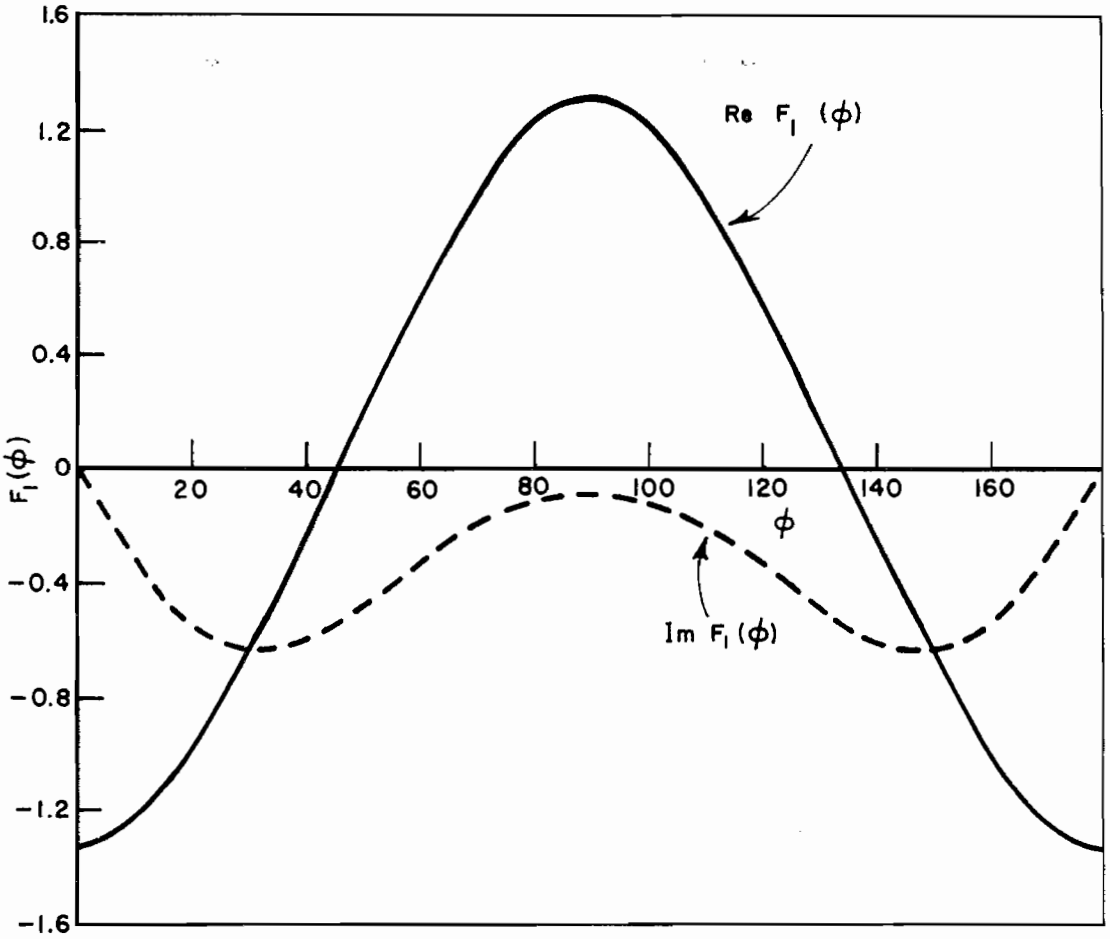


Fig. 8--The first characteristic mode pattern, 3-wire array.

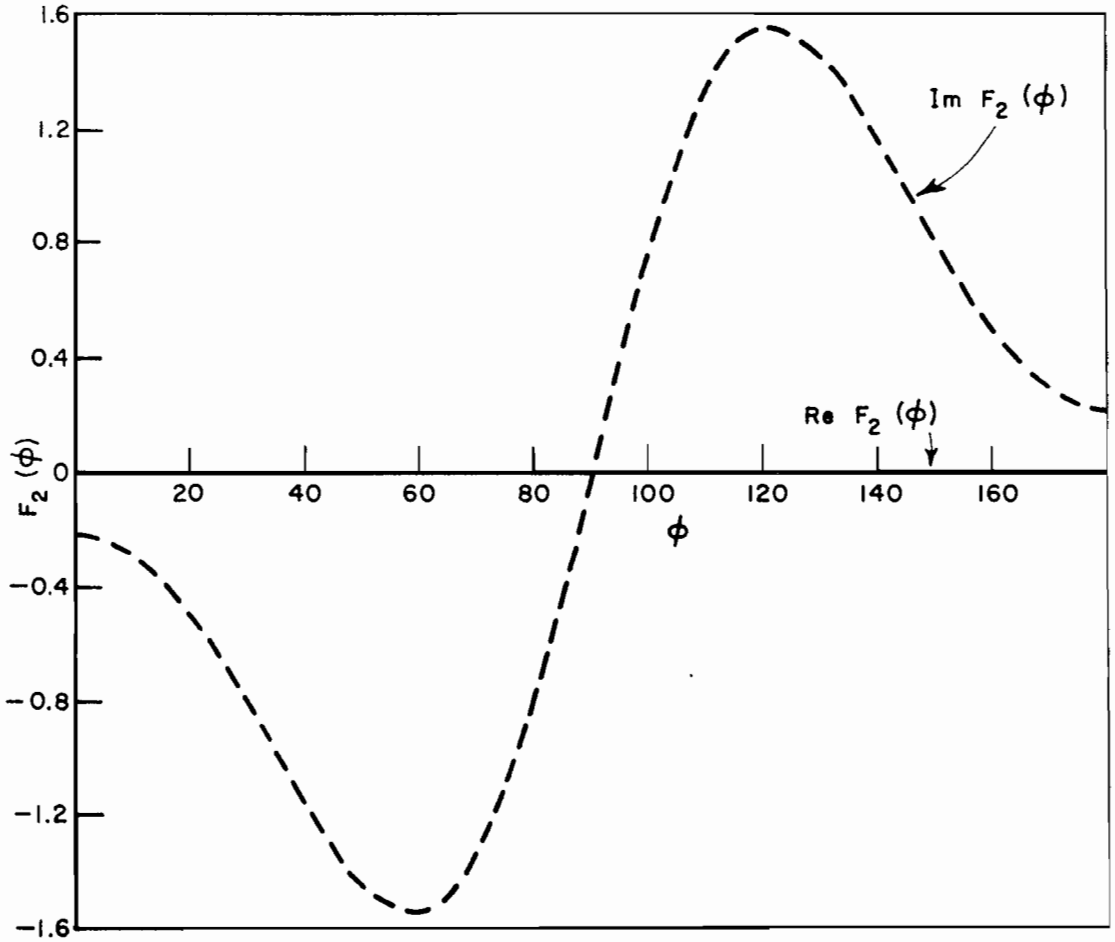


Fig. 9--The second characteristic mode pattern, 3-wire array.

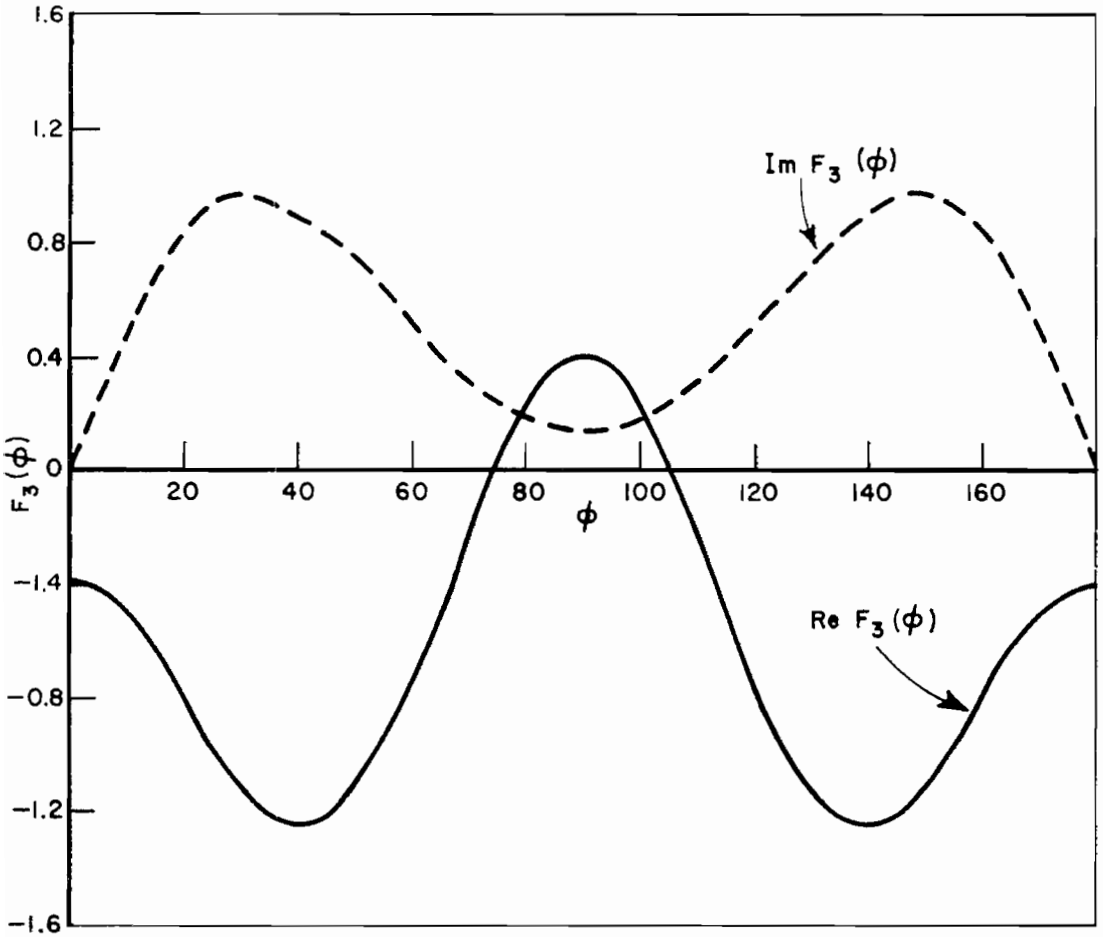


Fig. 10--The third characteristic mode pattern, 3-wire array.

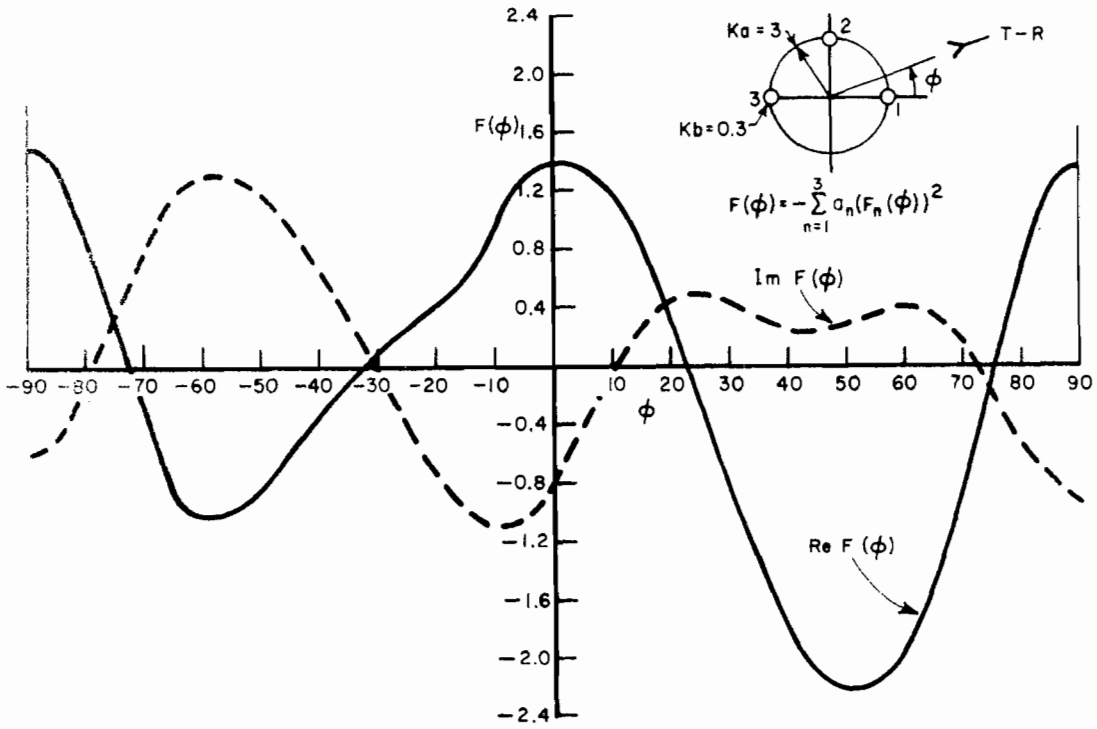


Fig. 11--The backscattered field pattern, 3-wire array.

The corresponding value of $\hat{P}_T$ is

$$(95) \qquad \hat{P}_T = \frac{4}{kZ_o} \sum_{n=1}^{3} |a_n|^2 = \frac{4}{kZ_o} \ (1.78), \text{ decoupled array.}$$

From Table II, the value of $\hat{P}_T$ for the coupled array is

$$(96) \qquad \hat{P}_T = \frac{4}{kZ_o} \sum_{n=1}^{3} |a_n|^2 = \frac{4}{kZ_o} \ (1.706), \text{ coupled array,}$$

indicating that on the basis of average total power, the coupling creates a slight disadvantage. If the average backscattered power per unit length is calculated for the two cases, the results indicate that they, too, are approximately the same and equal to

$$(97) \qquad \hat{P}_{B.S.} \approx \frac{1}{2\pi} \ \frac{4}{kZ_o} \ (1.78).$$

Since the wires are rather widely spaced, implying weak coupling among them, these results are not unexpected.

A less symmetrical array of eight wires is shown in Fig. 12. The wire circumferences in wavelengths are kb = 0.01 and their locations are given in Table V.

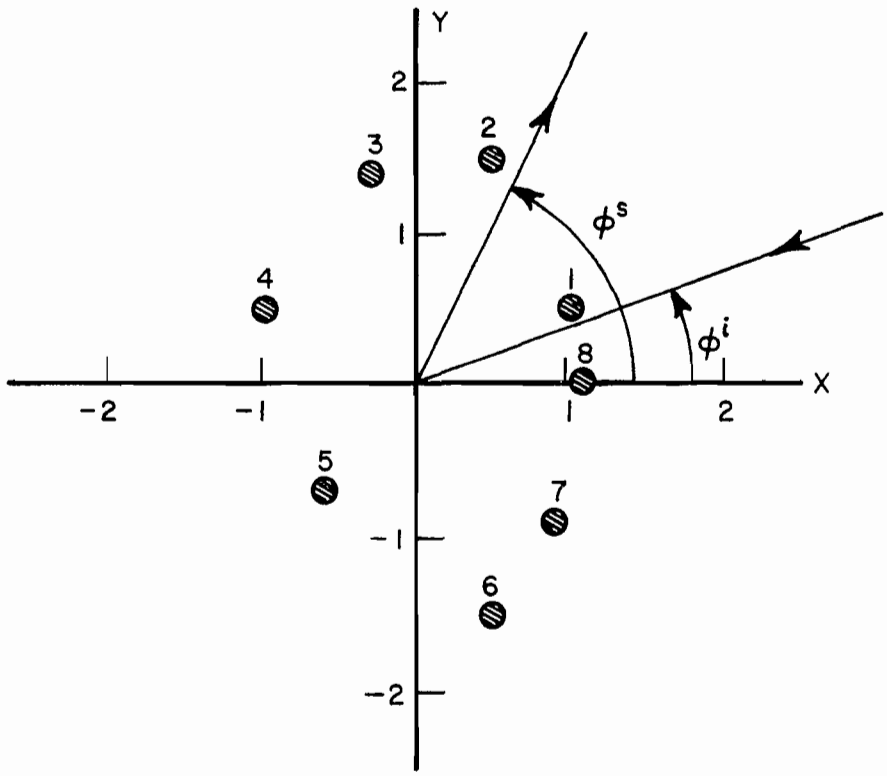


Fig. 12--An example of an 8-wire array.

TABLE V

Wire Locations - 8 Wire Array

| Wire No. | kx | ky |
|---|---|---|
| 1 | 1.0 | 0.5 |
| 2 | 0.5 | 1.5 |
| 3 | -0.3 | 1.4 |
| 4 | -1.0 | 0.5 |
| 5 | -0.6 | -0.7 |
| 6 | 0.5 | -1.5 |
| 7 | 0.9 | -0.9 |
| 8 | 1.1 | 0.0 |

The roots, $\lambda_n$, and the angles, $\alpha_n$, and coefficients, $a_n$, are given in Table VI.

TABLE VI
Values of $\lambda_n$, $\alpha_n$ and $|a_n|$
for 8 Wire Array

| Mode No. | $\lambda_n$ | $\alpha_n = \tan^{-1}(-\lambda_n)$ | $\lvert a_n\rvert = \lvert\cos \alpha_n\rvert$ |
|---|---|---|---|
| 1 | 0.16945 | $170.38^o$ | 0.9860 |
| 2 | 1.6375 | $121.42^o$ | 0.5213 |
| 3 | 2.7189 | $110.20^o$ | 0.3353 |
| 4 | 11.918 | $94.80^o$ | 0.0837 |
| 5 | 18.799 | $93.05^o$ | 0.0532 |
| 6 | 214.59 | $90.27^o$ | 0.0047 |
| 7 | 393.93 | $90.13^o$ | 0.0026 |
| 8 | 31659 | $\sim 90^o$ | $\sim 0.0$ |

The four most significant coefficients $a_n$ have been plotted in the complex plane in Fig. 13.

Similarly to the 3 wire array, the 8 wire array may be compared with a decoupled set of 8 wires of the same diameter with respect to the quantity $\hat{P}_T$. For the decoupled wires,

$$(98) \qquad a_1 = a_2 = \cdots a_8 = -\frac{1}{1 - j\dfrac{N_o(0.01)}{J_o(0.01)}} \quad ,$$

$$= 0.3156\, e^{j108.4^o},$$

and the corresponding value of $\hat{P}_T$ is

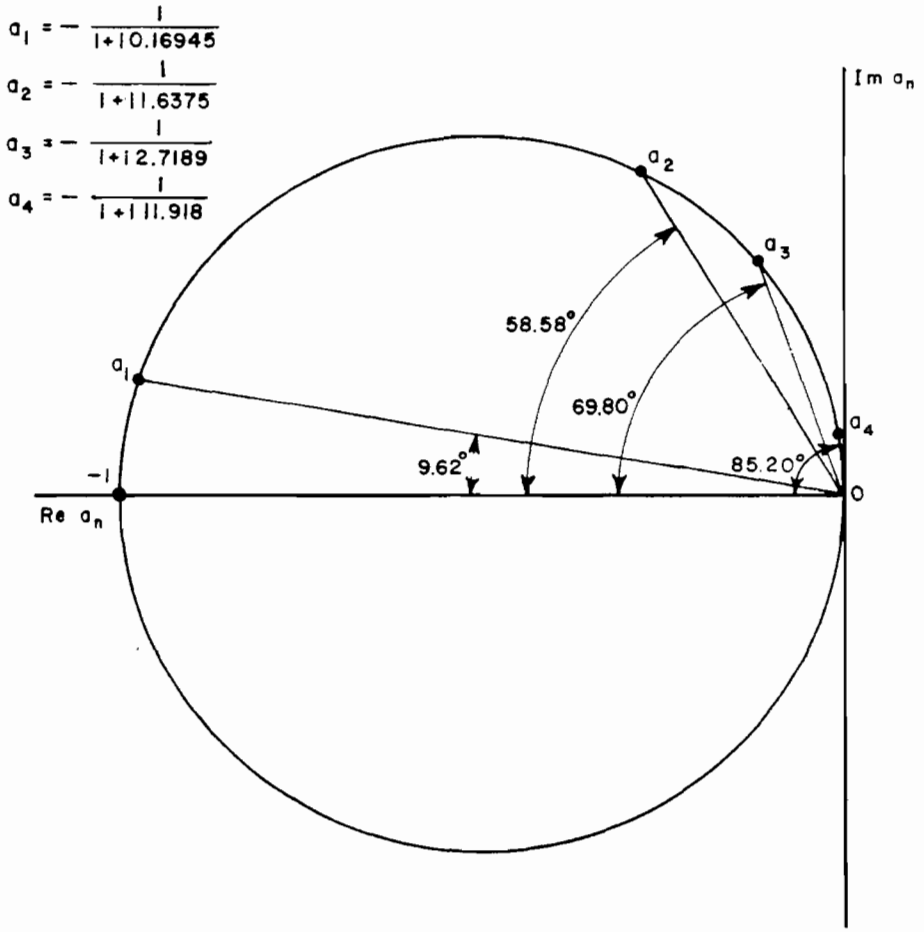


Fig. 13--The four most significant coefficients $a_n$ for the 8-wire array.

(99) $\hat{P}_T = \frac{4}{kZ_o}$ (0.7968), decoupled array.

From Table VI, the value of $\hat{P}_T$ for the complex array is

(100) $\hat{P}_T = \frac{4}{kZ_o}$ (1.3662), coupled array.

Hence, we conclude that in this case coupling has enhanced the average total power scattered.

The characteristic currents $(J_n)$, normalized such that $(J_m)^t \left[-\frac{4}{\omega\mu} R\right] (J_n) = \delta_{mn}$, are given in Table VII.

Assuming that a single mode current is forced to exist on the wires, a contour plot can be constructed of the equiphase lines of the resulting near electric field. Such a plot is shown in Fig. 14 for the lowest order mode, n = 1, associated with the eight wire array. The number assigned to each contour indicates the phase delay in degrees of the electric field with respect to the zero phase of the currents. The feature to note is the approximately equiphase plateau caused by a characteristic mode current in the region "enclosed" by the wires. As more wires are added to the array better "enclosing" this region, this plateau becomes flatter. In the case of a closed surface rather than a quantized one this plateau should represent a phase of $-\alpha_1$ degrees associated with the first mode of the closed contour. Outside the region "enclosed" by the wires, outward traveling fields are evident, the phase angle decreasing on successive contours as one progresses outward.

TABLE VII

Characteristic Currents for 8 Wire Array

| Mode No. | 1 | 2 | 3 |
|---|---|---|---|
| Wire No. | | | |
| 1 | 0.182500 | -0.054018 | 0.292452 |
| 2 | 0.187858 | -0.279852 | 0.242099 |
| 3 | 0.187122 | -0.299729 | -0.100081 |
| 4 | 0.218317 | -0.159926 | -0.480015 |
| 5 | 0.223291 | 0.142351 | -0.446582 |
| 6 | 0.179910 | 0.353085 | -0.062725 |
| 7 | 0.178142 | 0.236645 | 0.140012 |
| 8 | 0.178027 | 0.071283 | 0.274535 |
| | 4 | 5 | 6 |
| 1 | -0.542448 | 0.412859 | -2.34525 |
| 2 | 0.611046 | 1.05674 | -2.16842 |
| 3 | 0.801384 | -0.766030 | 4.27750 |
| 4 | -0.496285 | -0.921224 | -4.22445 |
| 5 | -0.273849 | 1.43922 | 3.08460 |
| 6 | 1.08536 | 0.59561 | -3.47798 |
| 7 | 0.118843 | -0.905579 | 1.80761 |
| 8 | -0.617696 | -0.382319 | 1.87558 |
| | 7 | 8 | |
| 1 | 4.50352 | -64.1309 | |
| 2 | -5.66507 | 21.4775 | |
| 3 | 4.03621 | -10.8736 | |
| 4 | -1.57486 | 8.71565 | |
| 5 | -0.238635 | -3.85685 | |
| 6 | 4.32441 | 18.4251 | |
| 7 | -6.93429 | -40.4532 | |
| 8 | 1.26945 | 77.1455 | |

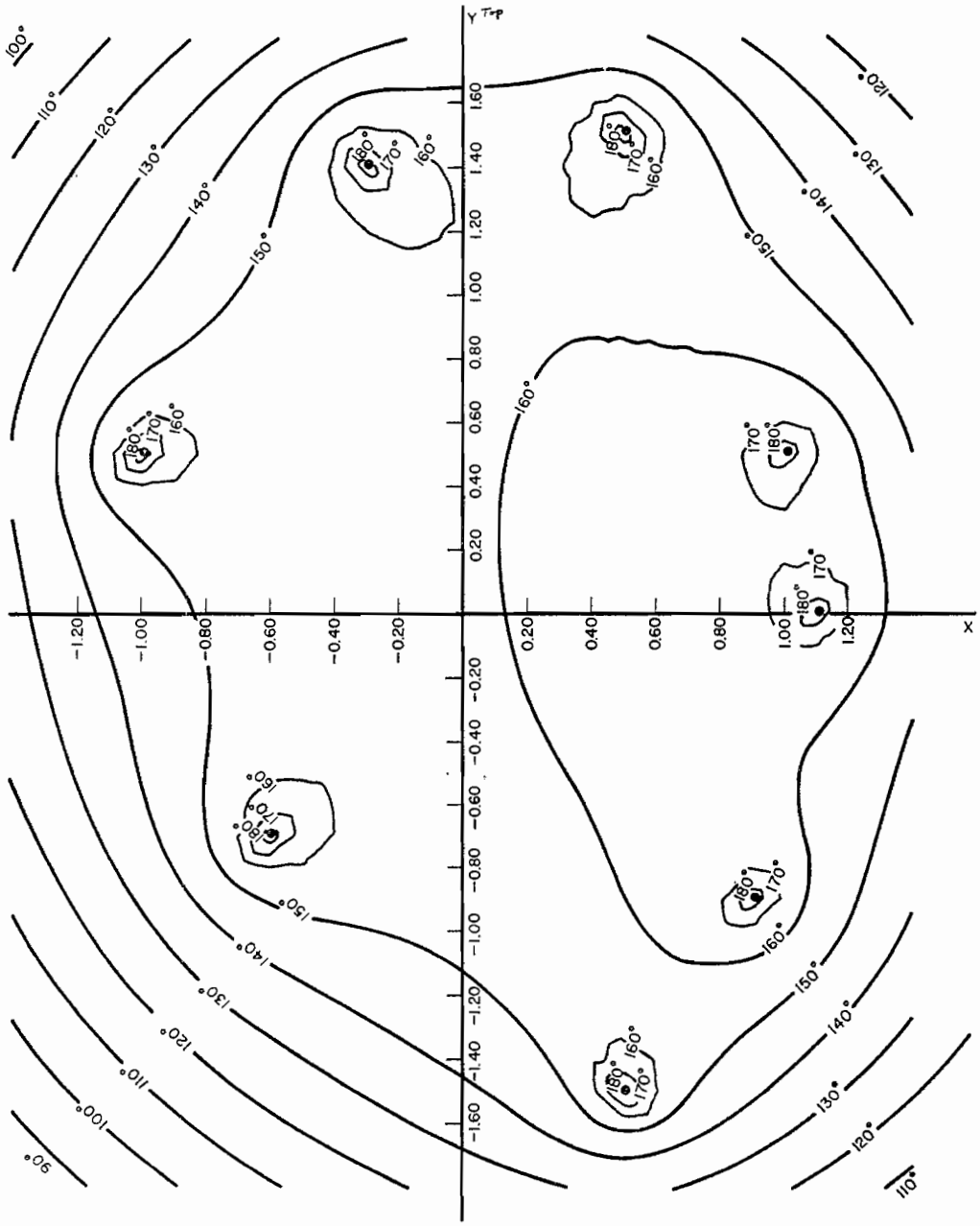


Fig. 14--Contour map of equiphase electric fields radiated by the major characteristic mode on the 8-wire array.

D. Two Coaxial Circular Loops of Wire

Although the previous example illustrated certain features of a characteristic mode expansion, it was somewhat over simplified in that it reduced to a two dimensional scalar problem and applied to an obstacle that is impossible to construct, i.e., wires of infinite length. A scatterer comprising two circular loops of wire, coaxially oriented in different planes in general, is a more practical example. In this case, the characteristic currents and fields are of known form around each loop, but vary in amplitude from loop to loop depending upon loop spacing, loop diameter, and frequency.

Before considering the two loop configuration, let us examine the characteristic-fields for the single circular loop (Fig. 15) which is simpler and for which there exists a substantial literature treatment both as an antenna[37][38][39] and as a scatterer.[40][41][42][43][44] The work of Harrington and Mautz[44] is of particular interest here because their formulation for plane wave scattering by a loop of thin wire is based upon a modal expansion which is almost directly interpretable in terms of the characteristic mode formalism.

Since the loop of Fig. 15 possesses rotational symmetry, the $\phi$-variation of the associated characteristic-mode currents and far radiated modal field patterns are already known to be of the form $\begin{Bmatrix} \cos n\phi \\ \sin n\phi \end{Bmatrix}$, $n = 0,1,2,\cdots$. The radiation zone fields of a real modal current $J^n$ flowing on the loop are[45]

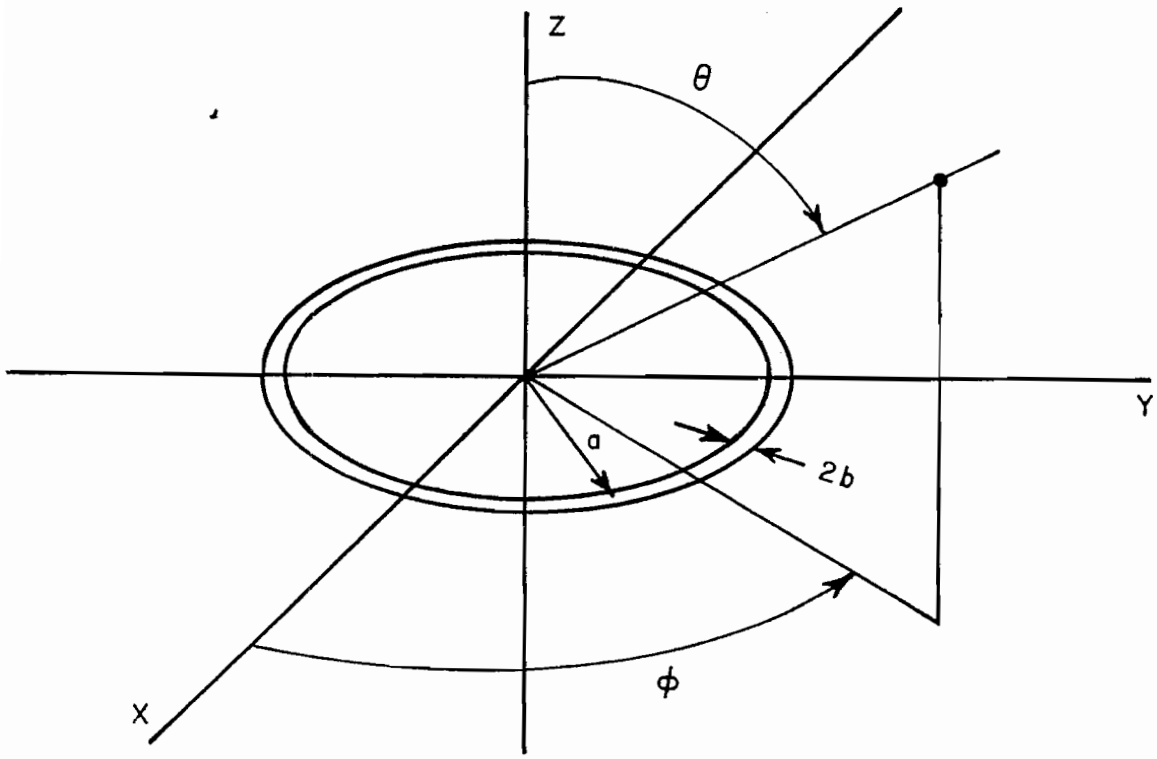


Fig. 15--Coordinates for the single circular loop.

$$(101)\qquad {}_{e}^{o}E_{\phi}(\theta,\phi) = -\frac{\omega\mu a}{2}\,\frac{e^{-ikr}}{r}\,J^{n}\left\{\begin{matrix}\cos n\phi\\ \sin n\phi\end{matrix}\right\}(i)^{n}\,J_{n}'(ka\sin\theta),$$

$$= \frac{-i\omega\mu}{4\pi}\,\frac{e^{-ikr}}{r}\left\{J^{n}\left\{\begin{matrix}\cos n\phi\\ \sin n\phi\end{matrix}\right\}(i)^{n+1}\,\pi a\times\right.$$

$$\left.[J_{n+1}(ka\sin\theta) - J_{n-1}(ka\sin\theta)]\right\}\quad,$$

and

$$(102)\qquad {}_{e}^{o}E_{\theta}^{n}(\theta,\phi) = \mp \frac{\omega\mu a}{2} \frac{e^{-ikr}}{r} J^{n} \begin{Bmatrix} \sin n\phi \\ \cos n\phi \end{Bmatrix} (i)^{n} \frac{n J_{n}(ka \sin\theta)}{ka \tan\theta},$$

$$= \frac{-i\omega\mu}{4\pi} \frac{e^{-ikr}}{r} \left\{ \mp J^{n} \begin{Bmatrix} \sin n\phi \\ \cos n\phi \end{Bmatrix} (i)^{n+1} \pi a \cos\theta \times \right.$$

$$\left. \left[ J_{n+1}(ka \sin\theta) + J_{n-1}(ka \sin\theta) \right] \right\} .$$

The factors inside the brackets in Eqs. (101) and (102) will be called the far field modal pattern functions, ${}_{e}^{o}F_{\phi}^{n}(\theta,\phi)$ and ${}_{e}^{o}F_{\theta}^{n}(\theta,\phi)$, respectively. The subscripts e or o refer to the use of cos $n\phi$ or sin $n\phi$ current modes, respectively.

According to the definition of modal impedances given in Appendix A, the power radiated by $J^{n}$ is

$$(103)\qquad P^{n} = R_{11}^{n} |J^{n}|^{2},$$

where $R_{11}^{n}$ is defined by the relationship

$$(104)\qquad {}_{e}^{o}\hat{E}_{\phi}^{n} = - \frac{\varepsilon_{n}}{2\pi a} (R_{11}^{n} + i X_{11}^{n}) J^{n} ,$$

and $\hat{E}_{\phi}^{n}$ is the maximum of the electric field tangential to the wire axis produced by $J^{n}$. Alternatively,

$$(105)\qquad P^{n} = \frac{1}{Z_{o}} \iint_{\Sigma} \left[ |{}_{e}^{o}E_{\theta}^{n}|^{2} + |{}_{e}^{o}E_{\phi}^{n}|^{2} \right] r^{2} \, d\Omega$$

$$= \left( \frac{k Z_{o}}{4\pi} \right)^{2} \frac{1}{Z_{o}} \iint_{\Sigma} \left[ |{}_{e}^{o}F_{\theta}^{n}|^{2} + |{}_{e}^{o}F_{\phi}^{n}|^{2} \right] d\Omega .$$

The currents are normalized to radiate unit power, i.e.,

$$J^n = \frac{1}{\sqrt{R_{11}^n}} \quad , \tag{106}$$

so that the characteristic patterns are

$$ {}_{e\atop o}F_{\phi}^{n}(\theta,\phi) = \frac{\pi a(i)^{n+1}}{\sqrt{R_{11}^n}} \left\{ \begin{matrix} \cos n\phi \\ \sin n\phi \end{matrix} \right\} \left[ J_{n+1}(ka \sin\theta) - J_{n-1}(ka \sin\theta) \right] , \tag{107}$$

and

$$ {}_{e\atop o}F_{\theta}^{n}(\theta,\phi) = \mp \frac{\pi a(i)^{n+1}}{\sqrt{R_{11}^n}} \left\{ \begin{matrix} \sin n\phi \\ \cos n\phi \end{matrix} \right\} \cos\theta \left[ J_{n+1}(ka \sin\theta) + J_{n-1}(ka \sin\theta) \right] . \tag{108}$$

Employing vector notation,

$$ {}_{e\atop o}\underline{F}^{n}(\theta,\phi) = \left( {}_{e\atop o}F^{n}(\theta,\phi) \right) = \begin{pmatrix} {}_{e\atop o}F_{\theta}^{n}(\theta,\phi) \\ {}_{e\atop o}F_{\phi}^{n}(\theta,\phi) \end{pmatrix} \quad , \tag{109}$$

the dyadic pattern function of the loop due to a plane wave arriving from $(\theta^i,\phi^i)$ is

$$ \underline{F}(\theta^i\phi^i;\theta^s,\phi^s) = -\sum_{n=0}^{\infty} \left[ a^n \left( {}_{e} F^{n}(\theta^i,\phi^i) \right) \left( {}_{e} F^{n}(\theta^s,\phi^s) \right)^t + a^n \left( {}_{o} F^{n}(\theta^i,\phi^i) \right) \left( {}_{o} F^{n}(\theta^s,\phi^s) \right)^t \right] \quad , \tag{110}$$

and the far scattered field is

$$(111) \qquad \underline{E} = \frac{-i\omega\mu}{4\pi} \frac{e^{-ikr}}{r} \underline{F}(\theta^i,\phi^i;\theta^s,\phi^s) \cdot \hat{\xi}^i,$$

where $\hat{\xi}^i$ is the polarization state of the incident plane wave. The coefficients $a^n$ are

$$(112) \qquad a^n = -\frac{1}{1 + i\lambda^n},$$

where

$$(113) \qquad \lambda^n = \frac{\mathrm{Im}\{\underset{\delta}{e}\, \hat{E}^n_\phi\}}{\mathrm{Re}\{\underset{\delta}{e}\, \hat{E}^n_\phi\}} = \frac{X^n_{11}}{R^n_{11}},$$

and $Z^n_{11} = R^n_{11} + i\, X^n_{11}$ are as defined in Eq. (104). From these last two equations

$$(114) \qquad a^n = -\frac{R^n_{11}}{Z^n_{11}}.$$

It may be verified that Eq. (111) is identical to Eq. (50) of Reference 44 with the observation that $Z_{nn}$ in that treatise is related to $Z^n_{11}$ in the present work by

$$(115) \qquad \epsilon_n Z^n_{11} = Z_{nn}.$$

Values of $Z_{nn}$, n = 0-4, for certain loop sizes are given in curve form in Reference 44 and a numerical tabulation is available[46] for values of n up to 20. Independently derived integral expressions for $Z^o_{11} = Z_{oo}$ and $Z^1_{11} = \frac{1}{2} Z_{11}$ have been derived by using a

transform method. Typical values for an $0.5\lambda$ average diameter loop of wire $0.005\lambda$ in diameter are

$$Z_{11}^{o} = 724 + i3055,$$

$$2Z_{11}^{1} = 380 + i1225.$$

Comparable results given by Harrington[46] are

$$Z_{oo} = 723.4 + i3041,$$

$$Z_{11} = 384.8 + i1219.$$

Table VIII lists the first six modal impedances for this loop as given by Harrington[46] as well as the associated scattering coefficient angles, $\alpha^n$. The corresponding coefficients $a^n$ are plotted in Fig. 16, where we recognize that for each $n \neq 0$, two values of $a^n$ are coincident, one for the even modes, one for the odd modes. We also recognize that the ordering of the modes is on increasing orders, n, of the trigonometric $\phi$ variations of the modal currents rather than on the magnitude of the $|a^n|$. This standard notation permits a direct correlation with the literature, similarly to the examples of the circular cylinder and sphere.

TABLE VIII
Modal Impedances and Scattering Coefficient Angles for the Single Loop, $a/\lambda = 0.25$, $b/\lambda = 0.0025$

| n | $\varepsilon_n Z_{11}^n = \varepsilon_n(R_{11}^n + iX_{11}^n)$ | $\lambda^n = X_{11}^n/R_{11}^n$ | $\alpha^n = \tan^{-1}(-\lambda^n)$ |
|---|---|---|---|
| 0 | 723.4 + i3041 | 4.204 | $103.4^o$ |
| 1 | 384.8 + i1219 | 3.168 | $107.5^o$ |
| 2 | 197.2 - i1620 | -8.215 | $263.1^o$ |
| 3 | 27.82 - i5860 | -210.6 | $269.7^o$ |
| 4 | 1.760 - i11060 | -6284 | $\sim 270^o$ |
| 5 | 0.0657 - i17070 | -259800 | $\sim 270$ |

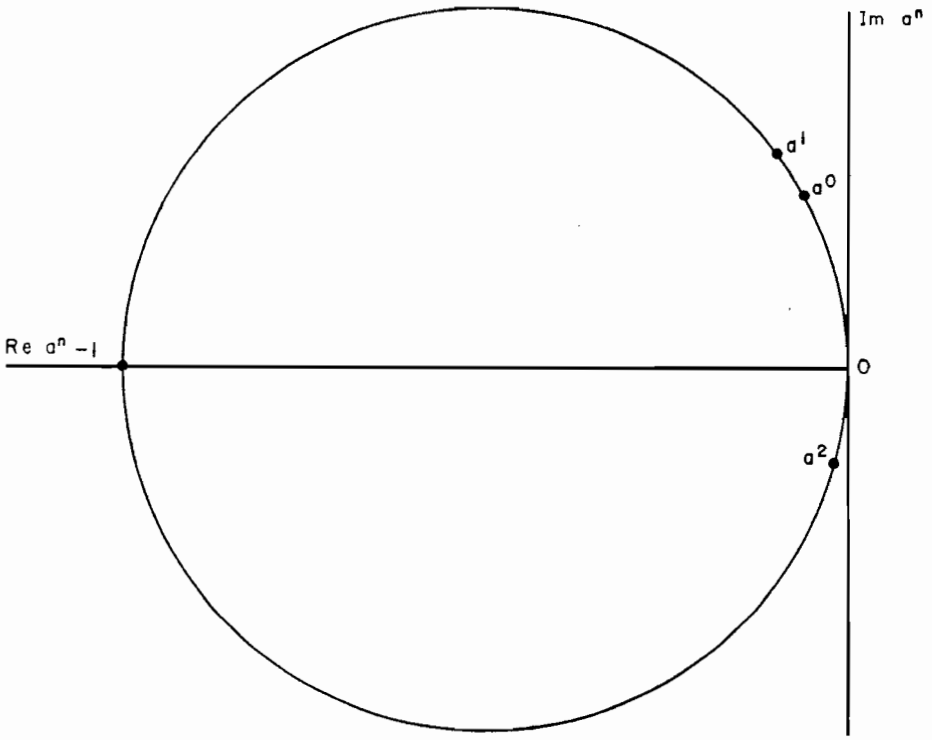


Fig. 16--The three major coefficients, $a^n$, associated with a circular loop, $a/\lambda = 0.25$, $b/\lambda = 0.0025$.

It is instructive to observe the variation in the phase angles, $\alpha^n$, for the same loop as functions of frequency. Utilizing the curves of Fig. 2, Reference 44, we have plotted these angles in Fig. 17 for n = 0, 1, 2, and 3. The scattering resonances for the n = 1 and 2 modes, i.e., those frequencies for which $\alpha^1 = 180^o$ and $\alpha^2 = 180^o$, are clearly evident as are the rather narrow bandwidths of these resonances. We suggest that such curves may play a role in evaluating the effectiveness of a scatterer in comparison with others, particularly when only a single mode is important. Here, the problem of ranking a variety of wire elements according to some figure-of-merit involving such curves, comes to mind.

If $P_T$ again is defined to be the total power scattered by the loop averaged over all possible directions of incidence and polarization states of an exciting plane wave of unit electric field intensity, then

$$\hat{P}_T = \frac{2\pi}{k^2 Z_o} \sum_{n=0}^{N} \varepsilon_n |a^n|^2, \tag{116}$$

where the factor $\varepsilon_n = \begin{cases} 2, & n \neq 0 \\ 1, & n = 0 \end{cases}$ accounts for the existence of both even and odd modes when $n \neq 0$. For the loops represented in Fig. 17, typical values of $\hat{P}_T$ at $a/\lambda = 0.25$ and $a/\lambda = 0.325$ are

$$\hat{P}_T = \frac{2\pi}{k^2 Z_o} (0.263), \quad a/\lambda = 0.25, \tag{117}$$

$$\hat{P}_T = \frac{2\pi}{k^2 Z_o} (2.2), \quad a/\lambda = 0.325. \tag{118}$$

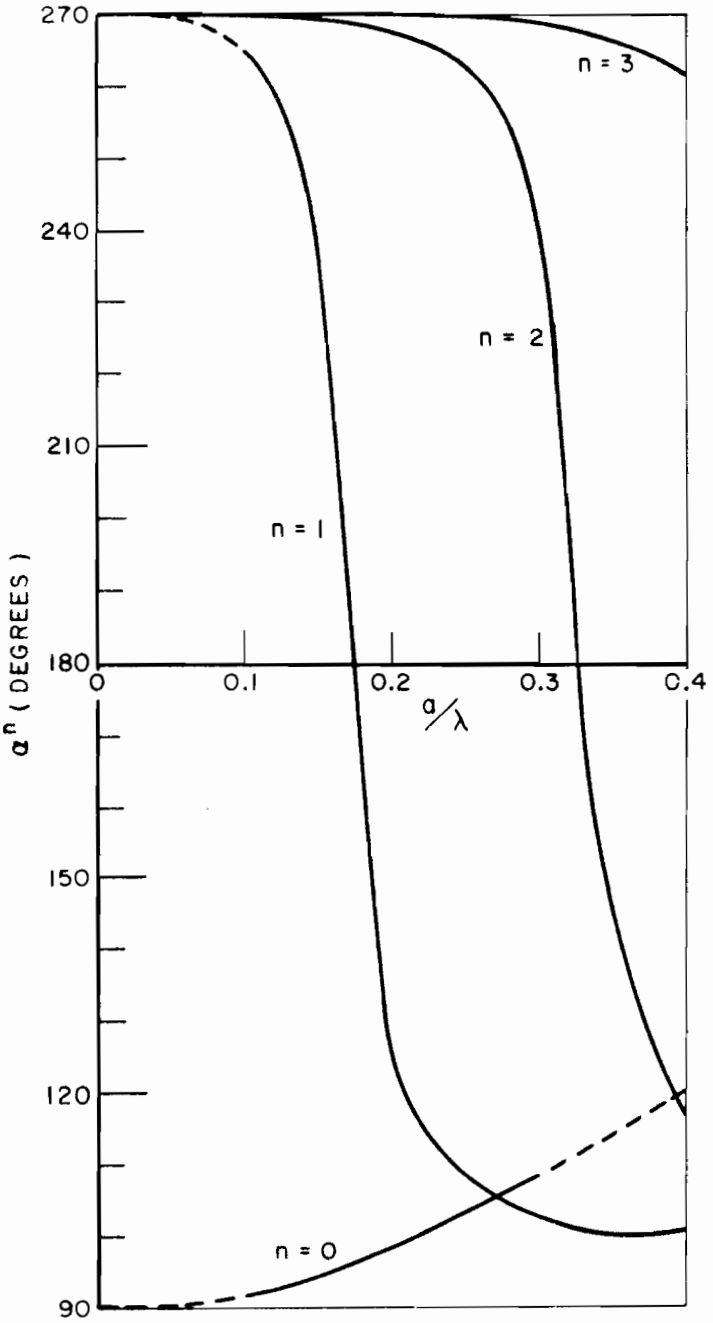


Fig. 17--Variation with frequency of phase angles, $\alpha^n$, n = 0,1,2,3, for a single loop of wire. a/b = 100, a = loop radius, b = wire radius.

In this last case, the overwhelming contribution to $\hat{P}_T$ comes from the resonant n = 2 mode, implying that a figure-of-merit based on $\hat{P}_T$ could safely be evaluated using this mode alone.

We proceed to the two loop geometry sketched in Fig. 18.

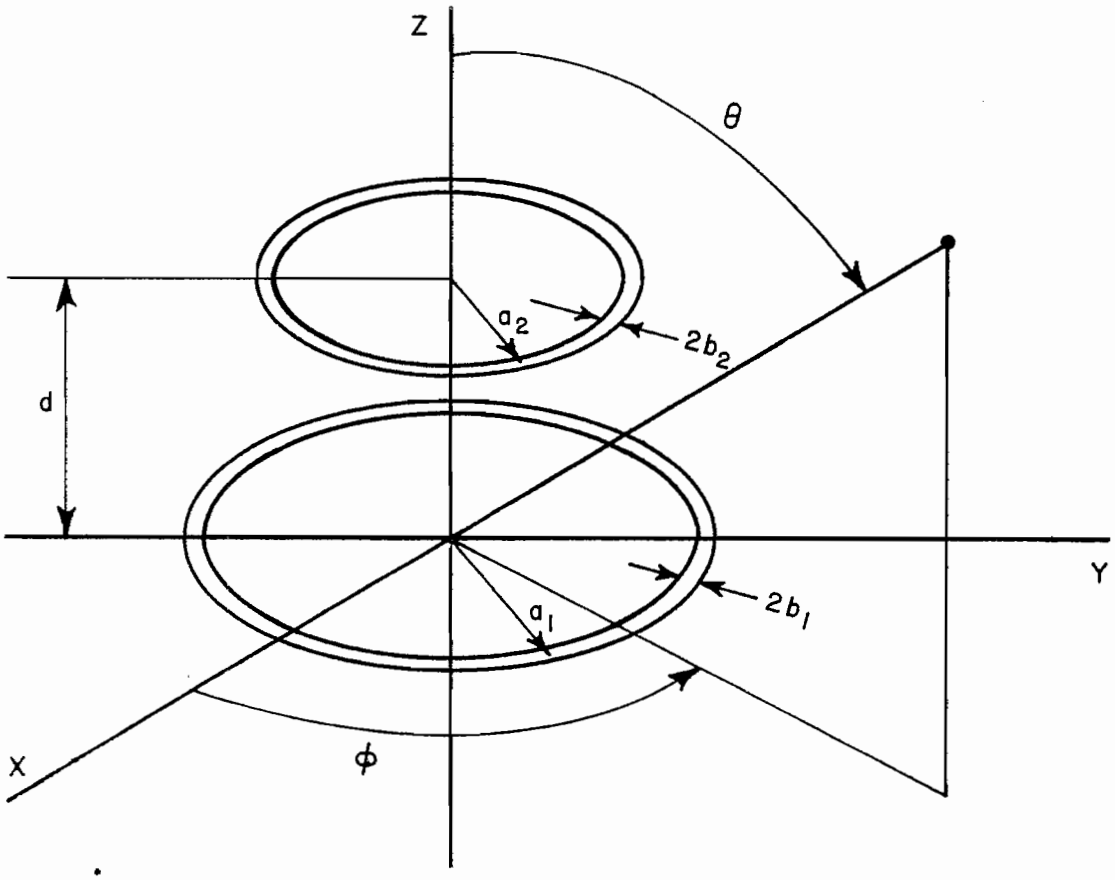


Fig. 18--Coordinates for two coaxial circular loops.

Similarly to the single loop, the $\phi$-variation of the characteristic mode currents and patterns is of the form $\begin{Bmatrix}\cos n\phi \\ \sin n\phi\end{Bmatrix}$, n = 0,1,2,$\cdots$. The problem lies in determining the proper combinations of amplitudes of such currents on each loop which give rise to characteristic mode

patterns in the $\theta$-variable. To this end, the Z operator is represented by a set of N $2 \times 2$ complex matrices, $[Z^n] = [R^n] + i[X^n]$, $n = 1,2,\cdots N$. In Appendix A the elements of the $n^{th}$ such matrix are related to the self and mutual modal impedances of the two loop configuration. (Clearly, if the method is extended to M coaxial loops, each matrix would be of the order $M \times M$.) These N matrices are diagonalized individually, leading to inverse characteristic values, $a_m^n$, and real characteristic current amplitudes, $({}_{e}^{o}J_m^n) = ({}_{e}^{o}J_{1m}^n \; {}_{e}^{o}J_{2m}^n)^t$, with $m = 1,2$, (number of loops). The radiation integral yields the associated fields,

$$(119) \qquad {}_{e}^{o}E_{m\phi}^n = \frac{-i\omega\mu}{4\pi} \frac{e^{-ikr}}{r} \{ \pi a_1 (i)^{n+1} \; {}_{e}^{o}J_{1m}^n \begin{Bmatrix} \cos n\phi \\ \sin n\phi \end{Bmatrix} \times$$

$$[J_{n+1}(ka_1 \sin\theta) - J_{n-1}(ka \sin\theta)]$$

$$+ \pi a_2 (i)^{n+1} \; {}_{e}^{o}J_{2m}^n \begin{Bmatrix} \cos n\phi \\ \sin n\phi \end{Bmatrix} [J_{n+1}(ka_2 \sin\theta)$$

$$-J_{n-1}(ka_2 \sin\theta)] \, e^{ikd\cos\theta} \} \; ,$$

$$= \frac{-i\omega\mu}{4\pi} \frac{e^{-ikr}}{r} \; {}_{e}^{o}F_{m\phi}^n (\theta, \phi),$$

and

$$(120)\qquad {}_{e\atop o}E^n_{m\phi} = \frac{-i\omega\mu}{4\pi}\ \frac{e^{-ikr}}{r}\{\pm\ \pi a_1 (i)^{n+1}\ {}_{e\atop o}J^n_{1m}\ \{{}^{\sin n\phi}_{\cos n\phi}\}\cos\theta\ \times$$

$$[J_{n+1}(ka_1\sin\theta) + J_{n-1}(ka_1\sin\theta)]$$

$$\mp\ \pi a_2 (i)^{n+1}\ {}_{e\atop o}J^n_{2m}\ \{{}^{\sin n\phi}_{\cos n\phi}\}\cos\theta[J_{n+1}(ka_2\sin\theta) +$$

$$J_{n-1}(ka_2\sin\theta)]\ e^{ikd\cos\theta}\}\ ,$$

$$= \frac{-i\omega\mu}{4\pi}\ \frac{e^{-ikr}}{r}\ \ {}_{e\atop o}F^n_{m\phi}\ (\theta,\phi),$$

where ${}_{e\atop o}F^n_{m\phi}(\theta,\phi)$ and ${}_{e\atop o}F^n_{m\theta}(\theta,\phi)$ are the characteristic patterns. As before, the subscripts e or o refer to use of $\cos n\phi$ or $\sin n\phi$ current modes, respectively.

The modal currents are normalized to radiate unit power, i.e.,

$$(121)\qquad P^n_m = ({}_{e\atop o}J^n_m)^t\ [R^n]\ ({}_{e\atop o}J^q_p) = \delta_{mp}\ \delta_{nq},$$

where the $[R^n]$ matrix is defined in Appendix A by

$$(122)\qquad ({}_{e\atop o}\hat{E}^n_m) = [\bar{Z}^n]\ ({}_{e\atop o}J^n_m) = [\bar{R}^n + i\bar{X}^n]\ ({}_{e\atop o}J^n_m),$$

$$= \begin{bmatrix} -\frac{\varepsilon_n}{2\pi a_1} & 0 \\ 0 & -\frac{\varepsilon_n}{2\pi a_2} \end{bmatrix} [R^n + iX^n]\ ({}_{e\atop o}J^n_m),$$

where the components of $({}_{e\atop o}E^n_{m\phi})$ are the maximum electric fields tangential to the loops produced by $({}_{e\atop o}J^n_m)$. Alternatively,

$$(123)\qquad P_m^n = \frac{1}{Z_o}\iint_\Sigma \left[\left|{}_e E^n_{m\theta}\right|^2 + \left|{}_e E^n_{m\phi}\right|^2\right] r^2\, d\Omega = 1,$$

$$= \left(\frac{kZ_o}{4\pi}\right)^2 \frac{1}{Z_o}\iint_\Sigma \left[\left|{}_e F^n_{m\theta}\right|^2 + \left|{}_e F^n_{m\phi}\right|^2\right] d\Omega = 1 .$$

The dyadic pattern function of the loops due to a plane wave arriving from $(\theta^i,\phi^i)$ is

$$(124)\qquad \underline{\underline{F}}(\theta^i,\phi^i;\theta^s,\phi^s) = -\sum_{n=0}^{\infty}\sum_{m=1}^{2}\left[a_m^n\left({}_e F_m^n(\theta^i,\phi^i)\right)\left({}_e F_m^n(\theta^s,\phi^s)\right)^t + a_m^n\left({}_o F_m^n(\theta^i,\phi^i)\right)\left({}_o F_m^n(\theta^s,\phi^s)\right)^t\right],$$

and the far scattered field is

$$(125)\qquad \underline{E}(\theta^i,\phi^i;\theta^s,\phi^s) = \frac{-i\omega\mu}{4\pi}\frac{e^{-ikr}}{r}\,\underline{\underline{F}}(\theta^i,\phi^i;\theta^s,\phi^s)\cdot\hat{\xi}^i,$$

where $\hat{\xi}^i$ is the polarization state of the incident plane wave. The coefficients $a_m^n$ are

$$(126)\qquad a_m^n = -\frac{1}{1+i\lambda_m^n},$$

where $\lambda_m^n$ are solutions of the second order polynomials,

$$(127)\qquad \det\left\{\left[\bar{\bar{X}}^n\right] - \lambda^n\left[\bar{\bar{R}}^n\right]\right\} = 0.$$

For the case, $a_1/\lambda = 0.5$, $a_2/\lambda = 0.333$, $b_1/\lambda = b_2/\lambda = 0.0167$, the modal impedances were calculated using a transform method for $n = 0,1$. The results are tabulated in Table IX.

TABLE IX

Modal Impedances for Two Coaxial Loops,

$a_1/\lambda = 0.5, a_2/\lambda = 0.333, b_1/\lambda = b_2/\lambda = 0.0167$

| n | $Z_{11}^n/Z_o$ | $Z_{22}^n/Z_o$ | $Z_{12}^n/Z_o = Z_{21}^n/Z_o$ |
|---|---|---|---|
| 0 | 5.832 + i6.182 | 4.031 + i6.347 | 1.762 - i2.721 |
| 1 | 2.052 + i4.299 | 0.605 + i1.833 | -0.0217 - i0.286 |

Using these impedances in Eqs. (127), values for $\lambda_m^n$ and $\alpha_m^n$ are found and tabulated in Table X. The coefficients $a_m^n$ are plotted in Fig. 18. For $n \neq 0$, the same coefficient, $a_m^n$, is associated with even and odd modes.

TABLE X

Values of $\lambda_m^n$ and $\alpha_m^n$ for Two Coaxial Loops,

$a_1/\lambda = 0.5$, $a_2/\lambda = 0.333$, $b_1/\lambda = b_2/\lambda = 0.0167$

| n | m | $\lambda_m^n$ | $\alpha_m^n = \tan^{-1}(-\lambda_m^n)$ |
|---|---|---|---|
| 0 | 1 | 0.523 | $152.4^o$ |
| 0 | 2 | 2.986 | $108.5^o$ |
| 1 | 1 | 2.047 | $116^o$ |
| 1 | 2 | 3.067 | $108.1^o$ |

Table XI lists the characteristic current amplitudes associated with the n = 1 mode.

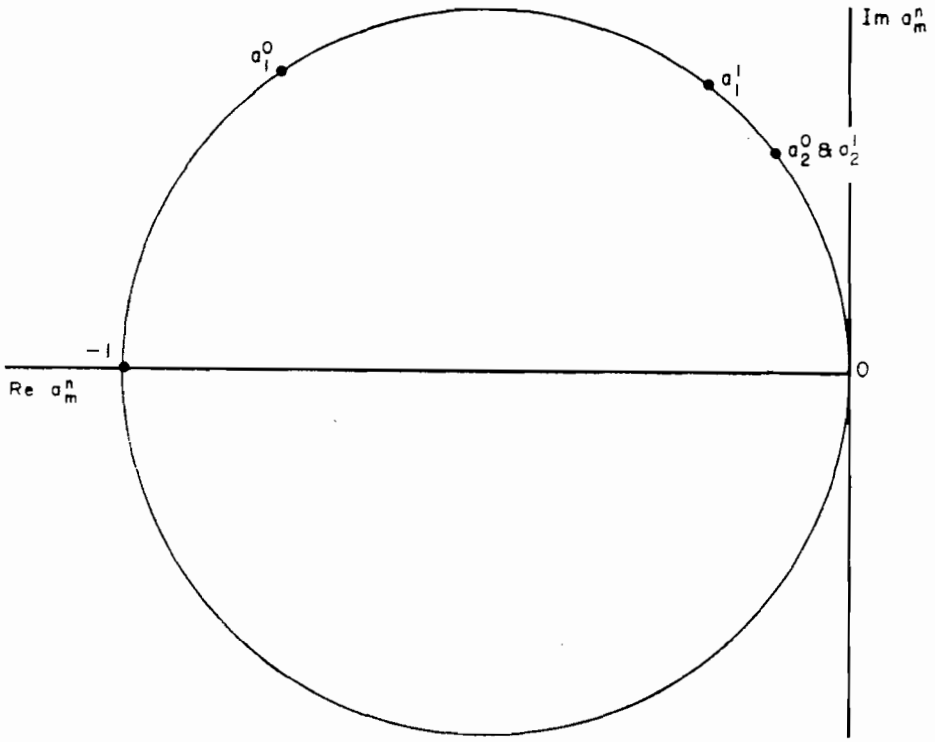


Fig. 10--Four scattering coefficients, $a_m^n$, associated with two coaxial circular loops, $a_1/\lambda = 0.5$, $a_2/\lambda = 0.333$, $b_1/\lambda = b_2/\lambda = 0.0667$, $d/\lambda = 0.333$.

TABLE XI

Characteristic Current Amplitudes for Two Coaxial Loops,

$a_1/\lambda = 0.5$, $a_2/\lambda = 0.333$, $b_1/\lambda = b_2/\lambda = 0.0167$

| n | m | $e^{J^n_{1m}}_{o}$ | $e^{J^n_{2m}}_{o}$ |
|---|---|---|---|
| 1 | 1 | +0.682 | +0.278 |
| 1 | 2 | -0.132 | +1.258 |

For broadside excitation of the two loops, only the n = 1 modes are induced. For the backscattering case, $\theta^i = \theta^s = 0$, $\phi^i = \phi^s = 0$, only the even mode is induced, and

$$(128) \qquad F(0,0;0,0) = -\{ a_1^1 [{}_eF_{1\phi}^1]^2 + a_2^1 [{}_eF_{2\phi}^1]^2 \},$$

$$= \frac{\pi^2}{1 + i\lambda_1^1} \left[ J_{11}^1 a_1 + J_{21}^1 a_2 e^{+ikd} \right]^2 +$$

$$\frac{\pi^2}{1 + i\lambda_2^1} \left[ J_{12}^1 a_1 + J_{22}^1 a_2 e^{+ikd} \right]^2 .$$

For the backscattering case, $\theta^i = \theta^s = \pi$, $\phi^i = \phi^s = 0$,

$$(129) \qquad F(\pi,0;\pi,0) = -\{ a_1^1 [{}_eF_{1\phi}^{1c}]^2 + a_2^1 [{}_eF_{2\phi}^{1c}]^2 \} ,$$

$$= \frac{\pi^2}{1 + i\lambda_1^1} \left[ J_{11}^1 a_1 + J_{21}^1 a_2 e^{-ikd} \right]^2 +$$

$$\frac{\pi^2}{1 + i\lambda_2^1} \left[ J_{12}^1 a_1 + J_{22}^1 a_2 e^{-ikd} \right]^2 .$$

For the loop of radius $a_1/\lambda$ alone,

$$(130) \qquad F_{a_1}(0,0;0,0) = \frac{\pi^2}{1 + i \frac{X_{11}^1}{R_{11}^1}} \left[ \frac{a_1}{\sqrt{R_{11}^1}} \right]^2 .$$

For the loop of radius $a_2/\lambda$ alone,

$$(131) \qquad F_{a_2}(0.0;00) = \frac{\pi^2}{1 + i \frac{X_{22}^1}{R_{22}^1}} \left[ \frac{a_2 e^{ikd}}{\sqrt{R_{22}^1}} \right]^2 .$$

Using the pertinent values given in Tables IX-XI, we obtain the ratios of echo areas,

$$(132) \qquad \frac{|F_{a_2}(0,0;00)|^2}{|F_{a_1}(0,0;00)|^2} = 1.2, \quad (1.3 \pm 0.06),$$

$$(133) \qquad \frac{|F(0,0;00)|^2}{|F(\pi,0;\pi,0)|^2} = 0.603, \quad (0.6 \pm 0.03),$$

where the numbers in parentheses are corresponding experimentally determined values.

E. Filamentary Scatterers of Finite Length

We shall now give some examples of characteristic modes for filamentary scatterers of finite length and arbitrary shape. Unlike the previous examples, the characteristic current distributions along the filaments are not known *a priori*. Nevertheless, computational techniques[47][48] have been developed which permit one to determine the induced current distributions for various directions of plane wave incidence and these may be interpreted for our purposes.

When the filament is thin, perfectly conducting* and less than about $0.5\lambda$ in length, one finds that to a good approximation, the current distribution induced by a plane wave does not change in form for arbitrary incidence directions. In fact, Fig. 4 of Reference 47 indicates that this invariance of the induced current distribution characterizes the linear wire even for dipole sources quite close to the wire. Moreover, the current distribution is characterized by a nearly-constant phase over the length of filament. In terms of characteristic modes, it is clear that such a scatterer possesses only a single dominant mode.

As an example, the dominant characteristic currents for several perfectly conducting filaments curved in the form of circular arcs, each $0.475\lambda$ in length and $0.0017\lambda$ in filament diameter have been determined. The current distributions, normalized to radiate unit power, are shown in Fig. 20 for several radii of curvature for the

---

*This statement also holds if the filament is merely a "good" conductor.

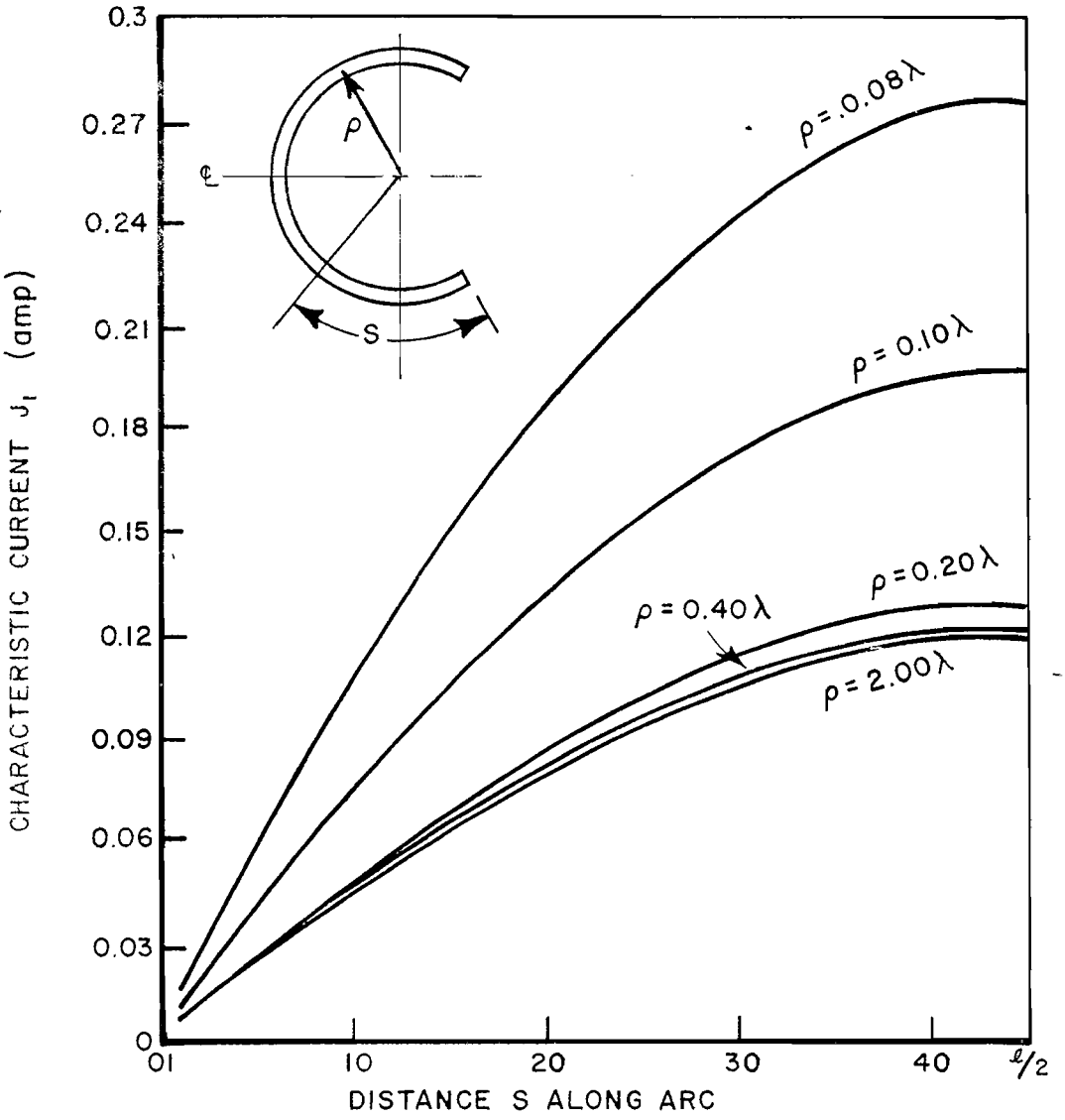


Fig. 20-- Dominant characteristic mode currents on circular arcs of wire. The wire length is $\ell = 0.475\lambda$ and its diameter is $d = 0.0017\lambda$. The currents are normalized to radiate unit power.

circular arcs. In Fig. 21, the corresponding phase angle, $\alpha_1$, is shown for each radius of curvature.

Significantly, one notes that the form of the current distribution does not change much with radius of curvature, suggesting a close relationship between the dominant characteristic current distributions for a range of filament shapes, provided that the overall filament length is held constant.

While the data shown in Figs. 20 and 21 were obtained from the induced current distribution and backscattered echo area for one direction of plane wave incidence, i.e., broadside to the plane of the circular arcs, it is possible to predict from this the scattering for any combination of source and observer directions. To do this one must calculate the pattern function, $\underline{F}_1(\theta,\phi)$, radiated by any normalized current distribution of Fig. 20. This, together with the phase constant $\alpha_1$ of Fig. 21, leads to an expression for the dyadic plane wave scattering pattern,

$$(134) \qquad \underline{\underline{F}}(\theta^i,\phi^i;\theta^s,\phi^s) = -|\cos\ \alpha_1| e^{i\alpha_1}\ \underline{F}_1(\theta^i,\phi^i)\ \underline{F}_1(\theta^s,\phi^s).$$

The total scattered power, averaged over all directions is

$$(135) \qquad \hat{P}_T = \frac{2\pi}{k^2 Z_o}\ |\cos\ \alpha_1|^2\ ,$$

and may be predicted from the values of $\alpha_1$ given in Fig. 21. It is also possible to determine the average backscattered signal over all directions from the data of Figs. 20 and 21, but this would

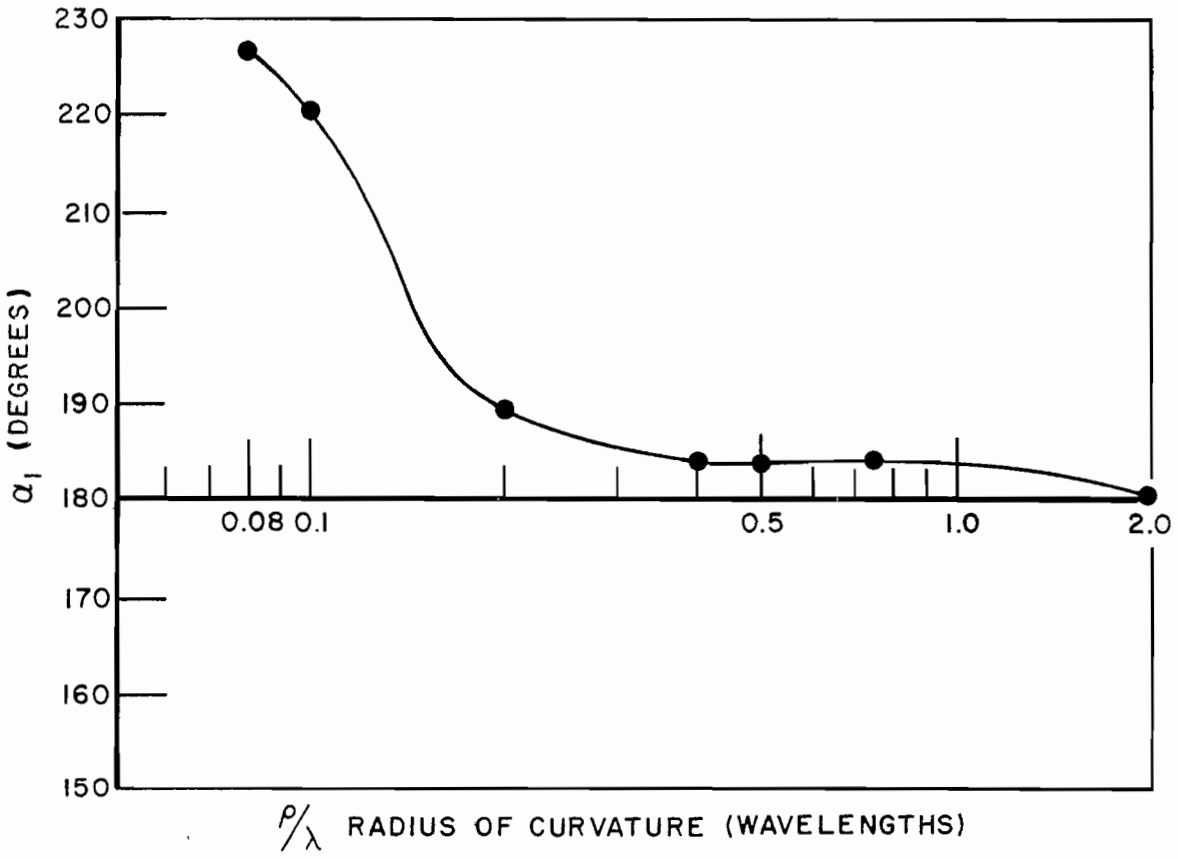


Fig. 21--Variation of phase angle, $\alpha_1$, with radius of curvature of circular arcs of wire. The wire length is $\ell = 0.475\lambda$ and its diameter is $d = 0.0017\lambda$.

involve additional calculations such as the averages of $[\underline{F}_1(\theta,\phi)]^2$ over $\Sigma$ and we shall not pursue this further, here.

When the length of the filamentary scatterers exceeds about $0.5\lambda$, the form of the current distribution varies appreciably with direction of plane wave incidence, indicating that more than a

single characteristic mode current must be considered. The induced current distribution in such cases can be decomposed into several characteristic mode components by a variety of techniques. As an example Fig. 22 presents modal current distributions for a straight wire $0.75\lambda$ in length and $0.01\lambda$ in diameter. The values of $\alpha_n$ associated with each current are also indicated and these may be used to calculate an average total scattered power,

$$(136) \qquad \hat{P}_T = \frac{2\pi}{k^2 Z_o} \sum_{n=1}^{4} |\cos \alpha_n|^2 \simeq \frac{2\pi}{k^2 Z_o} \quad (0.217).$$

For comparison purposes, we have presented in Fig. 23 similar curves of characteristic mode current distributions for a straight wire $0.5\lambda$ in length and $0.01\lambda$ in diameter. These data further support our earlier contention that essentially a single mode is important in the scattering from the wire. The average total scattered power in this case is

$$(137) \qquad \hat{P}_T = \frac{2\pi}{k^2 Z_o} |\cos \alpha_1|^2 \simeq \frac{2\pi}{k^2 Z_o} \quad (0.605).$$

The problem of determining the characteristic modes for a filamentary scatterer over $0.5\lambda$ in length may be approached in several ways. In each case, we assume that a finite-dimensional $(N \times M)$ representation of the Z operator, which carries an N-parameter current distribution into an M-parameter description of the related electric field intensity along the filament. Such would be the case, for example, if the current were specified by

N uniform currents (in each of N subintervals along the wire) or by an N-term Fourier series along its length, and if the tangential electric field intensity produced by this distribution were specified at M points along the filament. This is one of the accepted methods for computer solution of scattering by thin wires, wherein the Z operator is described by an N by M matrix with complex elements.[49] Methods for determining the characteristic mode currents for a specified [Z] matrix representation, determined by filament shape, radius, and frequency, fall into two general categories. In the first of these, the induced currents are determined for a selected set of incident field intensity vectors, which requires inversion of the Z operator, or a square matrix derived from it. If each of the set of incident field intensity vectors has only real components, a linear combination of the induced complex current distributions with real coefficients is sought which will have minimum phase variation along the wire length. There will be a number of such combinations which yield different equiphase current distributions, and each of these corresponds to a characteristic mode current distribution. In the second general method, a set of real current distributions are chosen and the associated set of electric field intensity distributions are determined through the [Z] matrix directly. A real linear combination of the set of electric field intensities is then sought which has minimum phase variation along the length of the filament. The same real linear

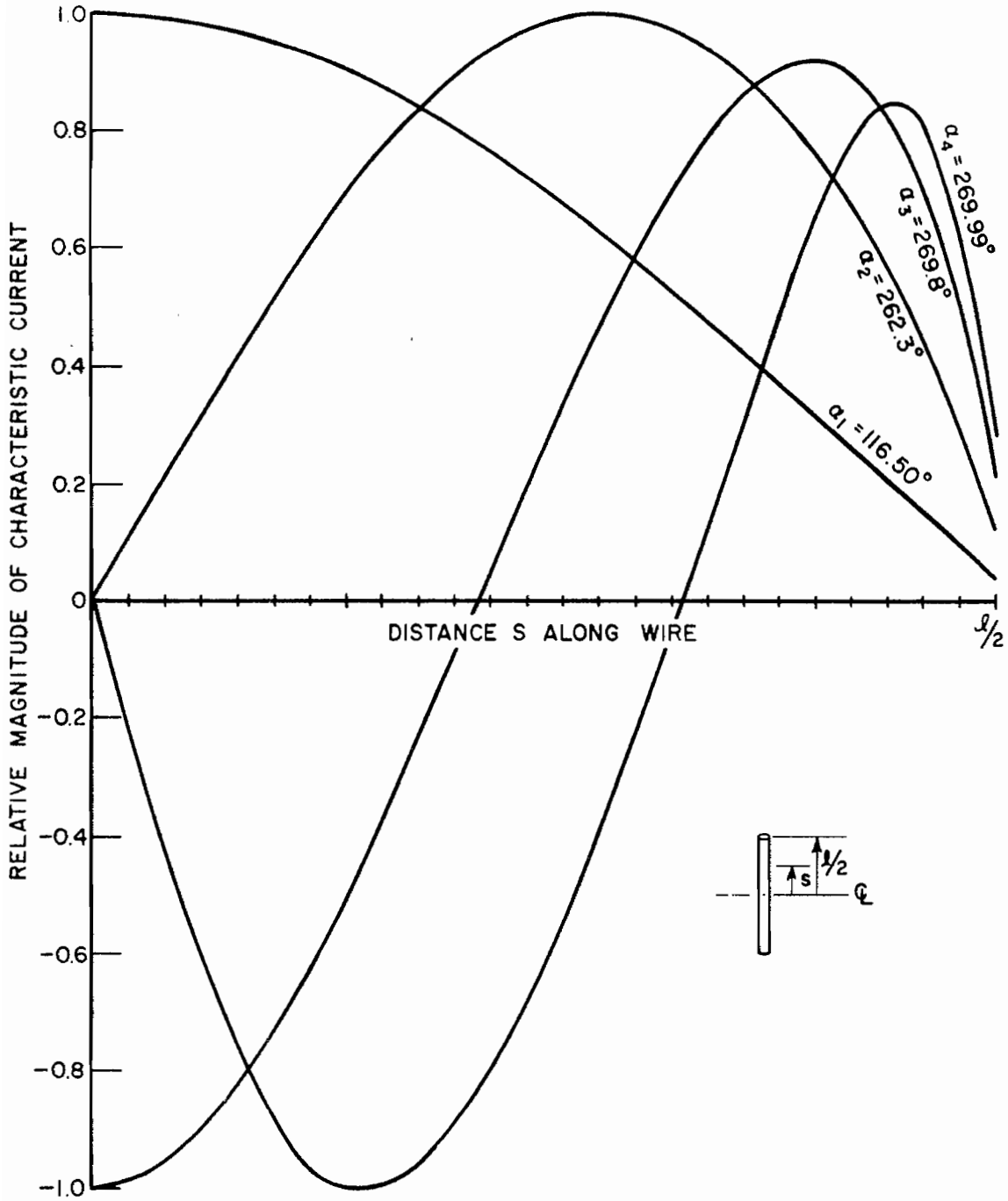


Fig. 22--Four characteristic mode current distributions on a straight wire of length $\ell = 0.75\lambda$ and diameter $d = 0.01\lambda$. The currents are normalized to unit maximum value.

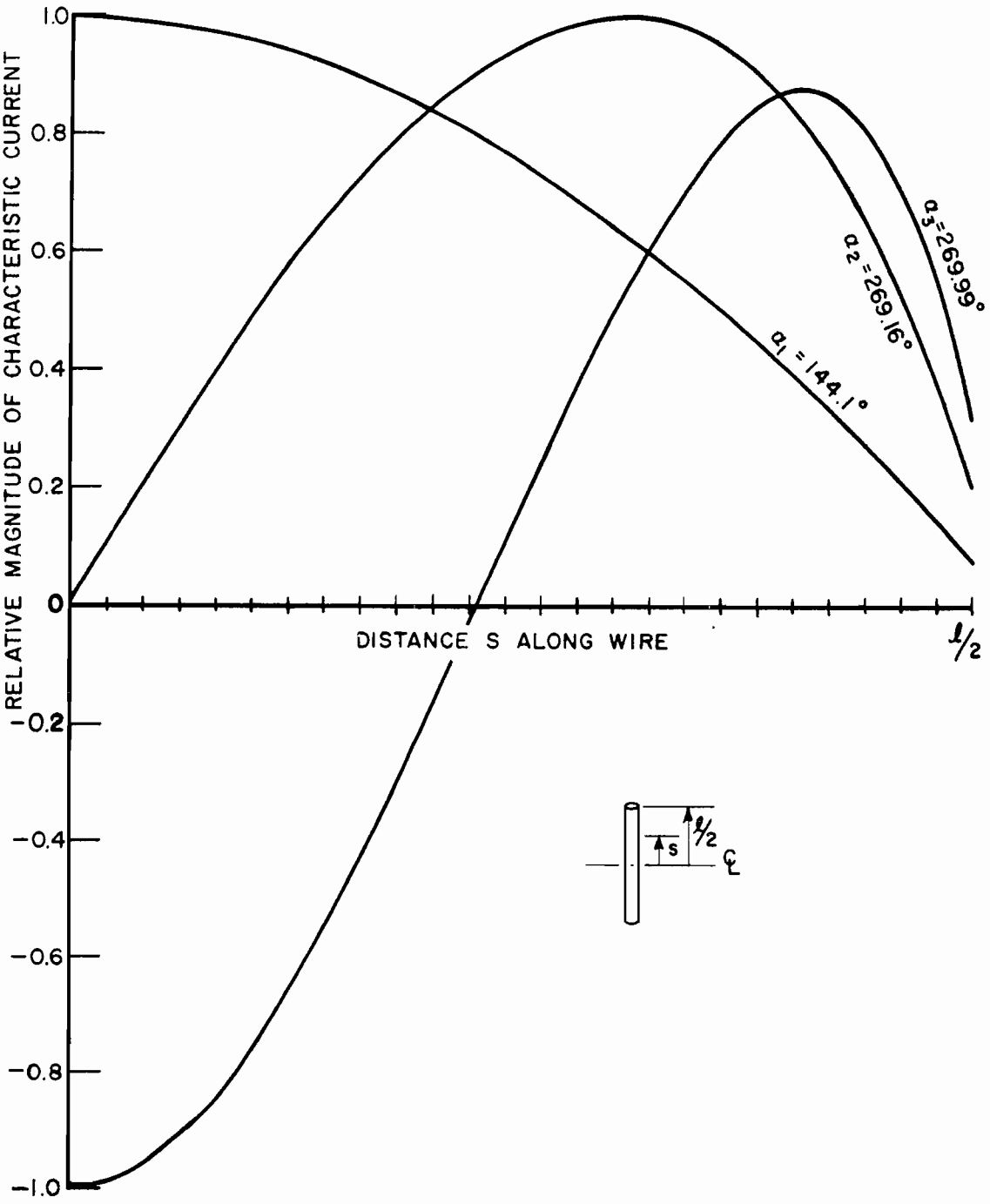


Fig. 23--Three characteristic mode current distributions on a straight wire of length $\ell = 0.5\lambda$ and diameter $d = 0.01\lambda$. The currents are normalized to unit maximum value.

combination of the current distributions is then a characteristic mode current distribution.

The data presented in Figs. 22 and 23 were obtained using the second of the general methods discussed above. In particular, the current distributions were specified by an N = 10 term (5 even, 5 odd) Fourier series with real coefficients and the resulting tangential electric field distributions were specified at M = 80 points along the linear wire. The resulting [Z] matrix is a rectangular array of M rows and N columns. This array may be decomposed into the sum of its real and imaginary parts, i.e., $[Z] = [R] + i[X]$, where [R] and [X] are real rectangular arrays. From previous considerations, if [Z] were a square array we would wish to determine the roots, $\lambda_n$, of $\det[X-\lambda R] = 0$ in order to find the phase constants, $\alpha_n = \tan^{-1}(-\lambda_n)$. Because in the present instance $M \neq N$, making [Z] rectangular, a related square matrix must first be devised before utilizing the determinantal equation procedure to find the $\lambda_n$. To this end, we form the rectangular array of real elements, $[M(\lambda)] = [X-\lambda R]$ and multiply it by its transpose to obtain the real, symmetric $N \times N$ array $[P(\lambda)] = [M(\lambda)]^t [M(\lambda)]$. We now are in a position to form the determinantal equation $\det[P(\lambda) - \gamma(\lambda)I] = 0$ and seek its N eigenvalues, $\gamma(\lambda)$, which must be all real and positive. By virtue of the process of multiplying $[M(\lambda)]$ by its transpose[50][51], it may be verified that the minimum eigenvalue (call it $\gamma_{min}(\lambda)$) represents the least mean square error of the phase variation of the

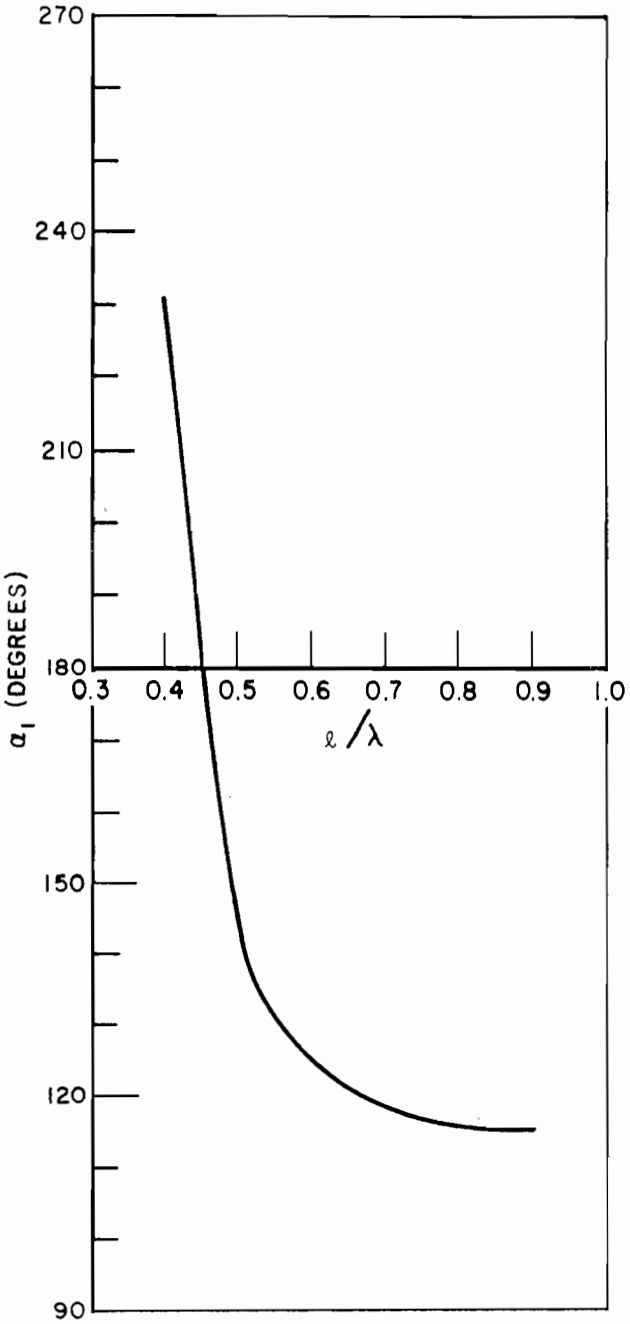


Fig. 24--Variation with frequency of phase angles, $\alpha_1$, of the dominant characteristic mode of a straight wire with diameter d = 0.01$\lambda$.

electric field along the filament caused by the current whose Fourier expansion coefficients are the N real components of the eigenvector associated with $\gamma_{min}(\lambda)$. By choosing various values of $-\infty \leq \lambda \leq \infty$, we can obtain a curve of $\gamma_{min}(\lambda)$ versus $\lambda$ (or alternatively, versus $\alpha = \tan^{-1}(-\lambda)$ where $\pi/2 \leq \alpha \leq 3\pi/2$) and center attention around those values of $\lambda$ for which $\gamma_{min}(\lambda)$ reaches relative minima. If these values of $\lambda$ are ordered according to non-descending values of their magnitudes, $|\lambda_1| \leq |\lambda_2| \cdots$, we obtain a set of phase constants $\alpha_1, \alpha_2, \cdots$ associated with a set of characteristic current distributions specified by the eigenvectors going with $\gamma_{min}(\lambda_1), \gamma_{min}(\lambda_2), \cdots$, respectively. Since $a_n = |\cos \alpha_n| e^{i\alpha_n}$ it is clear that the modes decrease in dominance with increasing n. In Figs. 22 and 23 we have plotted the first few characteristic mode current distributions and associated $\alpha_n$ found by the above procedure for two linear wires.[52] If desired, these currents may be normalized so that each radiates unit power. Figure 24 shows the variation with frequency of the phase angle, $\alpha_1$, associated with the dominant mode.

# CHAPTER V
# SUMMARY AND CONCLUSIONS

We have shown that it is useful to view a scattering obstacle as a device which transforms an incident wave converging (collapsing in) upon it into a scattered wave diverging away from it. Mathematically, this transformation is represented by a perturbation operator, $P$, which simply is a way of expressing the change in the diverging field which an observer at some distance from the obstacle would measure if the obstacle were suddenly removed and only the incident converging waves remained. Once such a transformation operation is postulated, it is necessary to determine some of its features which are useful to us.

One feature which every loss-free scatterer possesses is a set of special converging waves or modes, each of which is transformed into a diverging wave or mode of the same form as its incoming counterpart. That is, if $\underline{F}_n(\theta,\phi)$ is the far-zone pattern function of the $n^{th}$ such converging wave, the corresponding far zone pattern function of the scattered wave will also be $\underline{F}_n(\theta,\phi)$. They are related by,

$$a_n \underline{F}_{-n}(\theta,\phi) = P\underline{F}_n(\theta,\phi), \tag{138}$$

where $a_n$ is a complex constant of magnitude less than or equal to

unity. It is convenient to order the functions $\underline{F}_n(\theta,\phi)$, which are called characteristic pattern functions, such that they correspond to characteristic values, $a_n$, which satisfy $|a_1| \geq |a_2| \geq |a_3| \geq \cdots$. It is also convenient to normalize the $\underline{F}_n(\theta,\phi)$ such that they each represent unit radiated power. Every finite obstacle possesses an infinite set of $a_n$'s and $\underline{F}_n$'s, but the scattering operation is such that

$$\sum_{n=1}^{\infty} |a_n|^2$$

is finite, implying that only the first N waves are significant enough to include in practical problems. That is, we may treat the scattering operation as effectively a finite dimensional one to a good approximation.

The complex characteristic values, $a_n$, associated with any loss-free scatterer all must lie on the half-unit circle centered in the complex plane at $(-\frac{1}{2},io)$. That is,

$$a_n = |\cos \alpha_n| \, e^{i\alpha_n}, \quad \frac{\pi}{2} \leq \alpha_n \leq \frac{3\pi}{2} \quad . \tag{139}$$

The real angle, $\alpha_n$, is a measure of the "effectiveness" of the obstacle in scattering the associated $n^{th}$ order converging characteristic wave. Those waves which are scattered best are associated with angles $\alpha_n$ having values near $\pi$; those which scatter least, i.e., which behave almost as if the obstacle were not present, are associated with angles $\alpha_n$ having values near $\pi/2$ or $3\pi/2$. If

$\alpha_n = \pi$, $a_n = -1$ and we say that the $n^{th}$ characteristic wave or mode is in scattering resonance; if $\alpha_n = \pi/2$ or $3\pi/2$, $a_n = 0$ and we say that the $n^{th}$ characteristic wave is in scattering null. We may also remark that if the scatterer is not loss-free, i.e., is made of imperfect metal, dielectric, or magnetic materials, the numbers $a_n$ fall inside the aforementioned half-unit circle in the complex plane and the angles $\alpha_n$ become complex. This case is not discussed here.

The characteristic pattern functions, $\underline{F}_n(\theta,\phi)$, form a complete orthonormal set (with respect to radiated power) on the sphere $\Sigma$ at infinity, thereby permitting the expansion of any reasonably well behaved scattering pattern, $\underline{F}\ (\theta,\phi)$, on $\Sigma$ in terms of the $\underline{F}_n(\theta,\phi)$. That is

$$\underline{F}\ (\theta,\phi) = \sum_{n=1}^{N} A_n\ \underline{F}_n(\theta,\phi), \tag{140}$$

where the coefficients $A_n$ are found from knowledge of the primary source in terms of a "reaction" between the source current and the $n^{th}$ outgoing field (specified by $\underline{F}_n(\theta,\phi)$) analytically continued in to the primary source region.

If the primary source is a unit plane wave incident upon the obstacle from an arbitrary direction $(\theta^i,\phi^i)$, the scattered electric field intensity observed in a direction $(\theta^s,\phi^s)$ on $\Sigma$ is given by

$$\underline{E}(\theta^i,\phi^i;\theta^s,\phi^s) = -\frac{i\omega\mu}{4\pi}\ \frac{e^{-ikr}}{r}\ \underline{\underline{F}}(\theta^i,\phi^i;\theta^s,\phi^s)\cdot\hat{\xi}^i, \tag{141}$$

where $\hat{\xi}^i$ is the polarization state of the incident plane wave and $\underline{\underline{F}}(\theta^i,\phi^i;\theta^s,\phi^s)$ is the dyadic scattering pattern,

$$\underline{\underline{F}}(\theta^i,\phi^i;\theta^s,\phi^s) = -\sum_{n=1}^{N} a_n \underline{F}_n(\theta^i,\phi^i)\,\underline{F}_n(\theta^s,\phi^s). \tag{142}$$

Thus, knowledge of the characteristic pattern functions $\underline{F}_n(\theta,\phi)$ and the associated characteristic values, $a_n$ (or angles $\alpha_n$), permits a compact bilinear expression for the field scattered in any direction due to a unit plane wave incident from any direction.

The properties described above are common to all loss-free obstacles, but to simplify the problem of determining the forms of the characteristic waves, in this work we have restricted ourselves to perfectly conducting obstacles. In these cases it is always possible to define real characteristic current distributions, $\underline{J}_n$ induced on the surface S of the obstacle by the $n^{th}$ converging wave such that in the absence of the obstacle they each radiate a field with a characteristic field pattern $\underline{F}_n(\theta,\phi)$ on $\Sigma$ and an electric field intensity inside and on S which is equiphase and lags $\underline{J}_n$ by the angle, $\alpha_n$. Thus, for a particular surface S, determining those unique current distributions, $\underline{J}_n$, which possess this property, makes it possible to construct the bilinear expansion formula for plane wave scattering from the corresponding perfectly conducting obstacle. As suggested previously, those characteristic current distributions for which the phase angle $\alpha_n = \pi$ are in scattering resonance and are the most effective contributors to radiated energy; conversely, those current distributions for which $\alpha_n = \pi/2$

or $3\pi/2$ are in scattering null and do not contribute at all to radiated energy. In fact, these latter current distributions are precisely those which are associated with the perfectly conducting cavity formed by the region interior to S when this cavity is in resonance.

Having introduced the concept of a bilinear expansion for plane wave scattering in terms of characteristic mode functions, and having developed a property of such modes for perfectly conducting obstacles, which can be used to determine them, several examples were chosen as illustrations.

The infinite circular cylinder and the sphere under plane wave illumination were treated first in order to relate the characteristic mode formulation to the more familiar formulations of these problems. For these cases, the cylindrical and spherical wave functions, respectively, are shown to be essentially the characteristic modes.

Next, plane wave scattering by an arbitrary array of N thin, infinitely long, parallel wires was formulated and specific results were calculated for a 3-wire and an 8-wire array. The characteristic currents and associated phase angles, $\alpha_n$, were tabulated and in the case of the 3-wire array, the characteristic pattern functions, $\underline{F}_n(\phi)$, were plotted and combined in the bilinear form to yield the back-scattered field pattern for the array. In the case of the 8-wire array, the near fields of the lowest order characteristic current were calculated and an equiphase contour plot was calculated to

illustrate the near-constant nature of the modal field inside the region outlined by the eight wires.

Scatterers consisting of closed circular loops of thin wire were considered next. Plane wave scattering by a single loop was analyzed from the characteristic mode viewpoint and shown to be equivalent to formulations in the literature. We introduced the concept of an impedance associated with each modal current on the loop and using data extracted from the literature, related such impedances to the phase angles, $\alpha_n$. Derived curves of $\alpha_n$ versus frequency were plotted for the first few modes associated with a given loop. The characteristic mode approach was also applied to plane wave scattering by two coaxial circular loops of wire. The concept of modal impedances was extended to include such a geometry and expressions were derived for their evaluation. Phase angles, $\alpha_n$, and characteristic currents were computed for the lowest order modes associated with a chosen pair of loops.

The final example considered was plane wave scattering by a circular arc of thin wire. Using often-used computer techniques devised in the past few years for solving complicated boundary value problems, we have observed the essentially single mode behavior of plane wave scattering by arbitrarily shaped thin wires less than $0.5\lambda$ in length. To illustrate this behavior, we have plotted the induced current distributions along wire arcs $0.475\lambda$ in length and of various radii of curvature, together with the phase angle, $\alpha_n$,

associated with each arc. The invariance of these current distributions with change in shape suggests that this common feature may be exploited for comparing the elements. For example, using these current distributions to obtain the associated characteristic pattern functions permits the expression of the back scattering cross section for any angle of incidence, which in turn can be used to obtain cross sections averaged over all or selected tumble angles. Or, since the value of $|\cos \alpha_n|^2$ are proportional to the total cross section averaged over all tumble angles, a comparison of wires of different shapes based on this criterion is immediately available from knowledge of the phase angles, $\alpha_n$. For planar geometries of the wire these angles are easily found, as in the case of the circular arcs, by inspecting the phase of the computer derived current induced on each geometry by a broadside-incident plane wave. For three dimensional wire geometries, an excitation composed of two plane waves incident from opposing directions immediately would provide the same information. Comparison schemes based on these principles can be applied to wire dipoles, where warpage from the ideal straight element is common, and its effect on a tumble average is desired.

If the wire length exceeds $0.5\lambda$, such comparisons are complicated by the fact that higher order modes enter more significantly. Several methods have been devised to isolate the characteristic current and associated phase angle of each mode in these cases.

One such method is discussed in this work and is applied to a linear wire of length $0.75\lambda$ as an example.

Having summarized this treatise, we now suggest some possible topics for near-future study. In our opinion, efforts should proceed along the following lines of investigation:

(1) Just as in the case of the open circular arcs discussed in Section IVE, it should be possible to use standard computer techniques to determine the phase angles, $\alpha_n$, and characteristic current distribution on other wire configurations, both planar and non-planar, such as elliptical arcs, spirals, helices, and S shapes. It is recommended that these be obtained for a variety of shapes over a range of frequencies, and a comparison made with respect to backscattering cross section and total scattering cross section averaged overall aspect and polarization angles. Such comparisons would allow an ordering of various elemental scatterers according to a chosen figure-of-merit which accounts for tumble average cross section and bandwidth. Because we expect that the form of the current distribution is rather invariant with changes in wire shape, the modal expansion formulation should provide a rapid and efficient way of evaluating such figures-of-merit.

(2) Similarly, it should be possible to use standard computer techniques to determine the phase angles, $\alpha_n$, and characteristic current distributions on more complex scatterers of small size. In particular, bodies of revolution where distributions along a longitudinal curve suffice to describe the modal currents, can be attacked using computer methods presently in use.

(3) The methods suggested in this work for determining characteristic mode current distributions suffer from the fact that several such currents are postulated to exist simultaneously, the task being to isolate them and their associated phase constants all in one operation. This approach encounters difficulty because the higher order modes, even though only slightly excited, corrupt the determination of the dominant mode. At the same time these higher order modes are minor contributors to the overall scattered field and may even be neglected in the final analysis. Thus, future efforts should include the determination of characteristic mode currents by some method which isolates one mode at a time, refining it by an iterative procedure. In this way the dominant modes could be given preferential treatment and the higher order modes could be ignored or

determined without influencing the dominant ones. The exact procedure for accomplishing this has not been developed. Characteristic mode fields associated with a perfectly conducting obstacle are an extension of resonant cavity fields (the interior problem) to radiation and scattering by the obstacle (the exterior problem). As such, it may be possible to extend methods of determining resonant field distributions inside ideal cavities of arbitrary shape to the scattering problem. However, two basic differences exist between these two situations: whereas the cavity supports a single field distribution at resonance (discounting degenerate modes) and must have an associated phase angle, $\alpha_n = \pi/2$ or $3\pi/2$, the scatterer at the same frequency (or any frequency) supports an infinitude of modal field distributions for which the associated phase angles, $\alpha_n$, are not known *a priori*. This additional freedom of the phase angles will complicate any iterative method which seeks to converge upon the associated characteristic field distributions individually. However we speculate that it may prove useful to try as initial current distributions resonant cavity currents permitted to exist at the frequency of interest by considering the interior region filled with dielectric or magnetic material.

(4) Properties of the characteristic modes of lossless dielectric or magnetic obstacles should be investigated in order to aid the development of methods for their determination.

Up to this point, we have emphasized the use of characteristic modes for plane wave scattering by perfectly conducting obstacles. If, however, the primary source lies in or near the surface S, the whole complex forms an antenna and the associated characteristic currents and pattern functions may aid radiation pattern control, pattern synthesis, and feed design. For example, we may obtain the admittance of an infinitesimal slot in a conducting body in terms of its characteristic current densities according to the formula,

$$Y_{slot} = - \sum_{n=1}^{N} a_n \, |\underline{J}_n(u,v) \cdot \hat{w}|^2$$

where $(u,v)$ is the location of the slot on S and the unit vector $\hat{w}$ fixes its orientation.

We may generalize characteristic modes to N-element arrays of small elements, thereby obtaining characteristic-excitations and patterns for use as basis functions in array synthesis procedures. In contrast with other basis functions (for example, those devised by Müller[53]), the characteristic modes provide a natural set which simultaneously orthogonalize radiated and net stored energies.

Because of this property, for example, it is possible to devise an array excitation which simultaneously maximizes the directivity of the array and minimizes its net stored power.

Or, one may utilize the characteristic patterns of an array of elements to approximate a prescribed pattern in a least mean square sense and thereby obtain the appropriate array excitation. It may also be possible to incorporate a restriction on net stored energy in the manner of Rhodes[54][55][56][57], in which case we suggest that the lowest-order mode associated with $\lambda_1 = -\tan \alpha_1$ should possess the minimum super gain ratio, $\gamma_{min} = 1 + |\lambda_1|$.

# APPENDIX A
# DEFINITION OF MODAL IMPEDANCES FOR COAXIAL CIRCULAR LOOPS

In the development of a characteristic mode expansion suitable for the representation of far fields radiated or scattered by two coaxial circular loops, it is convenient to define and derive self and mutual modal impedances of such a structure. Although they are defined precisely in this appendix it may help to say here that these impedances relate a current on one loop to the tangential electric field it produces on itself or on the other loop, respectively. The descriptor, "modal", implies that not just any currents are assumed, but characteristic ones, which in this case are currents distributed sinusoidally around the loops.

Referring to Fig. 25, assume a time harmonic current on loop 1 of the form

$$\underline{J}^{n}_{1m} = \hat{\phi}\, J^{n}_{1m}(B) \cos n\phi, \tag{144}$$

where an $e^{i\omega t}$ time factor is understood. The resultant electric field tangential to loop 2 will be denoted by

$$\hat{E}^{n}_{2m\phi} = \dot{E}^{n}_{2m\phi}(B) \cos n\phi\ . \tag{145}$$

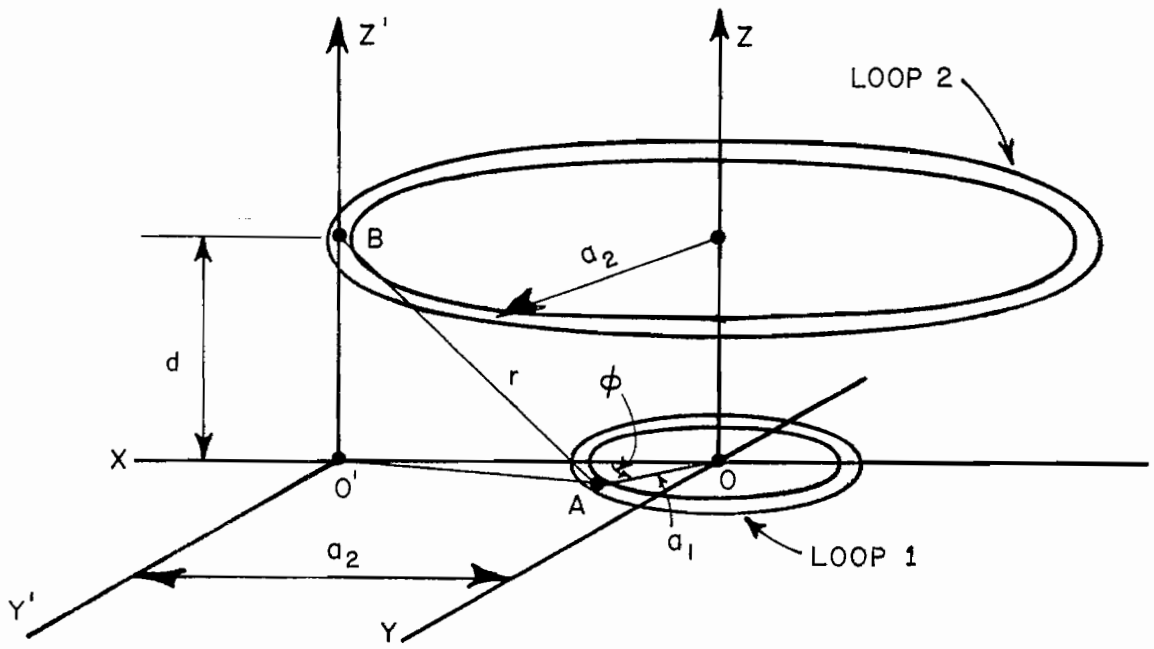


Fig. 25--Coordinates for two coaxial circular loops.

The voltage induced between two adjacent nodes of $\hat{E}^n_{m\phi}$ on loop 2 is

$$(146) \qquad V^n_{2m} = a_2 \int_{-\pi/2n}^{\pi/2n} \hat{E}^n_{2m\phi}\, d\phi = a_2\, \hat{E}^n_{2m\phi}\,(B) \int_{-\pi/2n}^{\pi/2n} \cos n\phi\, d\phi,$$

$$= \frac{2a_2}{n}\, \hat{E}^n_{2m\phi}\,(B).$$

Since there are 2n such voltages around the loop, the sum of their absolute values is

$$(147) \qquad 2n\, V^n_m = 4a_2\, \hat{E}^n_{2m\phi}\,(B).$$

The current on loop 1 averaged between two adjacent modes is

$$(148) \qquad \bar{J}^n_{1m} = \frac{n}{\pi} \int_{-\pi/2n}^{\pi/2n} J^n_{1m}(B) \cos n\phi \, d\phi \, ,$$

$$= \frac{2}{\pi} J^n_{1m}(B).$$

The mutual modal impedance is defined by

$$(149) \qquad Z^n_{21} = - \frac{2n \, V^n_{2m}}{\varepsilon_n \, \bar{J}^n_{1m}} = - \frac{2\pi a_2}{\varepsilon_n} \frac{\hat{E}^n_{2m\phi}(B)}{J^n_{1m}(B)} \, ,$$

with $\varepsilon_n = \begin{cases} 2, & n \neq 0 \\ 1, & n = 0 \end{cases}$. Definitions for $Z^n_{12}$, $Z^n_{11}$, and $Z^n_{22}$ are arrived at in an analogous manner.

In order to clarify this choice of definition for the modal impedances, consider the power radiated by a pair of loops with $J^n_{1m} = J^n_{1m}(B) \cos n\phi$ on loop 1 and $J^n_{2m} = J^n_{2m}(B) \cos n\phi$ on loop 2:

$$(150) \qquad P^n_m = - \mathrm{Re} \oint_S (J^n_m)^t \, (\hat{E}^n_{m\phi}) \, d\sigma \, , \; m = 1,2.$$

Using the definition for modal impedances

$$(151) \qquad \begin{pmatrix} E^n_{1m\phi} \\ E^n_{2m\phi} \end{pmatrix} = \begin{bmatrix} - \frac{\varepsilon_n}{2\pi a_1} & 0 \\ 0 & - \frac{\varepsilon_n}{2\pi a_2} \end{bmatrix} \begin{bmatrix} Z^n_{11} & Z^n_{12} \\ Z^n_{21} & Z^n_{22} \end{bmatrix} \begin{pmatrix} J^n_{1m} \\ J^n_{2m} \end{pmatrix} \, ,$$

or

$$(152) \qquad (\hat{E}^n_{m\phi}) = \begin{bmatrix} - \frac{\varepsilon_n}{2\pi a_1} & 0 \\ 0 & - \frac{\varepsilon_n}{2\pi a_2} \end{bmatrix} \left[ Z^n \right] (J^n_m) = [\bar{Z}^n] \, (J^n_m).$$

Substituting Eqs. (152) into Eq. (150),

$$(153) \qquad P_m^n = \varepsilon_n \{R_{11}^n [J_{1m}^n(B)]^2 + 2R_{12}^n J_{1m}^n(B) J_{2m}^n(B) + R_{22}^n [J_{2m}^n(B)]^2\} \times \int_{-\pi}^{\pi} \cos^2 n\phi \, d\phi,$$

$$= R_{11}^n [J_{1m}^n(B)]^2 + 2R_{12}^n J_{1m}^n(B) J_{2m}^n(B) + R_{22}^n [J_{2m}^n(B)]^2 \quad ,$$

where $J_{1m}^n(B)$ and $J_{2m}^n(B)$ are the maximum rms values of the current on loops 1 and 2 respectively.

Thus, the impedances as defined are related to the radiated power in such a way that they represent an extension of the concept of radiation resistance for the uniform loop of current.[58]

The above development of modal impedances for coaxial circular loops represents a particular case of a special class of scatterers, *viz.*, ones which are composed of individual coupled elements, each of which supports a known characteristic current distribution identical in form to that which it supports when isolated. In such cases, characteristic current distributions of the ensemble are a weighted combination of those for the individual elements. As an example, consider the two element scatterer (such as the loop pair). If $J_{11}$ is a characteristic current distribution on isolated element #1 and $J_{22}$ is a characteristic current on isolated element #2, then the characteristic current distributions on each element in the presence of the other are:

$w_{11}J_{11}$ on element #1
$w_{21}J_{22}$ on element #2
} characteristic current distribution #1

$w_{12}J_{11}$ on element #1
$w_{22}J_{22}$ on element #2
} characteristic current distribution #2

If we continue the convention of making all characteristic current distributions real, the $w_{ij}$ must be real quantities. We inquire what information is necessary to determine the $w_{ij}$ for perfectly conducting scatterers?

In addition to the phase angles, $\alpha_1$ and $\alpha_2$, by which the tangential electric field distribution on elements #1 and #2 lag their respective characteristic current distributions <u>when isolated</u>, we must know the strength and phase of the induced current on each element (neglecting multiple interactions) when excited by a characteristic current (isolated case) on the other and normalized to radiate unit power. These induced currents could be expressed as a dimensionless ratio between the isolated characteristic mode current and the induced (on the same element) current. That is,

$$z_{21} = \frac{J_{21}}{J_{11}} = \frac{\text{amplitude and phase of current induced on element \#1 by unit characteristic current on element \#2}}{\text{characteristic current amplitude on isolated element \#2}}$$

$$z_{12} = \frac{J_{12}}{J_{22}} = \frac{\begin{array}{l}\text{amplitude and phase of current induced}\\ \text{on element \#2 by unit characteristic}\\ \text{current on element \#1}\end{array}}{\begin{array}{l}\text{characteristic current amplitude on}\\ \text{isolated element \#1}\end{array}}$$

When modal impedances can be defined,

$$z_{21} = \frac{\bar{Z}_{21}}{|\bar{Z}_{11}|} \quad ; \quad z_{12} = \frac{\bar{Z}_{12}}{|\bar{Z}_{22}|} \quad .$$

We can form the matrix,

$$\begin{bmatrix} e^{-i\alpha_1} & z_{12}e^{-i\alpha_1} \\ z_{21}\,e^{-i\alpha_2} & e^{-i\alpha_2} \end{bmatrix} \sim \begin{bmatrix} \dfrac{\bar{Z}_{11}}{|\bar{Z}_{11}|} & \dfrac{\bar{Z}_{12}}{|\bar{Z}_{11}|} \\ \dfrac{\bar{Z}_{12}}{|\bar{Z}_{22}|} & \dfrac{\bar{Z}_{22}}{|\bar{Z}_{22}|} \end{bmatrix},$$

in which the off-diagonal elements have the same phase, but not necessarily the same amplitude. Continuing the normalization so that the real parts of the diagonal entries are unity,

$$[M] = \begin{bmatrix} \dfrac{e^{-i\alpha_1}}{\cos\alpha_1} & \dfrac{z_{12}}{\cos\alpha_1}\,e^{-i\alpha_1} \\ \dfrac{z_{21}}{\cos\alpha_2}\,e^{-i\alpha_2} & \dfrac{e^{-i\alpha_2}}{\cos\alpha_2} \end{bmatrix} \sim \begin{bmatrix} \dfrac{\bar{Z}_{11}}{\bar{R}_{11}} & \dfrac{\bar{Z}_{12}}{\bar{R}_{11}} \\ \dfrac{\bar{Z}_{21}}{\bar{R}_{22}} & \dfrac{\bar{Z}_{22}}{\bar{R}_{22}} \end{bmatrix} .$$

We seek the real matrix

$$[W] = \begin{bmatrix} w_{11} & w_{12} \\ w_{21} & w_{22} \end{bmatrix} ,$$

which satisfies the relation

$$[W]^t [M][W] = [I] + i [\Lambda]$$

where $[\Lambda]$ is a diagonal matrix with real elements, $\lambda_1$ and $\lambda_2$. In the absence of coupling $[W]$ is the unit matrix and we get the original characterisitc currents, $J_{11}$ and $J_{22}$, for the individual elements. With coupling, the columns of $[W]$ yield the linear combinations of $J_{11}$ and $J_{22}$ which form the characteristic currents of the pair of elements, and these are properly normalized. Clearly, the phase angles associated with these characteristic modes are

$$\alpha_1 = \tan^{-1}(-\lambda_1),$$

and

$$\alpha_2 = \tan^{-1}(-\lambda_2).$$

Using this method, it is unnecessary to define modal impedances, although when they can be defined, the results are entirely equivalent.

It may be proper here to reiterate that the above method rests upon the hypothesis that the <u>form</u> of the characteristic current on any element in the ensemble of scatterers is the same when the element is isolated or in the ensemble. For coaxial circular loops this hypothesis is valid even when the loops are extremely close; for linear elements this hypothesis is approximately valid beyond a certain (yet unknown) spacing which depends upon the lengths and relative orientations of the elements.

## REFERENCES


1. Schmeidler, W., Linear Operators in Hilbert Space, Academic Press, New York, 1965.
2. Schmeidler, W., op. cit., pp. 43-45.
3. Friedman, B., Principles and Techniques of Applied Mathematics, John Wiley and Sons, Inc., New York, 1956, pp. 38-42.
4. Mikhlin, S.G., Linear Integral Equations, Hindustan Publishing Corp., Delhi, India, 1960, pp. 114-115.
5. Schmeidler, W., op. cit., pp. 58-60.
6. Akhiezer, N.I. and H.M. Glazman, Theory of Linear Operators in Hilbert Space, Fredrich Ungar Publishing Co., New York, 1965, Vol. 1, pp. 129-132.
7. Montgomery, G.G., R.H. Dicke and E.M. Purcell, Principles of Microwave Circuits, MIT Radiation Laboratory Series, McGraw-Hill Book Co., Inc., New York, 1948, pp. 317-333, 405-411.
8. Tsu, R., "The Theory and Application of the Scattering Matrix for Electromagnetic Waves," Report 1073-2, 1 August 1960, ElectroScience Laboratory (formerly Antenna Laboratory), Department of Electrical Engineering, The Ohio State University; prepared under Contract No. AF 19(604)-6157 for Air Force Cambridge Research Center. (AD 243 689)

9. Newton, R.G., Scattering Theory of Waves and Particles, McGraw Hill Book Co., Inc., New York, 1966, pp. 177-213, 300-304, 452-457.

10. Lax, P.D. and R.S. Philips, Scattering Theory, Academic Press, New York, 1967.

11. Lusternik, L.A. and V.J.Sobolev, Elements of Functional Analysis, Hindustan Publishing Corp., Delhi, India, 1965, p. 249.

12. Montgomery, C.G., R.H. Dicke, and E.M. Purcell, ibid.

13. MacDuffee, C.C., The Theory of Matrices, Chelsea Publishing Co., New York, 1956, pp. 108-109.

14. Schmeidler, W., op. cit., p. 98.

15. Stone, H.S., Linear Transformations in Hilbert Space and Their Applications to Analysis, American Mathematical Society, 1932, p. 330.

16. Collatz, L., Functional Analysis and Numerical Mathematics, Academic Press, New York, 1966, p. 171.

17. Shilov, G.E., An Introduction to the Theory of Linear Spaces Prentice-Hall, Inc., Englewood Cliffs, New Jersey, 1961, p. 285.

18. Rumsey, V.H., "Reaction Concept in Electromagnetic Theory," Phys. Rev., Vol. 94, 1954, pp. 1483-1491.

19. Richmond, J.H., Reciprocity Theorems and Plane Surface Waves, Bulletin 176, Engineering Experiment Station, The Ohio State University, 1959.

20. Cohen, M.H., "Application of the Reaction Concept to Scattering Problems," I.R.E. Group on Antennas and Propagation, Vol. AP-3, pp. 193-199, April 1955.

21. King, R.W.P. and T.T. Wu, The Scattering and Diffraction of Waves, Harvard University Press, Cambridge, Mass., 1959, pp. 22-74.

22. Harrington, R.F., Time-Harmonic Electromagnetic Fields, McGraw-Hill Book Co., New York, 1961, pp. 232-235.

23. McLachlan, N.W., Theory and Application of Mathieu Functions Clarendon Press, Oxford, 1947, pp. 363-366.

24. Nomura, Y., "On the Propagation of Electric Waves from a Horizontal Dipole over the Surface of the Earth Sphere," Sci. Rep. Res. Inst. Tohoku University (Japan), Vol. 1-2, 1951, pp. 25-49.

25. Tai, C.T., Technical Report No. 29, Aircraft Radiation Systems Laboratory, Stanford Research Institute, Stanford, California, 1952.

26. Mie, G., "Beitrage zur Optik truber Median speziell kolloidaler Metallosumgen," Ann. Phys., Vol. 25, 1908, pp. 377-445.

27. Debye, P., "Der Lichtdruck auf Kugeln von beliebigem Material," Ann. Phys., Vol. 30, 1909, pp. 57-136.

28. Stratton, J.A., Electromagnetic Theory, McGraw-Hill Book Co., New York, 1941, pp. 564-570.

29. Harrington, R.F., Time-Harmonic Electromagnetic Fields, McGraw-Hill Book Co., New York, 1961, Chapter 6.

30. Stratton, J.A., **loc.cit.**

31. Tai, C.T., "Some Electromagnetic Problems Involving a Sphere," McGill Symposium on Microwave Optics, Part II, April 1959, pp. 185-195.

32. Newton, R.G., op. cit., Chapter 2.

33. Richmond, J.H., "Scattering by an Arbitrary Array of Parallel Wires," IEEE Trans. on Microwave Theory and Techniques, Vol. MTT-13, July 1965, pp. 408-412.

34. Gantmacher, F.R., The Theory of Matrices, Chelsea Publishing Co., New York, Vol. I, 1959, pp. 310-326.

35. Van de Hulst, H.C., Light Scattering by Small Particles, John Wiley and Sons, Inc., New York, 1957, pp. 302-304.

36. De Hoop, A.T., "On the Plane-Wave Extinction Cross-Section of an Obstacle," App. Sci. Res., Vol. 7, Sect. B, 1957, pp. 463-469.

37. Chen, C.L. and R.W.P. King, "The Small Bare Loop Antenna Immersed in a Dissipative Medium," IEEE Trans. on Antennas and Propagation, Vol. AP-11, No. 3, May 1963, pp. 266-269.

38. King, R.W.P., C.W. Harrison, Jr., and D.G. Tingley, "The Admittance of Bare Circular Loop Antennas in a Dissipative Medium," IEEE Trans. on Antennas and Propagation, Vol. AP-12, No. 4, July 1964, pp. 434-438.

39. Iizuka, K., "The Circular Loop Antenna Multiloaded with Positive and Negative Resistors," IEEE Trans. on Antennas and Propagation, Vol. AP-13, No. 1, January 1965, pp. 7-20.

40. Kouyoumjian, R.G., "The Back-Scattering from a Circular Loop," Appl. Sci. Res., Vol. 6, Sect. B, 1956, pp. 165-179.

41. Baghdassarian, A. and D.J. Angelakos, "Scattering from Conducting Loops and Solution of Circular Loop Antennas by Numerical Methods," Proc. of the IEEE, Vol. 53, No. 8, August 1965, pp. 818-822.

42. Harrington, R.F. and J.L. Ryerson, "Electromagnetic Scattering by Loaded Wire Loops," Radio Science, Vol. 1 (New Series), No. 3, March 1966, pp. 347-352; correction in Vol. 1 (New Series), No. 12, December 1966, p. iii.

43. Harrington, R.F. and J. Mautz, "Computations for Loaded Wire Loops," Technical Report No. RADC-TR-67-8, Syracuse University, Syracuse, New York, February 1967.

44. Harrington, R.F. and J. Mautz, "Electromagnetic Behavior of Circular Wire Loops with Arbitrary Excitation and Loading," Proc. IEE, Vol. 115, No. 1, January 1968, pp. 68-77.

45. Unpublished notes of Prof. J.H. Richmond, The Ohio State University, Columbus, Ohio.

46. Private correspondence with Prof. R.F. Harrington, Syracuse University, Syracuse, New York.

47. Richmond, J., "Digital Computer Solutions of the Rigorous Equations for Scattering Problems," Proc. of the IEEE, Vol. 53, No. 8, August 1965, pp. 796-804.

48. Thiele, G.A., "Final Technical Report (Scattering by Imperfectly Conducting Wires of Arbitrary Shape)," Report 2409-6, 21 June 1968, ElectroScience Laboratory, Department of Electrical Engineering, The Ohio State University; prepared under Contract AF 19(628)-5167 for Massachusetts Institute of Technology.

49. Harrington, R.F., Field Computation by Moment Methods, MacMillan Company, New York, 1968.

50. Berezin, I.S. and N.P. Zhidkov, Computing Methods, Pergammon Press, New York, 1965, pp. 442, 447.

51. Fischbach, J.W., "Solution of Least Squares Problems by an N Step Gradient Method," Technical Note No. 719, Ballistic Research Laboratories, Aberdeen Proving Ground, Maryland, July 1962.

52. These curves were calculated by Mr. R.H. Turpin. His work will be treated more completely in a future ElectroScience Laboratory report.

53. Muller, C., "Electromagnetic Radiation Patterns and Sources," IEEE Trans. on Antennas and Propagation, Vol. AP-4, No. 3, July 1956, pp. 224-232.

54. Rhodes, D.R., "The Optimum Line Source for the Best Mean Square Approximation to a Given Radiation Pattern," IEEE Trans. on Antennas and Propagation, Vol. AP-11, No. 4, July 1963, pp. 440-446.

55. Rhodes, D.R., On a Fundamental Principle in the Theory of Planar Antennas," Proc. of the IEEE, Vol. 52, No. 9, September 1964, pp. 1013-1021. See also two comments by G.V. Borgiotti and R.E. Collin and response by Rhodes in IEEE Trans. on Antennas and Propagation, Vol. AP-15, No. 4, July 1967, pp. 565-569.

56. Tang, T.S., "On the Problem of Optimum Antenna Aperture Distribution," Jour. of the Franklin Institute, Vol. 283, No. 3, March 1967, pp. 235-249.

57. Hill, P.C.J., "Analytic Determination of Dipole Reactance by Radiation-Pattern Integration," Proc. IEE, Vol. 114, No. 7, July 1967, pp. 853-858.

58. Kraus, J.D., Antennas, McGraw-Hill Book Company, 1950, p. 166.